UC Berkeley
UC Berkeley Electronic Theses and Dissertations

Title
Regulation of Dynein Motility and Force Generation by Lissencephaly-1

Permalink
https://escholarship.org/uc/item/7rv79490

Author
Kusakci, Emre

Publication Date
2022

Peer reviewed|Thesis/dissertation

Regulation of Dynein Motility and Force Generation by Lissencephaly-1

By

Emre Kusakci

A dissertation submitted in partial satisfaction of the

requirements for the degree of

Doctor of Philosophy

in

Biophysics

in the

Graduate Division

of the

University of California, Berkeley

Committee in charge:

Professor Ahmet Yildiz, Chair

Professor Andreas Martin

Professor Eva Nogales

Professor Randy Schekman

Summer 2022

Abstract

Regulation of Dynein Motility and Force Generation by Lissencephaly-1

By

Emre Kusakci

Doctor of Philosophy in Biophysics

University of California, Berkeley

Professor Ahmet Yildiz, Chair

Molecular motors hydrolyze ATP to produce mechanical work by stepping along the cytoskeleton network and carrying cargos. Dynein has many cellular roles which require its minus end-directed motility and force generation along the microtubules (MTs). All dynein activity needs to be tightly regulated by its many associated factors. Lis1 is the only associated factor that directly binds to dynein's ATP hydrolyzing AAA ring, and it is involved in most, if not all, cellular processes that require dynein activity. In my thesis work, working with both mammalian and yeast proteins, I showed how dynein motility and force generation is regulated by Lis1 and its yeast homolog Pac1 (both Lis1 from here on).

Mammalian dynein is mostly autoinhibited, that is, it cannot take many steps before detaching from the microtubules, a property that is essential for dynein-mediated cargo transportation. For processive motility, dynein needs to be relieved from this autoinhibition and needs to bind to dynactin and a cargo adapter. Using protein engineering, single molecule motility, optical trapping, and biophysical characterization assays, we have shown that Lis1 relieves dynein from autoinhibition, thus allowing the formation of dynein dynactin cargo adapter complex (DDX). Through the same mechanism, Lis1 increases the copy number of dynein in DDX complexes which enables faster motility and higher force generation. However, even after the formation of these complexes Lis1 can remain bound to dynein. In that case, we see an inhibitory effect of Lis1.

In my thesis, I have shown the mechanism by which Lis1 binding affects dynein motility I switched my research to *S. cerevisiae* cytoplasmic dynein which has inherently processive motility without needing any cofactors, unlike mammalian dynein. I showed that Lis1 binding to the motor domain slows down dynein motility thus confirming previous studies done on yeast dynein and Lis1. Through multicolor TIRF colocalization assays, I have demonstrated that binding of individual Lis1 molecules causes dynein to pause or stop, and its unbinding restores dynein velocity. I have made three discoveries:

1. Lis1 binding to dynein has been proposed to inhibit or slow dynein motility by tethering dynein to the microtubule. I ruled out this model by showing that Lis1 only weakly interacts with the microtubule lattice, and this interaction does not slow dynein motility.
2. Lis1 binding has been proposed to block the force-generating conformational changes of the dynein linker domain. Using optical trapping, we ruled out this model by showing that Lis1 does not reduce the dynein stall force.
3. I observed that Lis1 binding decreases the asymmetry in detachment kinetics of force-induced detachment of dynein from the microtubule. Mutations that disrupt Lis1's

interactions with dynein's stalk (an anti-parallel coiled-coil that leads to dynein's microtubule-binding domain) partially restore the asymmetry. Because dynein's stalk "slides" or changes its coiled-coil registry in a nucleotide-dependent manner, my data suggest that Lis1's interaction with the dynein stalk interferes with the stalk sliding mechanism. I propose that this is what leads to slowing the detachment of dynein from the microtubule under force.

These results are compatible with studies of Lis1 in live cells and provide a mechanistic explanation for why Lis1 needs to dissociate from dynein for efficient minus-end-directed motility. They also suggest an additional regulatory role for Lis1, such as anchoring dynein to the microtubule in order to facilitate the proper assembly of dynein with dynactin. I believe that the studies presented in this thesis will be broadly interesting to biophysicists studying the mechanics of motor proteins in vitro, cell biologists interested in the mechanism and regulation of intracellular transport, and neurobiologists who study the molecular basis of neurodevelopmental disorders.

This dissertation is dedicated to my family. I will always need their support, guidance, love, and patience throughout my life.

Acknowledgments

I consider myself lucky to be surrounded by many great people who guided me and shaped my personality throughout my life and I owe my deepest gratitude to them. From them, I learned to push my limits, be positive, and have big plans. I followed an interesting academic path. I used to think that, I can master many science and engineering disciplines and do wonderful things combining them. As I learned more, however, I realized that life is simply too short to master even one, and not every question deserves an answer.

My Ph.D. life at UC Berkeley Biophysics was a challenging one. Being an international student and coming to biophysics with an engineering mindset, I was worried if I could thrive academically. I would like to thank my PI Ahmet Yildiz for his guidance and unlimited supply of baklava. He made himself available when I needed help and provided me with an environment where I can push my limits. In his lab, I have learned cutting-edge biophysics and microscopy techniques. I will not forget his support and guidance throughout my life, especially in my last year.

Next, I would like to thank all Yildiz laboratory members Merve Aslan, Vladislav Belyy, Sinan Can, John Canty, Alex Chien, Yavuz Dagdas, Mohamed Elshenawy, Yasin Ezber, Jon Fernandes, Luke Ferro, Yifei He, Andrew Hensley, Amanda Jack, Nicole Luk, Joseph Slivka, Ruensern Tan, Yuanchang Zhao. I would not have made it this far without their support. I also want to thank my thesis committee members Eva Nogales, Randy Schekman, and Andy Martin for helpful discussions, David Drubin for allowing us to use his microscopes, and my biophysics buddies for their friendship.

I am extremely grateful for my parents Ayse and Mustafa, my brother Ali Osman and my sisters Guldane and Merve. I always had your unconditional support, guidance, and love throughout my life wherever I am. Mom, thank you for always keeping me in your duas. I do not think I will be able to repay you ever.

Most importantly, I want to thank my loving wife Zehra and our little baby Saliha. Zehra, thank you for moving across the ocean with me, your energy and optimism made my bad days joyful and full of love and hope. Thank you for being patient when I come from the lab at midnight after another failed experiment. Saliha, my daughter, you climbed a steep hill in your first few months. Your smile is the loveliest gift I have ever received and I find an immense source of power every time I see it. We had the challenges of life until now, I wish it will be a smoother path for us from now on. Without you, I would not be near as happy as I am now.

Table of Contents

Chapter 1: Structure and Mechanics of Dynein

Introduction

Dynein is the primary molecular motor responsible for a myriad of cellular functions that require motility and force generation towards the minus end of MTs in eukaryotic cells[1,2]. These functions include but are not limited to retrograde cargo transportation, separating the sister chromatids during cellular division, and flagellar beating[3-5]. There is a single isoform of dynein (cytoplasmic dynein) that localizes in the cytoplasm and drives almost all of the minus-end-directed functions along the microtubules[6], whereas other dynein isoforms localize to cilia[7,8]. Defects in cytoplasmic dynein-mediated transport have been implicated in many neurodegenerative[9,10] and neurodevelopmental[11] diseases. In my thesis, I have studied the regulation of mammalian and yeast cytoplasmic dynein (dynein hereafter) by a dynein-associated factor, Lis1. This chapter will primarily summarize the structure and regulation of dynein which was also explained in more detail in our annual review[12].

Cytoplasmic Dynein

Dynein-1 is a huge protein complex with 1.4 MDa molecular weight and it is composed of 6 polypeptides. Dynein heavy chain is the largest chain with a molecular weight of 530 kDa and it is composed of an AAA+ ring and N-terminal tail domain[13,14]. Dynein motor domain self assembles into a AAA+ ring with nonidentical six subdomains named as AAA1 – AAA6. Each of these subdomains requires Walker A and Walker B motifs to be able to bind and hydrolyze ATP, respectively[14,15]. Not all subdomains bind or hydrolyze ATP. AAA1-AAA4 can bind ATP, however, AAA5 and AAA6 do not have a nucleotide-binding pocket. Therefore, AAA5 and AAA6 are catalytically not active. The main ATPase site is AAA1, mutations that disrupt ATP hydrolysis at this site fully abolish dynein motility[16,17]. Although AAA2 binds ATP, it cannot hydrolyze ATP because it lacks the catalytic glutamate in the Walker B motif[14,15,18]. AAA3 and AAA4 can bind and hydrolyze ATP although the hydrolysis rate is much slower than AAA1[16,19]. ATP binding to AAA2 and its hydrolysis at AAA3-4 is necessary for transducing the AAA ring's rigid body motion and regulating dynein motility. I will explain the mechanism in detail in the dynein mechanochemical cycle part.

Dynein has an MT binding domain (MTBD) at the end of a 15-nm coiled stalk, which protrudes between AAA4 and AAA5[20]. ATP hydrolysis in AAA1 causes sliding in this coiled-coil stalk leading to a change in MTBD's affinity for MTs[21,22]. A short coiled-coil named buttress extends from AAA5 to transduce the conformational changes in the ring to the stalk[14,15]. The dynein motor domain is structurally homologous across different species.

The N-terminus of the dynein AAA+ ring is connected to the dynein tail via an α-helical bundle referred to as the linker. The linker is the flexible element that undergoes nucleotide-
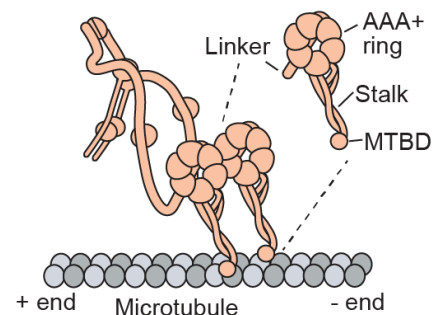
Figure 1.1: Cytoplasmic Dynein. Dynein heavy chain is composed of AAA+ ring, coiled coil stalk, MTBD, linker and tail domains. Two copies of LC, LIC, and IC bind along dynein tail.

dependent conformational changes leading to net movement and force generation by dynein[23,24]. Therefore, it is the element that dynein generates mechanical work. Dynein heavy chains dimerize through the N-terminal tail domain. The tail is the part to which the two copies of each dynein-associated light (LC), light-intermediate (LIC), and intermediate chains (IC) bind[25] (Fig. 1.1).

Assembly of Mammalian Dynein-Dynactin-Cargo Adaptor Complexes

One feature of motors that allows them to carry cargoes and do mechanical work is their ability to take multiple steps before detaching, referred to as processivity. Through many studies, it is known that dynein purified from *Saccharomyces cerevisiae* can walk processively without needing any other cofactors[26]. However, mammalian dynein adopts an autoinhibited conformation which is known as the φ-particle[27]. AAA rings of "φ-particle" have mirror symmetry, and the pairwise interactions between the tails, AAA rings, and the stalks of the two monomers do not allow them to simultaneously bind MTs and walk processively[28-30]. Abolishing these pairwise interactions through mutations allows dynein to adopt an "open conformation" where parallel symmetry is restored and the phi-particle is relieved.

Mammalian dynein in open-conformation still cannot walk processively because it needs to form a complex with two more critical components: dynactin and cargo-specific cargo adaptors (DDX complex hereafter). Dynein in open conformation has a higher affinity for dynactin and cargo adaptors than φ-particle. Dynactin is a ~1 MDa protein complex that contains a short Arp1 filament and it is essential for all dynein-mediated cargo transportation in the cytoplasm[31-33]. The cargo adaptors such as BicD2, BicDR, and Hook3 are generally long coiled coils that interconnect dynactin to dynein, and they bind to the cargoes by their N-terminal region[34-36]. Some of the cargo adaptors such as BicDR1 recruit predominantly two dynein dimers whereas some other cargo adaptors such as BicD2N predominantly recruit one dynein dimer[37,38]. This leads to some DDX complexes having two dynein dimers instead of one dynein dimer. DDX complexes with two dynein dimers have higher velocity and force generation[38,39](Fig. 1.2).

What relieves dynein from autoinhibition and is there a way to increase the dynein copy number in DDX complexes? Part of my thesis studies has shown that Lissencephaly-1 (Lis1 hereafter) is the critical component that favors the open over the phi conformation and facilitates the formation of DDX complexes. Moreover, a larger ratio of DDX complexes will have two dynein dimers in the complexes since there are more dyneins available in the open state. This will result in higher velocity and force generation DDX complexes. This will be explained in detail in Chapter 3.
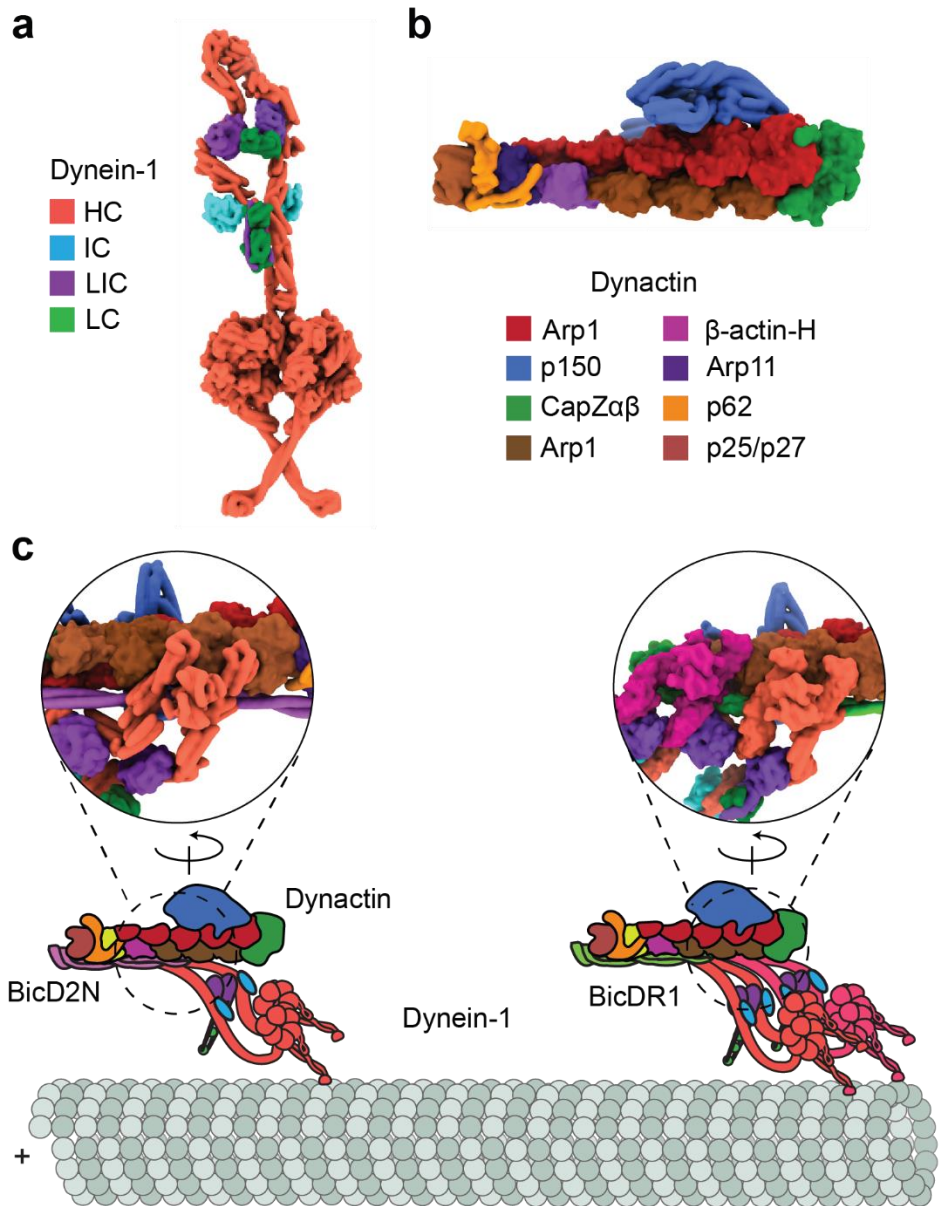
Figure 1.2: The assembly and activation of the dynein-1 transport machinery. (a) The φ-particle conformation of the dynein-1 complex (PDB accession code 5NVU) [25]. Dynein-1 is inhibited by the self-dimerization of the motor domains at multiple contact sites. **(b)** The structure of the dynactin complex (PDB accession code 5ADX)[25]. **(c)** Dynein-1 forms a ternary complex with dynactin and a coiled-coil cargo adaptor. The dynein-1 tail binds to the Arp1 filament of dynactin. Due to the translational symmetry of the Arp1 filament, the dynein-1 HCs form a parallel orientation and walk processively along MTs. Dynactin recruits a second dynein-1 motor, which results in a faster and stronger motor complex. Insets represent a 180°-rotated view of ternary interactions among the dynein-1 tail, dynactin, and the N-terminal fragment of the BicD2 adaptor (PDB accession code 5AFU)[31]. Abbreviations: HC, heavy chain; IC, intermediate chain; LC, light chain; LIC, light-intermediate chain; MT, microtubule; PDB, Protein Data Bank (The Figure is from Reference[12]).

Mechanochemical Cycle of Dynein

Dynein undergoes a series of conformational changes which allows it to successively bind and unbind from the tubulin allowing it to move towards the minus end of MT while carrying its many cargoes. To do this mechanical work, dynein harvests the energy stored in ATP by hydrolyzing it in the AAA ring during the mechanochemical cycle. The mechanochemical cycle of a dynein monomer is mainly dictated by the nucleotide state of AAA1 (apo, ATP, ADP-Pi, ADP)[13-15,40,41]. During this cycle the linker alters between "straight" and "bent" conformation and the coiled-coil stalk changes its registry between strongly bound "α" and weakly bound "β" states (Fig. 1.3).

When there is no nucleotide in AAA1 (ie. AAA1 is in the apo state), the linker has a "straight" conformation and it is docked on AAA5[14,15]. In this state, the coiled-coil stalk is in the α registry during which dynein is tightly bound to MT. Upon ATP binding or ATP hydrolysis (ADP+Pi) state, the AAA ring undergoes a rigid body movement[40,42]. The rotation in AAA5 and AAA6 pulls the returning coil of the stalk, causing it to slide with respect to the other coil. This leads the coiled-coil stalk registry to shift to the β state which relieves dynein from MT binding[22,43]. The linker undocks from AAA5 and moves to the bent (pre-power stroke) conformation[42]. This process creates a net bias in dynein's movement towards the minus end of MTs[42,44].

After a brief diffusional search, MTBD rebinds the MT in the post hydrolysis (ADP.Pi) state. This triggers the series of conformational changes in reverse order this time. The stalk slides back to the strongly bound α registry and this rotates AAA5 and AAA6 back to their original position[14,45]. The inorganic phosphate is released from AAA1, leaving AAA1 in ADP state[46]. The linker restores its straight conformation, pulling its cargoes towards the minus end in the meantime[47]. This process is known as the Powerstroke mechanism. The docking of the linker on AAA5 will be followed by ADP release from AAA1. Now, dynein is back to its initial apo state and ready for the next cycle.

During this cycle, AAA4 and AAA2 remain in the ATP state[48] and AAA3 remains in the ADP state. It is thought that the presence of nucleotides in these sites completes the mechanical circuitry so that the conformational changes in the AAA ring can be relayed down to the rest of the motor. The ATP hydrolyzing mutation in AAA4 has very little effect on dynein motility whereas the ATP binding mutation fully inhibits the motor[48]. The nucleotide-binding or hydrolyzing mutations in AAA3 severely inhibit dynein motility although dynein is still able to walk approximately 20 times slower[16,19]. Dynein can hydrolyze ATP in AAA1, bind and unbind from MTs and take successive steps when there is ADP in AAA3. The function of ADP release from this site remains unanswered. Lis1 is known to interact with dynein rings and stalk. Lis1's interaction site on the ring is close to the catalytic site of AAA3[49]. Whether Lis1 blocks the nucleotide exchange to allow AAA1 to have a more hydrolysis cycle (therefore take more steps) until ADP is released from AAA3 is also not known.
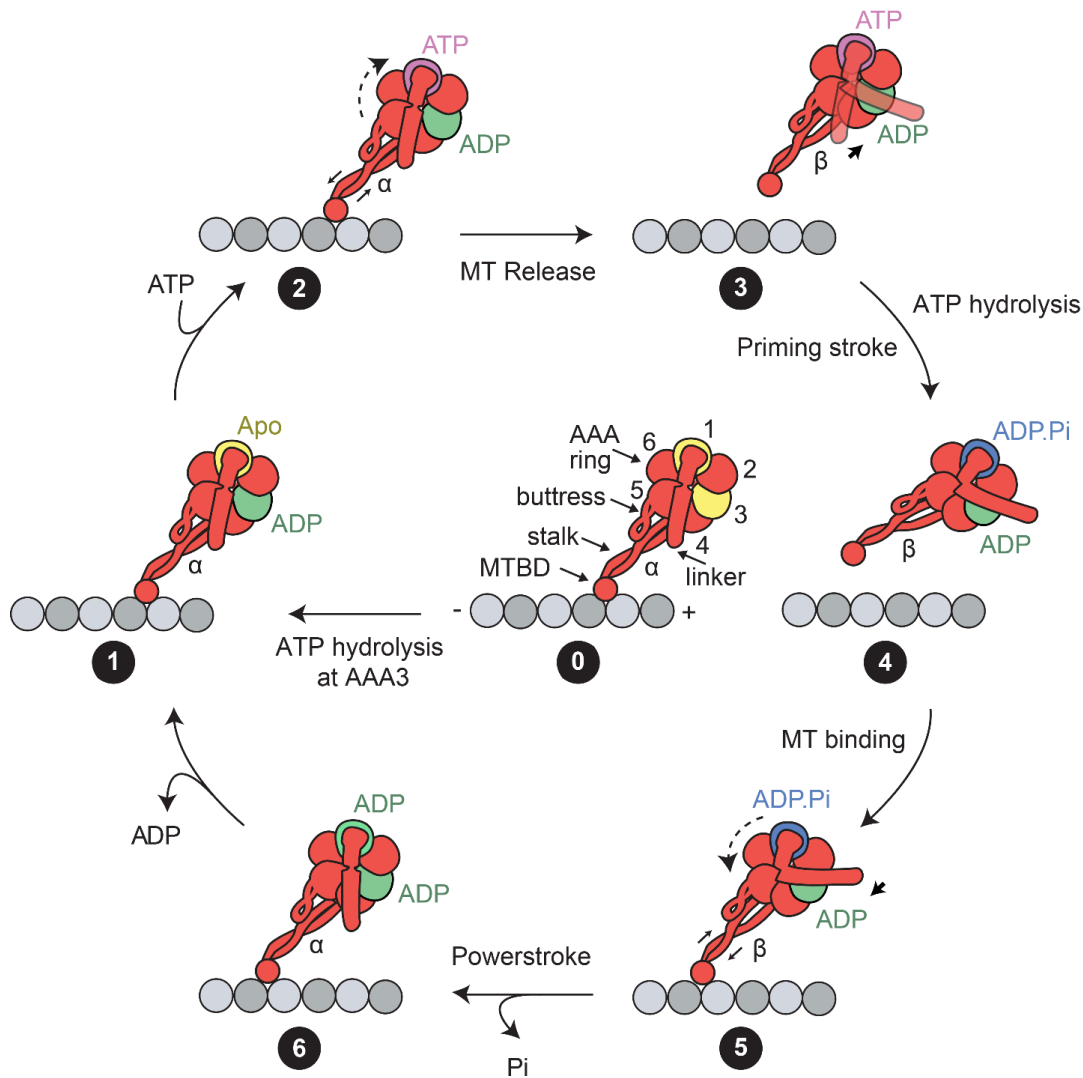
Figure 1.3: The mechanochemical cycle of the dynein-1 motor domain. (*State 0*) Schematic representation of the dynein-1 motor domain. The AAA ring (subunits are numbered 1–6) is attached to the MTBD through a coiled-coil stalk. The linker resides at the surface of the ring and connects to the tail (not shown). The prerequisite of the mechanochemical cycle is ATP binding and hydrolysis at the AAA3 site. AAA3 remains in a posthydrolysis (i.e., ADP-bound) state to enable the nucleotide state of AAA1 to control the linker conformation and stalk registry. (*State 1*) In the apo state of AAA1, dynein-1 is bound to the MT, the coiled-coil stalk is in the α registry, and the linker is in the straight conformation. (*State 2*) Upon ATP binding at AAA1, AAA5–6 undergo rigid body motion (*dashed arrow*), which triggers the buttress to slide stalk coiled-coils relative to each other (*solid arrow*). (*State 3*) The stalk shifts to the β registry, and the motor releases from the MT. The linker is allowed to move freely across the surface of the ring. (*State 4*) Upon ATP hydrolysis, the linker converts to the bent conformation, and this priming stroke moves the MTBD toward the minus end. (*State 5*) The MTBD undergoes a diffusional search and rebinds to the MT lattice. MT binding triggers shifting of the stalk coiled-coils (*solid arrow*) and rigid body motion in the AAA ring (*dashed arrows*). (*State 6*) The stalk adopts the α registry. The inorganic phosphate is released from AAA1. The linker moves the straight conformation through the force-generating powerstroke. Following ADP release, the motor returns to the initial apo state (*State 1*). Abbreviations: MT, microtubule; MTBD, MT-binding domain The Figure is from Reference[12].

Dynein's Stepping and Minus End Directionality

One ATP hydrolysis in a dynein monomer results in its detaching and reattaching to the MT on a different (or same) tubulin binding site. There is no tight coordination between ATP hydrolysis

cycles of dynein monomers in the dimer. This results in dynein monomers taking uncoordinated steps with varying step sizes[50,51]. Dynein can also switch protofilaments by taking side steps[26]. This gives dynein the ability to navigate through the physical obstacles on its track[52,53]. Since dynein monomers are dimerized, there is intramolecular tension between the monomers through the dimerization domain as dynein walks[54,55]. Because of this tension, two monomers cannot separate much and this provides partial coordination between the monomers resulting in the overall movement towards the minus-end without overextending the dimer[50,55].

Dynein stepping behavior is markedly different from plus-end directed kinesin motors. Kinesin-1 (kinesin from here on) walks on a single protofilament, it does not take side steps and therefore cannot change protofilaments. Kinesin takes tightly coordinated steps with an 8.2 nm step size. This is identical to the distance between adjacent tubulin-binding sites[56,57]. Kinesin steps always initiate from the monomer in the rear position, which results in kinesin stepping in a "hand-over-hand" fashion. Dynein's stepping characteristics are more complex than kinesin, which makes understanding dynein's regulation more challenging.

The minus-end directionality of dynein stepping is determined by two factors: the linker swing vector and the stalk angle. During the priming stroke of the linker, the AAA+ ring needs to move towards the minus-end to preserve the location of the dynein's center of mass. The evidence for this model is shown by reversing the linker swing towards the plus-end of the microtubules. This was achieved by flipping the AAA ring around the vertical axis by elongating the length of the stalk by half a turn and reversing the stalk angle relative to the micorubule[58,59] (Figure 1.4). The engineered dynein mutant processively walked towards the plus-end, strongly supporting the linker swing model for dynein directionality. Since residues determining stalk's length and angle are preserved across species[60], all dyneins are expected to have minus-end directionality.
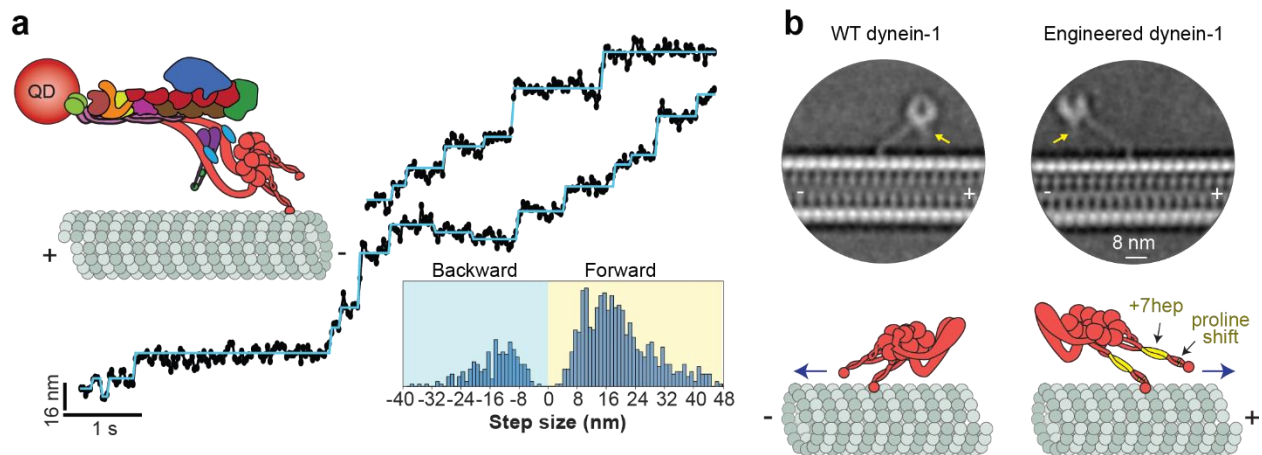
Figure 1.4: Stepping, directionality, and force generation of dynein-1. (a) (*Top right*) The stepping of a QD-labeled DDX motor was tracked on surface-immobilized MTs. (*Middle*) Representative stepping traces (*black dots*) are fit to a step-finding algorithm (*horizontal lines*). (*Bottom*) The histogram reveals that dynein-1 takes steps that are highly variable in size and direction. Panel adapted from Reference[39]. **(b)** (*Top*) Cryo-EM 2D class averages of WT and engineered yeast dynein-1 monomers. Arrows point to the N terminus of the linker. (*Bottom*) In engineered dynein-1, the angle that the stalk makes relative to the MT is reflected by shifting the positions of proline residues in both coiled-coils, and the AAA ring is flipped around the stalk axis by a seven-heptad insertion to the stalk coiled-coils (*highlighted in yellow*). These modifications reversed the direction of the linker swing and resulted in the plus end–directed motility (*blue arrow*). Panel adapted from Reference [58].

Chapter 2: Single-Molecule Techniques

TIRF Microscopy

Total internal reflection fluorescence (TIRF) Microscopy is indispensable when conducting single-molecule biophysical studies on molecular motors. Using organic dyes is more advantageous because they have higher quantum efficiency and they are more photostable thanks to their larger photon budget. Using singlet oxygen scavenging systems such as PCA-PCD and gloxy-dextrose prevents photobleaching and extends the lifetime of the fluorescent dyes during imaging.

At the critical incident angle, the excitation light refracts and gets total-internally reflected from the glass water interface. Total internal reflection generates an evanescent field, which decays exponentially into the water. This wave excites fluorescent molecules only if they are very close (0 -200 nm) to the surface and therefore creates minimal background by restricting the excitation volume to a thin disk of water. The excited molecules on the surface will emit a redshifted photon which can be detected and recorded by a CCD camera. In fluorescent microscopy, the resolution is limited by the diffraction of the emission wavelength, which corresponds to 250 nm in visible light ($\frac{\lambda}{2NA} = \sim 250\ nm$). This is substantially larger than the size of the cytoskeletal motors. However, if there is only one light emitting object in a diffraction limited volume, we can localize its position by determining the center of the fluorescent emission, referred to as the point-spread function (PSF). The precision of localization can be increased by collecting more photons ($\sigma_\mu = \frac{1}{\sqrt{N}}$), N being the collected photon count. This technique is particularly critical when studying motor stepping characteristics which requires nanometer precision.

In my research, I have extensively used TIRF microscopy when studying Lis1's effect on dynein motility. I have labeled my proteins mostly with organic dyes or also used fluorescent proteins (such as GFP) for imaging. I have polymerized MTs using tubulins purified from pig brains and stabilized them with taxol. MTs labeled with biotin were stabilized on streptavidin functionalized surfaces. To prevent non-specific binding, I have coated the glass surface with PEG, pluronic acid, and casein. For simultaneously imaging multiple components (up to 3 colors) I have used a time-shared approach. The z- stacks of the image frames of individual MTs will give the position (x-axis) vs time (y-axis) of the individual molecules. With ImageJ/FIJI I have quantified motile characteristics of the motors, such as velocity, run lengths, and run times.

Studying Dynein's Force Generation Using Optical Trapping

Dynein generates piconewton (pN) level forces to carry large cargoes in a viscoelastic medium or to stably anchor the spindle poles to the cell periphery. It is also exposed to forces by other motors carrying the same cargo and by active polymerization of MTs. Some of the dynein-driven processes require forces higher than what a single dynein dimer can generate. However, how the forces generated by a concerted action of multiple dyneins scale with copy number of dynein needs to be studied. Therefore, it is important to understand the force-related characteristics of dynein motors.

Optical trapping is the most commonly used technique to study dynein's force-related characteristics because it allows tracking single molecules with sub-nanometer and sub-millisecond spatiotemporal resolution. Commonly a 1064 nm focused IR laser beam is used to trap dynein attached to a micrometer-sized polystyrene bead. Because the light carries momentum, its refraction while passing through the bead generates a net force, with this force you can manipulate the bead and the motor attached to it. It is also possible to combine trapping with fluorescence microscopy and do simultaneous fluorescence characterization.

Measuring Stall Forces

To measure dynein's stall force I usually use fixed-beam optical trapping (Fig. 2.1a). Fluorescently labeled MTs are immobilized on the surface of the glass slide. Fluorescent labeling is necessary to find the location of the MTs. Since their thickness is smaller than the diffraction limit, one cannot see them without fluorescently labeling them. To guarantee the data is coming from single motors, I decreased the dynein/bead ratio by diluting dyneins. Typically, one should see an activity (i.e. MT binding, walking, etc) from less than 30% of the beads to ensure that at least 95% of the beads are driven by single dyneins[61]. The trapped bead is brought to the top of a long MT. Since the bead is spherical and it floats in liquid there is nothing to prevent its rotation. If one of the motors on the bead binds to the MT, it will start to walk away towards the minus end, pulling the bead along with it. At short distances (<~100-150 nm) from the center of the trapping beam, the beam acts like a Hookean spring, applying a restoring force on dynein towards the center. Dynein reaches a certain distance from the beam center such that it cannot go further, because the restoring force is equal to the force that the motor can generate. This force is called the stall force (Fig. 2.1b). A single dynein dimer can generate a 3-4 pN stall force on average. This is lower than kinesin's ~6 pN forces. However, dynein's stalls persists much longer than kinesin's stalls.
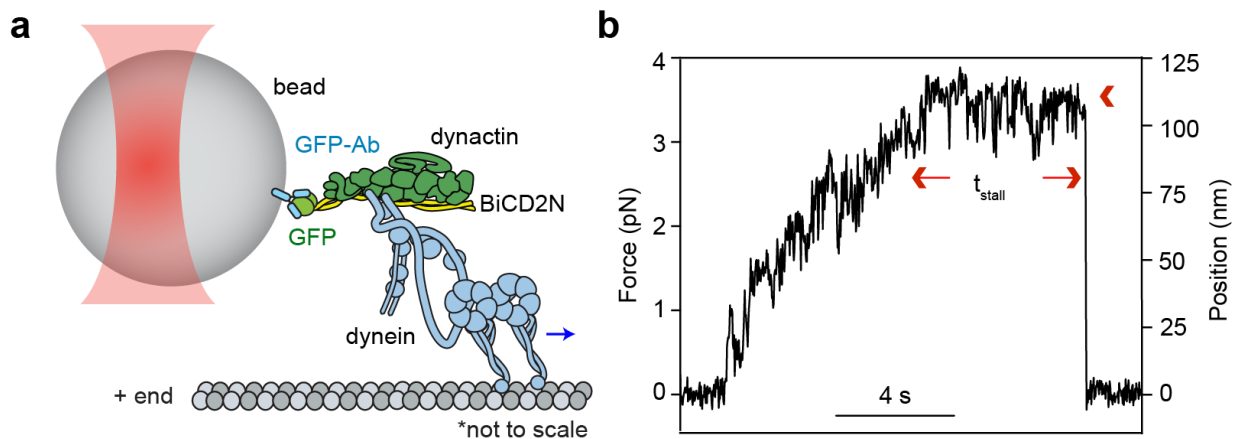
Figure 2.1: Measuring dynein stall forces with a fixed trapping assay. a) Graphical representation of optical trapping of the mammalian dynein-dynactin-BicD2N (DDB) complex attached to an 800 nm diameter polystyrene beads coated with anti-GFP antibodies. The arrow shows dynein's natural direction of motility towards the minus end of the microtubule. **b)** Sample recording of a stall event. The arrows show the beginning and the end of a stalling event (t_{stall}: stall duration). The arrowhead indicates the detachment of the motor from the microtubule, which is immediately followed by the rapid return of the bead to the trap center (Figure is modified from[62]).

Measuring Force-Velocity Relationship

To understand how dynein's motile characteristics change under load, force feedback experiments are used. The main difference in force feedback experiments is that the trapping beam leads or trails the bead at a certain position. At constant laser power, this means that we are applying a constant force while dynein moves along the MT. Depending on whether the trapping beam is leading or trailing the bead, this force will aid or hinder dynein motility (Fig. 2.2a,b). In addition to several previous studies, part of my thesis work is to develop an understanding of the motile characteristics of dynein under a range of aiding and hindering loads. For this, I created a Force-Velocity (FV) curve. Dynein behaves strikingly asymmetric to the applied load (Fig. 2.2c)[63]. Its velocity increases exponentially under aiding forces and will slowly decrease under hindering forces. Under a hindering force equal to dynein's stall force, the velocity should be 0 nm s^{-1}, theoretically. Interestingly, under hindering force exceeding the stall force, the trapping force will win against the motor pulling it backward and the motor will walk backward. After a certain hindering force, the dynein will release from the MTs much faster, leading to an exponential increase in the velocity toward the plus end.
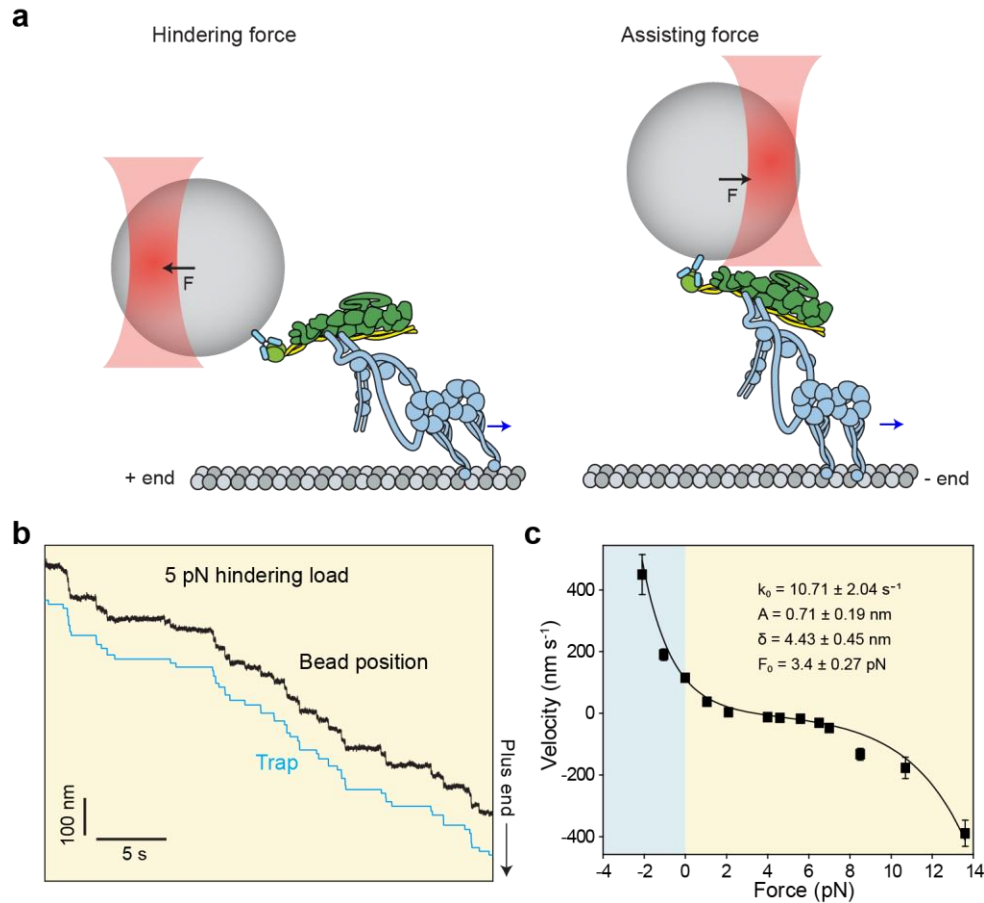
Figure 2.2: Measuring the force-velocity behavior of dynein using a force-feedback controlled trap. a) Dynein walks under constant hindering (left) or assisting (right) forces in force-feedback controlled trapping assays. **b)** Processive motility of yeast cytoplasmic dynein in the backward direction (towards the plus-end of the microtubule) under 5 pN constant hindering load. The assay was performed in 1 mM ATP. The black trace shows the position of the bead with respect to time and the blue trace shows the trapping beam tracking the bead at a constant distance. **c)** The force-velocity (F-V) relationship of yeast cytoplasmic dynein (mean ± s.e.m) under a set of various assisting (blue) and hindering (yellow) forces and in the presence of 1mM ATP. The solid

curve represents a fit to $V(F) = 2d(F)k_0^{ATP} e^{-\frac{(F-F_{stall})A}{k_BT}} sinh\left(\frac{-(F-F_{stall})\delta}{2k_BT}\right)$ where $V(F)$ is the velocity under load F, $d(F)$ is the average step size of dynein at a given force, k_0^{ATP} is the microtubule release rate of dynein in the absence of load, k_B is the Boltzmann constant and T is the absolute temperature (Figure is modified from [63]).

Measuring Detachment Rate

We also study the kinetics and the asymmetric behavior of dynein detachment rate under load using an optical trap by applying force oscillations to a dynein monomer[55]. When dynein is pulled forward, the coiled-coil stalk will shift to the γ registry, during which dynein is weakly bound (Fig. 2.3a-c)[64]. Similarly, when pulled backward the stalk will be in a strongly-bound α registry. Locking the registry of the coiled-coil stalk by cysteine crosslinking will abolish this asymmetry. This indicates force induced stalk registry shift is the responsible mechanism creating the asymmetry[63] (Fig. 2.3d).
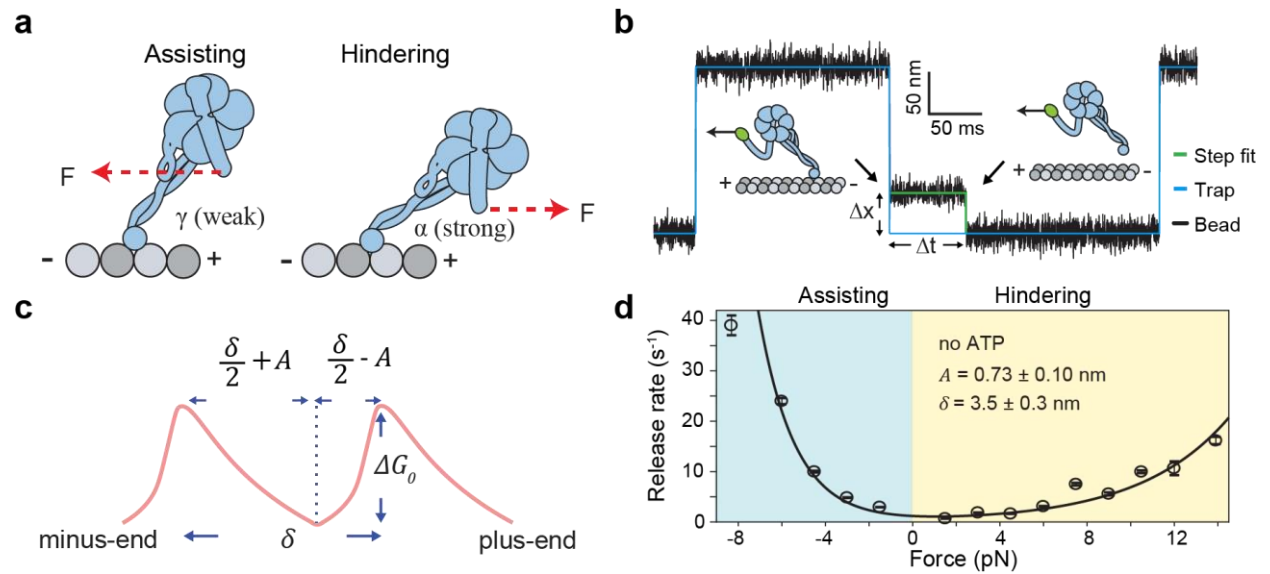
Figure 2.3: Measuring the force-induced microtubule detachment kinetics of dynein using an oscillatory trapping assay. a) Assisting forces shift the registry of the stalk coiled-coils such that the microtubule binding domain (MTBD) adopts a low microtubule binding affinity state (known as the g registry), whereas hindering forces shift this registry to induce a high microtubule binding affinity state (a registry), leading to asymmetric detachment rates of dynein from the microtubule. **b)** Sample trace showing a dynein monomer detaching from a microtubule under square-wave force oscillations. **c)** The model for the asymmetric potential landscape of dynein bound to a microtubule. The stepping in plus or minus direction needs to bypass the energy barrier (ΔG_0). A is the asymmetric distance that biases the energy barrier for release from the microtubule and δ is the width of the energy barrier. **d)** The microtubule release rate $k(F)$ of yeast cytoplasmic dynein under a set of applied forces are fitted to $k(F) = 2k_o^{apo} e^{-\frac{FA}{k_BT}} cosh\left(\frac{F\delta}{2k_BT}\right)$, where k_o^{apo} is the release rate in the absence of force. The experiment was performed in the absence of ATP (Figure is modified from [63]).

Some of the challenges in optical trapping for the characterization of molecular motors

Limitations of force-feedback and force-oscillation experiments

Optical trapping allows us to manipulate motors by applying forces, however, there is a limit on the range of forces on which we can make a healthy characterization of the motors. Under aiding forces larger than 3 pN and hindering forces larger than 15 pN dynein quickly detaches from the

MT. To get reliable data, one needs to update the trap needs to update the position of the beam with respect to the bead. The trap simply is not fast enough to catch up with dynein velocity (or detachment rate if we use dynein monomer for measurement) under forces beyond this range. The bead "slips" under larger forces. It is still possible to catch some of the slower dyneins, but one will miss the fast ones. This will create an underestimation problem in the velocity measurements.

Trapping under very low laser power is another problem. Usually, measurements under forces smaller than 0.5 pN will be dominated by the Brownian motion of the bead. This means the noise in your data will be so high, preventing a reliable analysis. In stall force experiments and force feedback experiments, this usually creates an overestimation problem. This can be avoided by simply using TIRF measurements as dynein velocity under 0 pN when building an FV curve. However, if we want to characterize a slow motor mutant or test our motors under conditions that make them move very slowly (< 3 nm s^{-1}) using an optical trap this will add another complexity to our data collection. In TIRF, we can catch very slow motors. In force feedback experiments, however, because the motor needs to move beyond the threshold distance so that forces may be applied, one will miss the slower events since no motility is observed. One trick to solve this problem is to apply the load right after the bead reaches stability (ie. since the bead is lowered on MTs to make the measurements, the initial touch of the bead to MT will create an initial jump in the position readout, this is why the bead needs to reach stability before recording the bead postion.) and record for longer times allowing the slower motors to reach the threshold distance.

Considering the Z-force in molecular motors characterization

The beads used in optical trapping are much larger (~800 nm, typically polystyrene beads) compared to the length of the molecular motor (20 nm - 50 nm) (Fig. 2.4a). Using simple geometry, this means, the vertical (azimuthal) component of the force (z-force) applied by the trap is much larger than the horizontal component, although the horizontal component is what we are measuring in an optical trap. Reducing the bead size will reduce the z-force, however, this will also limit our spatial resolution as the bead will fluctuate more.

The z-force can cause the motors' early detachment from the microtubules. For instance, this might be the reason why kinesin cannot create stalls but instead force spikes. Dynein can be more resistant to z-force as it can remain bound to MTs for longer times. However, one may see even longer stalls for dynein in the absence of z-force.

Several methods are being tested to overcome this problem. In the first method, a dumble trap is used to lower an MT on the motors attached to a surface-immobilized bead[65]. However, if the motor is not in the right orientation with respect to the MT, this may create torsion in the motor. Since the bead is fixed on the surface there is no way for the motor to rotate the bead in order to align itself with the MT. Another method for addressing the z-force problem is to use a long DNA handle to connect motors to beads instead of directly binding it (Fig. 2.4b). This will reduce the z-force. However, we are limited by the processivity of the motors since the motor need to travel a long distance before we actually record the data. Another challenge in this approach will be doing force-feedback or force oscillation experiments. In these experiments, we need to set how far the trapping beam should reposition itself from the bead. Since we are using

11

long DNA handles, determining this position will be challenging. A final approach is to use much smaller beads with a higher refraction index. A group used Germanium to create 70 nm beads which are comparable to motors size (Fig. 2.4c)[66]. However, we may not be able to see such small beads in bright fields, meaning that we need to either fluorescently label them to trap or will be fishing in the dark. Fishing in the dark can be risky, because we may accidentally trap multiple beads. Each of these methods have advantages and limitation. Although I have not used these techniques in my optical trapping experiments, I have explained them here for future reference. These techniques may enable one to measuring longer events (stalls, runs) without detaching the motor. In this case, kinesin may have stalls that lasts as long as dynein's stalls or dynein can show even greater asymmetry to aiding and hindering forces.
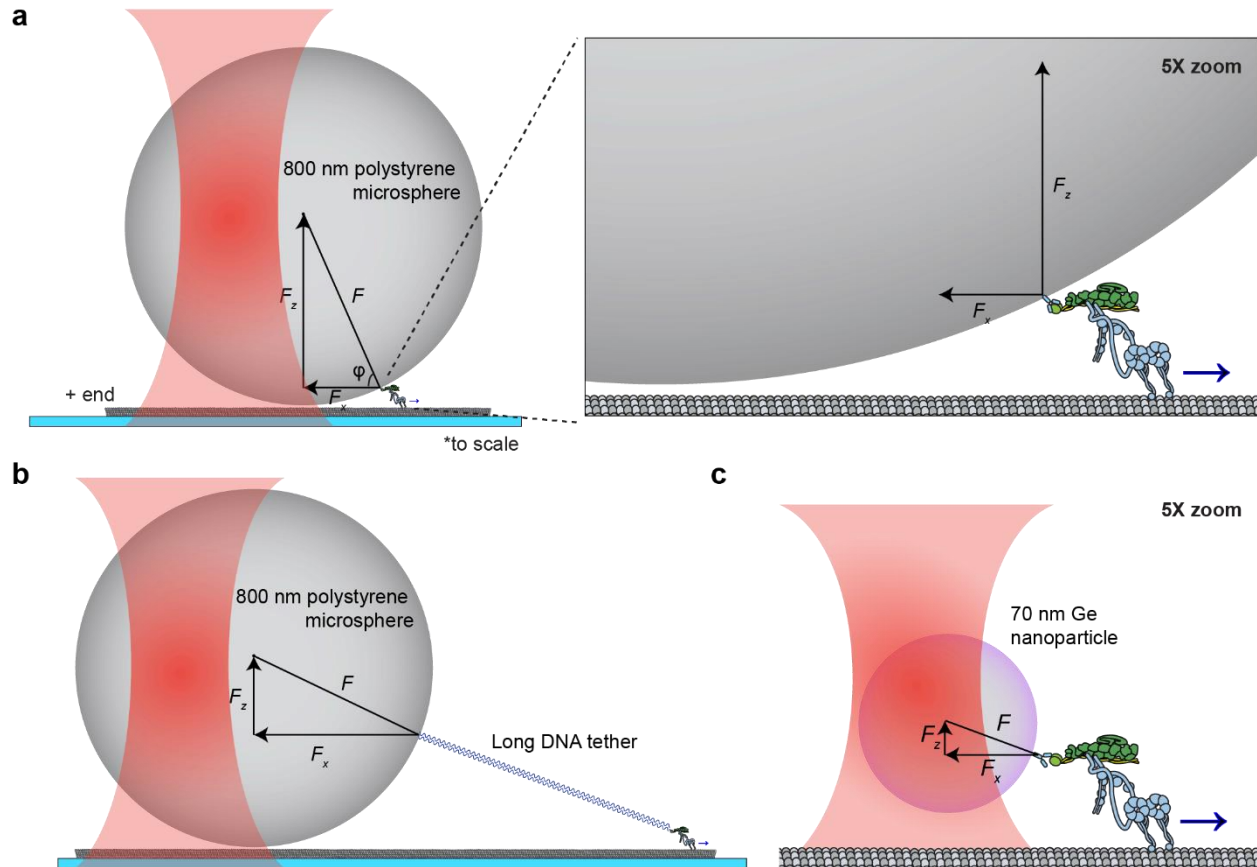
Figure 2.4: Minimizing the azimuthal force in single bead assays. a) Graphical representation of a single bead optical trapping assay using an 800 nm diameter polystyrene bead (drawn to scale). Due to the mechanical equilibrium, the total force F acts through the center of the bead and is transmitted to the tether formed by the motor on the microtubule. Magnitudes of the azimuthal (F_z) and horizontal (F_x) components depend on the angle φ, defined as $sin\varphi \approx \frac{R}{R+L}$ where R is the radius of the bead and L is the length of the tether formed between the microtubule and the bead by the motor. **b)** The magnitude of the azimuthal force can be reduced by increasing the length of the tether via a long double-stranded DNA. **c)** The magnitude of the azimuthal force can be reduced by reducing the size of the trapped bead, such as 70 nm diameter Germanium nanoparticles used for optical trapping of kinesin.

Chapter 3: Lis1 activates dynein motility by modulating its pairing with dynactin

The work presented in this chapter was published in the following paper: "Lis1 activates dynein motility by modulating its pairing with dynactin" written by Mohamed M. Elshenawy, Emre Kusakci, Sara Volz, Janina Baumbach, Simon L. Bullock, Ahmet Yildiz. Nature Cell Biology (2020)

Abstract

Lissencephaly-1 (Lis1) is a key cofactor for dynein-mediated intracellular transport towards the minus-ends of microtubules (MTs). It remains unclear whether Lis1 serves as an inhibitor or an activator of mammalian dynein motility. Here we use single-molecule imaging and optical trapping to show that Lis1 does not directly alter the stepping and force production of individual dynein motors assembled with dynactin and a cargo adaptor. Instead, Lis1 promotes the formation of an active complex with dynactin. Lis1 also favors the recruitment of two dyneins to dynactin, resulting in increased velocity, higher force production and more effective competition against kinesin in a tug-of-war. Lis1 dissociates from motile complexes, indicating that its primary role is to orchestrate the assembly of the transport machinery. We propose that Lis1 binding releases dynein from its auto-inhibited state, which provides a mechanistic explanation for why Lis1 is required for efficient transport of many dynein-associated cargoes in cells.

Introduction

Cytoplasmic dynein (dynein hereafter) is an AAA+ motor responsible for nearly all motility and force generation towards the MT minus-end[67-70]. Dynein is involved in a wide variety of cellular functions, such as positioning of intracellular organelles, breakdown of the nuclear envelope and assembly of the mitotic spindle[68,69,71]. The partial loss of dynein function has been implicated in a range of neurogenerative and neurodevelopmental conditions, including spinal muscular atrophy, amyotrophic lateral sclerosis, Alzheimer's disease, and schizophrenia[70,72,73].

The core of the dynein complex (1.4 MDa) is a homodimer of two heavy chains[74]. The C-terminal motor domain of the heavy chain is a catalytic ring of six AAA modules (AAA1-6). Unlike kinesin, dynein's MT binding domain is separated from the catalytic domain by a coiled-coil stalk[20]. Nucleotide-dependent conformational changes of the linker drive the motility towards the MT minus-end[75,76]. The N-terminal tail dimerizes the heavy chains[13-15] and binds smaller polypeptides[4,77,78]. When dynein is not bound to its cargo, it forms two distinct conformations, the phi-particle, and open conformation, both of which move poorly along MTs[30,79]. In the phi conformation, two motor domains self-dimerize through interactions between their linker, AAA+ ring and stalk regions and dynein weakly interacts with MTs. In the open conformation, the motor domains are more flexible and point towards each other, which is unfavorable for processive motility[25,30]. Transitions between the phi and open conformation are proposed to be an important part of dynein regulation[25,30], but the molecular cues that govern this transition remain unclear.

Recent studies suggested that dynein and its cofactor dynactin are recruited to cargos through coiled-coil adaptor proteins in a mutually dependent manner (Fig. 3.1a)[36,80,81]. Formation of a

dynein-dynactin-cargo adaptor complex aligns the dynein motor domains in a parallel conformation and activates processive motility along MTs[31,82]. These adaptors recruit dynein to a specific set of cargos[32,81], enabling a single dynein gene to be responsible for nearly all minus-end directed functions along MTs. Members of the BicD family, BicD2 and BicDR1, are well-characterized coiled-coil adaptors that link dynein to Golgi-derived Rab6 vesicles, as well as nuclear pore complexes and viruses[31,35,83]. *In vitro* reconstitution studies showed that BicDR1 recruits two dyneins to dynactin, while the N-terminal coiled-coil domain of BicD2 (BiCD2N) mostly recruits a single dynein[37,38]. Recruitment of two dyneins per dynactin results in complexes assembled with BicDR1 (DDR) moving faster and producing more force than complexes formed with BicD2N (DDB)[38,84]. The differences elicited by BicD2 and BicDR1 in dynein motility may play a critical role in the sorting of Rab6 vesicles during neuronal differentiation[35,80].

Dynein motility is also regulated by Lis1, which directly interacts with the dynein motor domain[85]. Lis1 inhibition reduces the transport of a wide variety of cargoes in eukaryotic cells, including endosomes, lysosomes, mRNAs, centrosomes and nuclei[86-93]. The critical role of Lis1 is underscored by the discovery that haploinsufficiency of the Lis1 gene causes a smooth brain disorder (lissencephaly) in humans, which is associated with a failure of nuclear migration[94]. Lis1 forms a homodimer, with each monomer comprising of an N-terminal dimerization domain and a C-terminal β-propeller domain that binds dynein at the interface between AAA3/4 and the coiled-coil stalk (Fig. 3.1a)[49,85].

The mechanism by which Lis1 regulates dynein motility is controversial. *In vitro* studies on yeast dynein revealed that a Lis1 homolog, Pac1 increases MT affinity, blocks nucleotide-dependent remodeling of the linker domain, and significantly reduces dynein velocity[45,85]. However, the view of Lis1 as a dynein inhibitor is difficult to reconcile with the ability of Lis1 to promote dynein-mediated cargo transport *in vivo*[86-93]. Studies on isolated mammalian dynein proposed that Lis1 transiently interacts with dynein, enhances dynein's affinity to MTs on high-load cargos by inducing a persistent-force generation state[89,95]. However, Lis1's function is not restricted to high-load cargos, and it is also required for the transport of smaller cargos[88,90,91,93]. These studies were performed before it was understood that isolated dynein motors are autoinhibited in the absence of dynactin and a cargo adaptor, and may not reflect the force generation mechanism of active dynein-dynactin complexes[32,62,81]. *In vivo* studies gave rise to models that Lis1 is only required for targeting dynein to the MTs, with dissociation of Lis1 triggering the initiation of transport[86,90,96-98] and that Lis1 promotes the interaction of dynein and dynactin[91,92]. Consistent with these models, recent *in vitro* studies showed that mammalian Lis1 can increase the frequency and velocity of DDB motility[98-100], but the underlying mechanism remained unknown.

In this study, we determined the effect of Lis1 binding on the motility, stepping, and force generation of DDB and DDR using single-molecule imaging and optical trapping *in vitro*. We found that Lis1 has no significant effect on the stepping and force generation of single dyneins after they have associated with dynactin and the cargo adaptor. Instead, Lis1 promotes the assembly of dynein with dynactin. Lis1 also favors the association of two dyneins to dynactin, and this accounts for the increase in both velocity and force generation of the complex. The presence of Lis1 shifts the force balance towards dynein's direction during a tug-of-war with a

plus-end directed kinesin. Our work reveals how Lis1 activates the motility of mammalian dynein-dynactin and is thereby required for efficient transport of cargos in cells.

Results

Lis1 increases the stepping rate of dynein-dynactin

We first tested the effect of human Lis1 on the velocity of DDB and DDR complexes assembled with wild-type human dynein (wtDyn). In agreement with previous measurements[99,100], wtDDB moved 30% faster in 600 nM Lis1 (two-tailed t-test, $p = 10^{-4}$). We also observed a modest (10%) increase in wtDDR velocity by Lis1 addition (Fig. 3.2). Similar results were obtained using a dynein mutant (mtDyn) that disfavors the autoinhibited phi conformation[25] (Fig. 3.1a-c). By titrating the Lis1 concentration, we found that 20 nM Lis1 is sufficient for the increased velocity of mtDDB (Fig. 3.1d). Because mtDyn favors the assembly of active dynein-dynactin complexes[25], we used this construct to study the effect of Lis1 on dynein motility and force generation.

We altered the order of dynein-dynactin assembly and Lis1 addition to determining whether Lis1 is needed before or after the assembly of mtDDB for its faster movement. First, mtDDB was assembled in the presence of 75 nM Lis1. Removal of excess Lis1 from the flow chamber as the complexes moved along MTs did not lead to the slowdown of motility. Second, we assembled mtDDB without Lis1 and removed excess dynein, dynactin, and BicD2N from the flow chamber before adding Lis1. We observed that the addition of Lis1 after the complexes were being formed had no positive effect on mtDDB speed (Fig. 3.1e). These results show that Lis1 must be present during the assembly of dynein-dynactin to increase velocity, and it is dispensable after the complexes walk along the MT.

To distinguish whether Lis1 addition increases dynein step size or stepping rate for faster movement, we determined the stepping behavior of dynein-dynactin with and without 600 nM Lis1 at limiting (2 µM) ATP concentrations. We labeled dynein with a bright quantum dot (QD) at its N-terminus and tracked the motility of single mtDDB complexes at nanometer precision. In the absence of Lis1, mtDDB has a highly variable step size, frequently taking backward steps (Fig. 3.1f)[84]. Lis1 addition did not alter the size and direction of steps taken by dynein. Instead, mtDDB stepped more frequently in the presence of Lis1 (2.9 ± 0.05 vs. 1.9 ± 0.02 s^{-1}, ±SE; two-tailed t-test, $p = 10^{-13}$; Fig. 3.1f and Fig. 3.3). We concluded that Lis1 increases the dynein stepping rate, not the mean step size, which accounts for the faster movement.

Lis1 increases the force production of dynein-dynactin

We tested whether Lis1 addition affects the force generation of dynein when this motor forms an active complex with dynactin and a cargo adaptor using an optical trap. We sparsely coated polystyrene beads with BicD2N and BicDR1 adaptors and assembled mtDDB and mtDDR complexes on beads[84]. Using a fixed trap, we observed that the stall force of mtDDB increases by 22% in 600 nM Lis1 (4.1 ± 0.1 vs. 5.4 ± 0.1 pN, mean ± SEM; two-tailed t-test, $p = 10^{-11}$; Fig. 3.4a-c). Lis1 addition also resulted in a modest increase in mtDDR stall force (5.4 ± 0.1 vs. 6.1 ± 0.1 pN; two-tailed t-test, $p = 10^{-4}$; Fig. 3.4c). Unlike isolated dynein[95], we did not observe an increase in the stall duration of mtDDB and mtDDR in the presence of Lis1 (Fig. 3.4d and Fig. 3.5).

We then tested whether the increase in mtDDB force production by Lis1 also increases the likelihood of DDB to win a tug-of-war against a plus-end-directed kinesin-1. We labeled mtDyn and tail-truncated wild-type human kinesin-1 with different fluorescent dyes and pitted one mtDDB against one kinesin-1 using a DNA tether. Consistent with our previous measurements[62], the majority (87%) of kinesin-DDB assemblies moved towards the plus-end in the absence of Lis1. The median velocity (185 nm s^{-1} towards the plus-end) was noticeably higher than previous measurements (26 nm s^{-1}) that used a cysteine-light mutant of kinesin-1[62], likely because the cysteine-light kinesin mutant, but not native kinesin, can be forced to move backward under resistive forces[101]. The addition of Lis1 increased the percentage of complexes moving towards the minus-end from 13% to 22% and increased the mean velocity of minus-end-moving assemblies by 6-fold (353 ± 68 vs. 55 ± 8 nm s^{-1}; two-tailed t-test, p = 0.02; Fig 3.4e-g). Collectively, these results demonstrate that Lis1 addition increases the likelihood of DDB winning against kinesin in a tug-of-war.

Lis1 does not affect force generation of complexes with single dynein

We next turned our attention to understanding how Lis1 increases the velocity and force production of mtDDB and mtDDR. To test whether Lis1 alters mechanochemical properties of single dynein assembled with dynactin, we mixed LD650-labeled full-length mtDyn and a TMR-labeled dynein tail construct (Dyn$_{LT}$, containing residues 1–1,074 of the heavy chain and associated chains)[38]. Because Dyn$_{LT}$ lacks the motor domain, processive runs of this construct can only be achieved through its side-by-side recruitment with single full-length mtDyn to dynactin. We measured the velocity of dual-labeled complexes that contain both mtDyn and Dyn$_{LT}$ in the presence of BicD2N (mtDTB) and BicDR1 (mtDTR). Remarkably, Lis1 addition did not affect the mean velocity of complexes containing single dynein (Fig. 3.6a-c). To test whether Lis1 alters the stepping properties of single dynein bound to dynactin, we tracked beads driven by single mtDTR under constant 1 pN hindering force exerted by the trap. Unlike mtDDB, Lis1 addition did not alter the stepping rate of mtDTR in 1 mM ATP (two-tailed t-test, $p = 0.83$; Fig. 3.6d-e and Fig. 3.7a). In addition, Lis1 addition did not affect the stall force and duration (two-tailed t-test, $p = 0.6$; Fig. 3.6f-g and Fig. 3.7b). We concluded that Lis1 does not directly affect the mechanical properties of single dynein bound to dynactin.

Lis1 promotes the recruitment of two dyneins to dynactin

The effect of Lis1 on DDB velocity and force production is strikingly similar to the recruitment of second dynein to dynactin[38,84], leading us to hypothesize that Lis1 regulates the stoichiometry of dynein per dynactin. To test this possibility, we mixed TMR- and LD650-labeled dynein with dynactin and BicD2N. Dual-colored complexes contain two dyneins, while single-colored complexes contain either one or two dyneins. Lis1 addition increased the percentage of dual-colored complexes from 14% to 24% ($p = 0.018$, two-tailed t-test, Fig. 3.8a-b). After correction for labeling efficiency and complexes dual-labeled with the same color[38], we estimated that Lis1 addition increases the percentage of complexes containing two dyneins from 22% to 42%. Consistent with our hypothesis, Lis1 addition did not increase the velocity of dual-colored complexes that contain two dyneins (Fig. 3.8c). Similar results were obtained when BicDR1 was used as a cargo adaptor, but the effect of Lis1 addition was modest, presumably because DDR complexes are already predisposed to contain two dyneins[38]. Collectively, these results demonstrate that Lis1 favors the recruitment of two dyneins to dynactin, which accounts for the faster velocity of these complexes[38,84,99,100]. We did not observe an increase in the recruitment of

16

Dyn$_{LT}$ side-by-side with mtDyn to dynactin in the presence of Lis1 (Fig. 3.8d-e and Fig. 3.9), suggesting that Lis1 favors the recruitment of two dyneins to dynactin through its interactions with the motor domain, not with the tail domain[102,103] of dynein.

Lis1 dissociates from motile complexes

To determine whether Lis1 remains stably bound when dynein moves along MTs[98-100], we mixed LD650-mtDyn and 50 nM TMR-Lis1 in the presence of dynactin and BicD2N. 30% of the motile mtDDB complexes contained Lis1. Removal of free Lis1 in assay solution after the initiation of processive motility reduced Lis1-dynein colocalization to 9%, suggesting that Lis1 can dynamically interact with dynein-dynactin as it moves along MT. In both cases, Lis1-bound complexes had a lower velocity than other mtDDB complexes (Fig. 3.10a-c, Fig. 3.11a-c). On rare occasions, Lis1 diffused on an MT, hopped onto a motile DDB complex on the same MT (Fig. 3.11d) and slowed down the motility[85,99]. Therefore, Lis1 typically dissociates from motile complexes but reduces velocity if it remains bound to dynein. These results are not fully consistent with previous reports that Lis1 remains bound to nearly all motile complexes[100] and Lis1-bound complexes have the same velocity[99] or move faster than complexes that move without Lis1[100]. The disparities may be related to differences in assay conditions and *in vitro* reconstitution methods.

Stoichiometry of Lis1 binding to dynein is also not well understood. DDB can concurrently recruit two Lis1 dimers[99]. However, it remains unclear whether each of the two dyneins in DDB binds to Lis1 or single dynein can simultaneously bind to two Lis1 dimers. To address this, we tested if two Lis1 molecules could bind to single full-length dynein recruited side-by-side with Atto488-Dyn$_{LT}$ (Fig. 3.10d). By quantifying DTR complexes colocalized with both TMR- and Cy5-Lis1, we estimated that 33% of DTR complexes with at least one Lis1 bound contain two Lis1s (Fig. 3.10e, Fig. 3.11e). Recruitment of two Lis1s leads to a further slowdown of the motility in comparison to single Lis1 (Fig. 3.10f). These results showed that single dynein can simultaneously recruit two Lis1 dimers.

Lis1 promotes the assembly of active dynein-dynactin complexes

Lis1 stimulates the frequency of minus-end-directed transport under conditions insufficient to induce motility, such as when BicD2N concentration is low[100]. To determine how Lis1 favors initiation of dynein motility when the complex formation is strongly limiting, we quantified wtDDB motility while we lowered the wtDyn concentration 10-, 20-, and 50-fold compared to our standard assay condition (see Methods). In the absence of Lis1, the percentage of complexes exhibiting motility was decreased at lower dynein concentrations, and motility was almost fully abolished with the 50-fold dilution. Lis1 addition increased the percentage of motility by ~5-fold (Fig. 3.12a-b), which is consistent with Lis1 favoring association of dynactin with dynein and the BicD2 orthologue in *Drosophila* cell extracts[91]. However, when we used mtDyn that does not form the phi conformation, we observed robust motility even in the 50-fold dilution condition and no significant increase in the percentage of motile complexes with the addition of Lis1 (Fig. 3.12a-b). We also mixed equal amounts of TMR- and LD650-wtDyn with dynactin and BicD2N and quantified the percentage of colocalizing complexes moving along the MTs under limiting dynein conditions (Fig. 3.13). Only ~ 5% of these complexes were assembled with two dyneins and we did not observe an increase in wtDDB velocity by Lis1 addition (Fig 3.12c-e), suggesting that Lis1 promotes motility by recruiting single dynein to dynactin under these conditions.

Therefore, Lis1 is also required for the assembly of the first dynein to dynactin and recruitment of the second dynein does not have to occur together with the first dynein.

Discussion

Our results challenge previous views on how Lis1 binding regulates dynein motility. A previous study on isolated dynein suggested that Lis1 binding induces pausing of dynein motility and enhances MT affinity when dynein is subjected to force[95]. Studies on yeast dynein also suggested that Lis1 binding interferes with the powerstroke of the linker domain[45], suggesting that Lis1 binding reduces dynein force generation. Our results with mammalian dynein-dynactin suggest a different mechanism. We found that the presence of Lis1 has no major effect on force generation of single dynein motors bound to dynactin and does not increase the time dynein stalls before dissociating from MTs under resistive loads. Therefore, our results do not support the view that the primary function of Lis1 is to regulate the tenacity of isolated dynein complexes to MTs[45,85]. Instead, Lis1 favors the recruitment of dynein to dynactin, thereby promoting the assembly of an active complex for dynein motility. This finding explains the requirement for Lis1 for transport initiation *in vivo*[86,90]. Consistent with two recent reports that studied the role of Lis1 in mammalian and yeast dynein-dynactin motility[104,105], we show that Lis1's ability to promote the association of dynein with dynactin also favors the adoption of the two-motor state, which accounts for more frequent stepping and higher force generation per complex. The increased probability of recruiting two dyneins to dynactin also means that Lis1 induces more effective competition against kinesin in a tug-of-war, a result consistent with an increase in anterograde velocity observed when Lis1 is inhibited in cells[89,91]. Remarkably, Lis1 does not have to be part of the complex to exert its effects on motility. Lis1 dissociates from most complexes before initiation of movement (Fig. 3.10), revealing that its primary role occurs during complex assembly. These results also provide an explanation for the recruitment of two dyneins to dynactin when the complex was pulled down by BicD2N from the brain lysate in which Lis1 is present[37], compared to the recruitment of mostly a single dynein when the complex is assembled from purified components in the absence of Lis1[38].

Our results provide insights into how Lis1 enhances the affinity of dynein to dynactin. We show that this function is not dependent on reported interactions between Lis1 and the dynein tail, pointing instead to a mechanism that involves Lis1's binding to the motor domain. Structural studies on yeast dynein showed that Lis1 binds to the motor domain at the interface between AAA3 and AAA4, and the coiled-coil stalk[49,85]. Assuming that mammalian Lis1 binds dynein in a similar orientation, Lis1 binding sites are positioned close to the dimerization interface on the AAA+ ring and stalk in the phi particle[25]. We propose that Lis1 binds to the open conformation of dynein and prevents switching back to the phi conformation (Fig. 3.12f), thereby reducing dynein autoinhibition[97]. Because the open conformation has a higher affinity to dynactin than the phi conformation[25], Lis1 promotes the assembly of dynein with dynactin and the cargo adaptor and favors the recruitment of two dyneins to each dynactin. The model explains why mtDDB is more likely to have two dynein motors and moves faster than wtDDB in the absence of Lis1 (Fig. 3.4c-d). The model is also consistent with a recent report that the requirement of Lis1and NudE in HookA-mediated dynein activation in *A. nidulans* can be bypassed by expressing a mtDyn[106]. Since we obtained a similar increase in the velocity of mtDDB and wtDDB in the presence of Lis1, it is possible that Lis1-bound dynein has additional structural features not present in the open conformation and further stimulates the assembly of dynein and dynactin

after the opening of the phi conformation. High-resolution structural studies will be needed to determine whether Lis1 binding induces conformational changes on the dynein heavy chain.

Our results are not consistent with a model in which a Lis1 dimer forms a bridge between two dyneins and recruits them simultaneously to dynactin, as we find that Lis1 is required for the assembly of complexes with single dynein at limiting dynein concentrations (Fig. 3.12 and Fig. 3.13). Moreover, monomeric Lis1, which cannot crosslink two dyneins, also stimulates the assembly of dynein-dynactin[104]. Therefore, Lis1 favors assembly of the first dynein to dynactin, which does not have to occur simultaneously with the second dynein. It remains to be studied whether Lis1 remains bound to dynein motors for the assembly of the fully activated complex, or early dissociation of Lis1 from the first dynein could occur before the recruitment of the second Lis1-bound dynein (Fig. 3.12f).

Mutagenesis studies have indicated that the transition between the phi-particle and open conformation is a tightly regulated process in cells[25]. Future studies are required to test whether Lis1-mediated opening of the phi conformation is also regulated by other dynein-associated proteins, such as the Lis1 binding proteins NudE and NudEL[96,107-109].

Figures
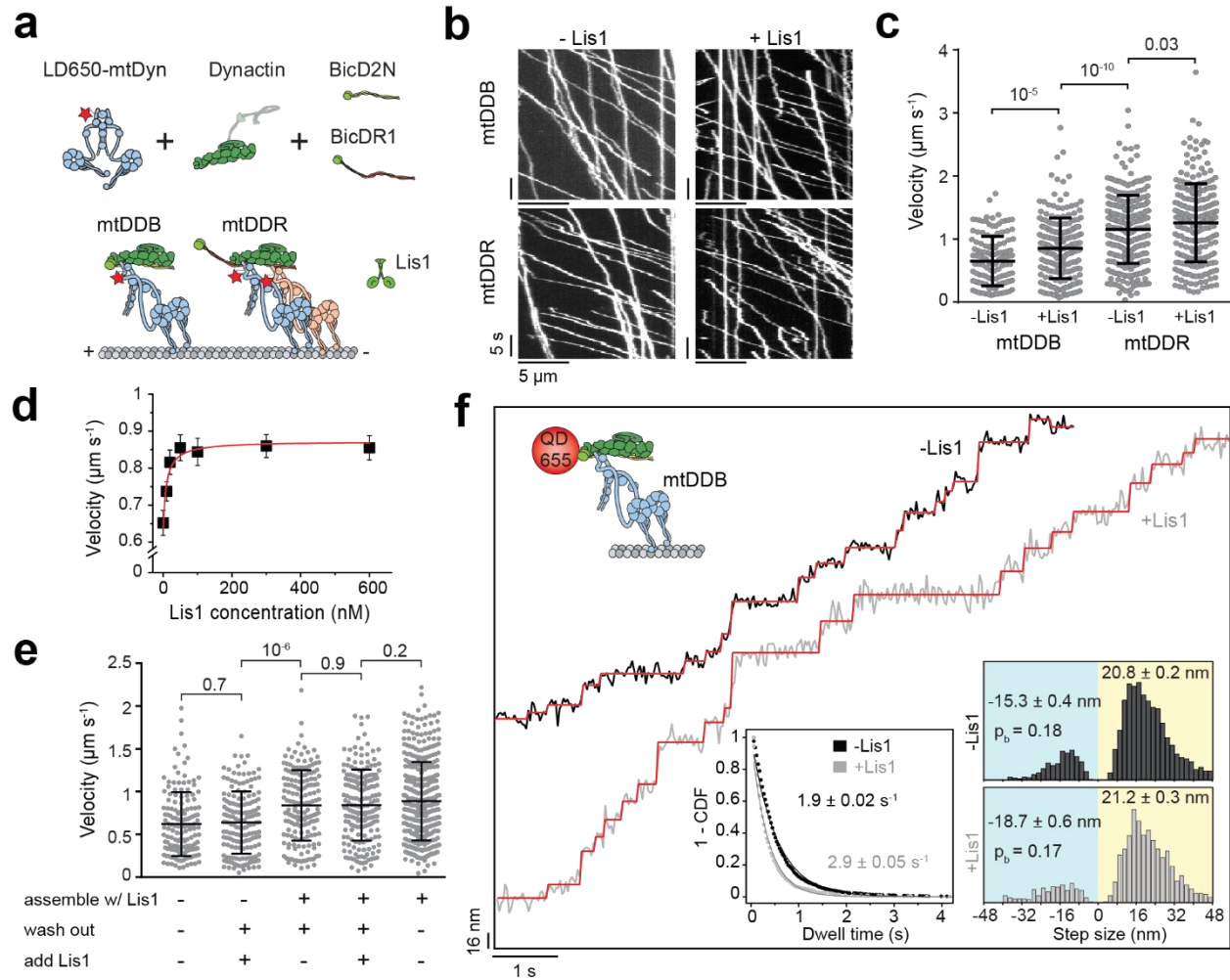
Figure 3.1: Lis1 increases the stepping rate of dynein-dynactin. (a) Schematic depiction of the mammalian dynein-dynactin-cargo adaptor complexes. BicD2N primarily recruits single dynein to dynactin (DDB), whereas BicDR1 recruits two dyneins (DDR). Lis1 binds to the dynein motor domain. **(b)** Kymographs show the motility of mtDDB and mtDDR on MTs. **(c)** Velocity distribution of mtDDB and mtDDR with and without 600 nM Lis1. The centerline and whiskers represent the mean and SD, respectively. From left to right, n = 132, 217, 307, and 241, and mean values are 652, 854, 1155, and 1259 nm s^{-1}. In a-c, four independent experiments were performed per condition. **(d)** The velocity of mtDDB under different Lis1 concentrations (mean ± SEM). mtDDB complex was assembled in the presence of Lis1, followed by removing excess protein and introducing Lis1 into the flow chamber. The red curve represents a fit to a Hill equation with n = 1. From left to right, n = 132, 216, 177, 204, 156, 179, and 217 (three independent experiments). **(e)** Velocity distribution of mtDDB assembled in the absence and presence of 600 nM Lis1 under different assembly conditions. The line and whiskers represent the mean and SD, respectively. From left to right, n = 152, 161, 170, 183, and 387 and mean values are 622, 638, 838, 842, and 888 nm s^{-1} (three independent experiments). **(f)** Step analysis of QD-labeled mtDDB (top insert) at 2 μM ATP in the presence and absence of 600 nM Lis1. Red staircases represent a fit to a step finding algorithm. (Bottom, left) Inverse cumulative distribution of dwell times between consecutive steps along the longitudinal axis. Solid curves represent fitting to an exponential decay (decay rate ± SE, n = 2138 for -Lis1 and 1441 for +Lis1). (Bottom, right) Normalized histograms of step sizes (n = 2,076 steps for -Lis1 and 1,374 for +Lis1, six independent experiments). Average forward and backward step sizes and the probability of backward stepping (p_b) are shown (± SEM). In c and e, p values are calculated from a two-tailed t-test.
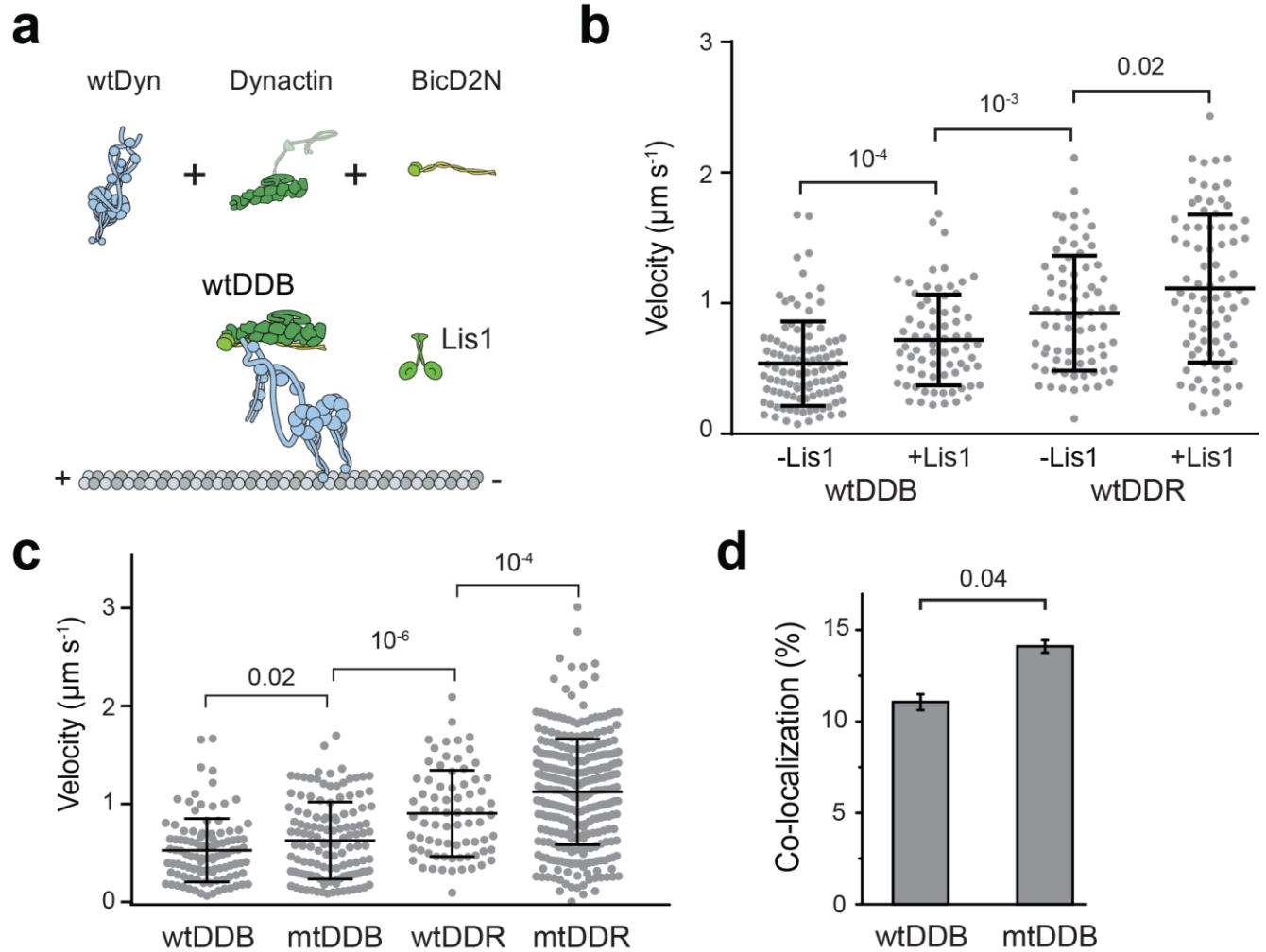
Figure 3.2: Lis1 increases the velocity of complexes with wtDyn. a, Assembly of wtDDB and wtDDR. **b**, Velocity distribution of wtDDB and wtDDR complexes assembled in the presence and absence of 600 nM Lis1. The line and whiskers represent the mean and SD, respectively. From left to right, $n = 106$, 72, 75, and 81, and mean values are 538, 718, 924, 1113 nm s^{-1} (three independent experiments). p-values are calculated from a two-tailed t-test. **c**, Velocity distribution of complexes assembled with wtDyn and mtDyn in the absence of Lis1. The line and whiskers represent the mean and SD, respectively. From left to right, $n = 106$, 132, 75, and 307, and mean values are 538, 652, 924, 1155 nm s^{-1} (three independent experiments). p-values are calculated from a two-tailed t-test. **d**, The percentage of processive wtDDB complexes that are dual-labeled when an equimolar mixture of TMR- and LD650-dynein motors were assembled with dynactin and BicD2N in the absence of Lis1 (mean ± SEM, $n = 246$ and 178 from left to right). Error bars represent SE calculated from multinomial distribution and the p-value is calculated from the two-tailed z-test.
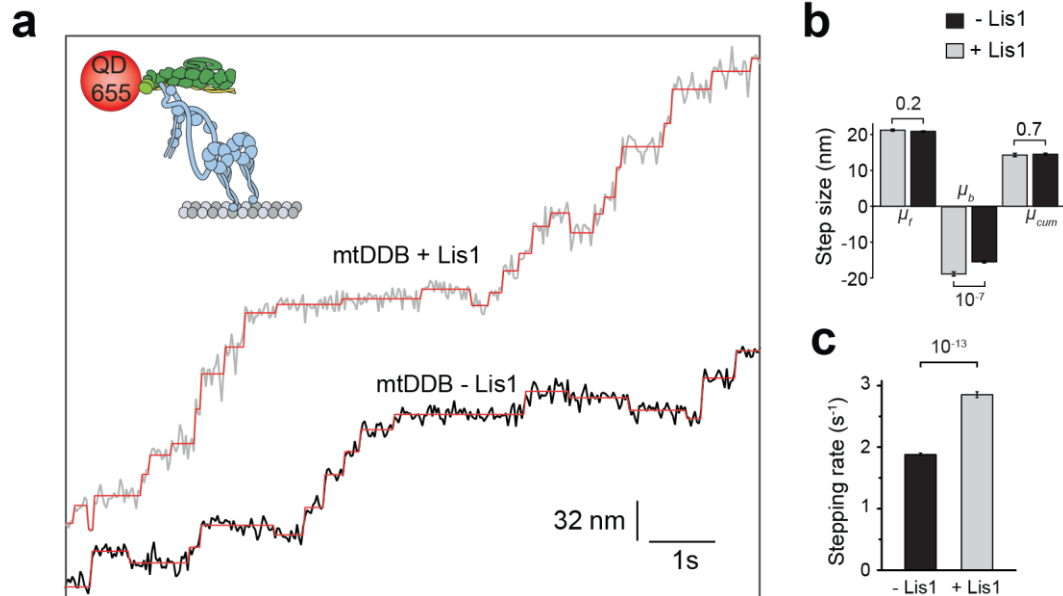
Figure 3.3: Step analysis of mtDDB in the presence and absence of Lis1. a, Additional examples of mtDDB stepping in the presence and absence of 600 nM Lis1. **b**, The average size of steps taken in forward (μ_f), backward, (μ_b), and both (μ_{cum}) directions along the longitudinal axis of the MT. Error bars are SEM. In a and b, six independent experiments were performed per condition. **c**, Stepping rates estimated from the exponential fit in Fig. 3.1f. Error bars are SE of the fit. In b and c, p values are calculated from a two-tailed t-test; sample size *(n)* distribution of data are provided in Fig, 3.1f.
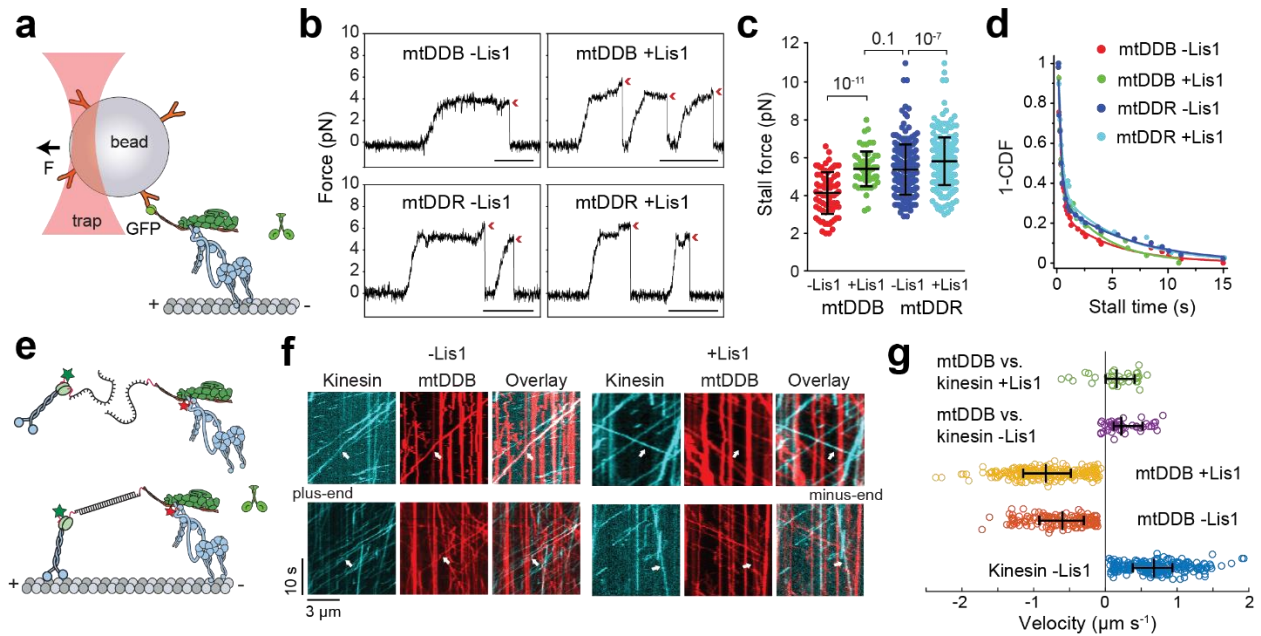
Figure 3.4: Lis1 increases the force production of dynein-dynactin. (a) Schematic of a fixed optical trapping assay for measuring the dynein stall force. **(b)** Typical stalls of beads driven by a single mtDDB or mtDDR. Red arrowheads denote the detachment of the motor from the MT after the stall event. Scale bars are 1 s. **(c)** Distribution of motor stall forces in the absence and presence of 600 nM Lis1. The centerline and whiskers represent the mean and SD, respectively. From left to right, n = 80 from 19 beads, 61 from 15 beads, 212 from 38 beads, and 152 from 32 beads, and mean values, are 4.1, 5.4, 5.4, and 6.1 pN. p-values are calculated from a two-tailed t-test. In b and c, four independent experiments were performed per condition. **(d)** Inverse cumulative distribution of stall durations of mtDDB and mtDDR in the presence and absence of Lis1. Solid curves represent fitting to a two-exponential decay (decay time ± SE, n = 53, 27, 50, and 39 from left to right). **(e)** Schematic depiction of the *in vitro* tug-of-war assay. DDB and kinesin were labeled with different-colored fluorescent dyes and tethered using a DNA scaffold. **(f)** Representative kymographs show the motility of LD650-dynein (red) and TMR-kinesin (cyan) in the absence and presence of 600 nM Lis1. White arrows show DDB-kinesin colocalizers. **(g)** Velocity distribution of mtDDB, kinesin, and mtDDB-kinesin assemblies in the absence and presence of Lis1. The centerline and whiskers represent the median and 65% CI, respectively. From top to bottom, n = 33, 45, 217, 132, and 210, and median values are 233, 185, −836, −604, and 670 nm s^{-1}. In f and g, three independent experiments were performed per condition. Negative velocities represent movement towards the MT minus-end.

23
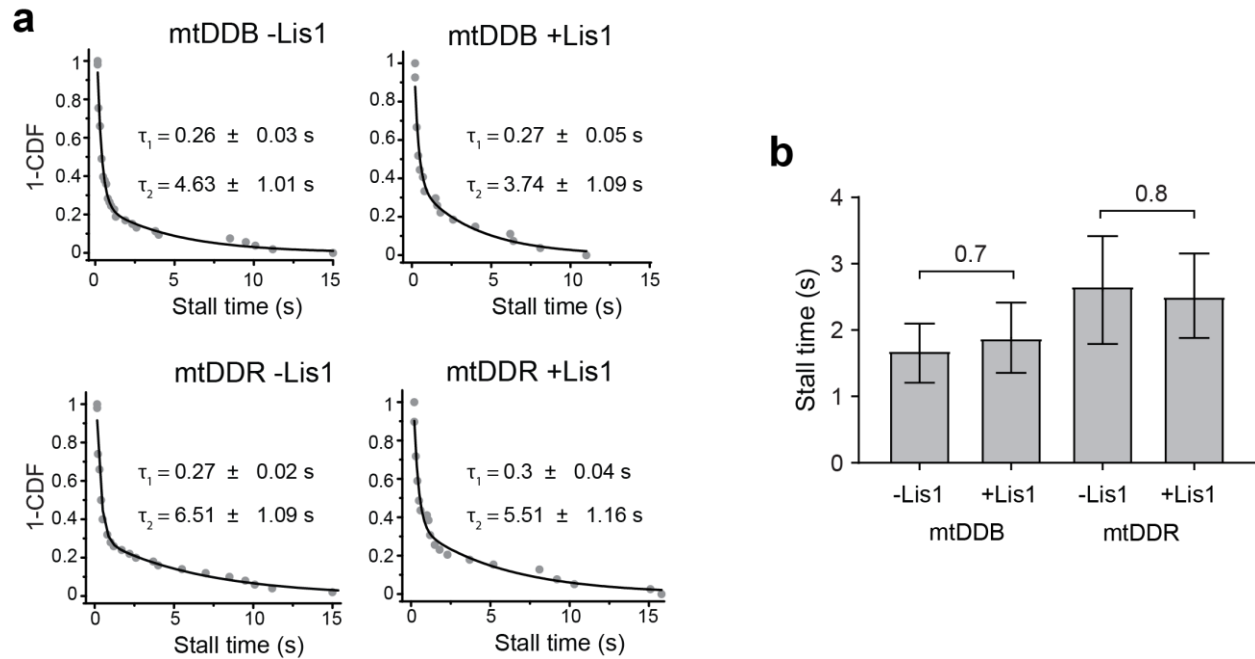
Figure 3.5: Lis1 does not increase the stall duration of dynein bound to dynactin and a cargo adaptor. a, Inverse cumulative distribution of stall durations in the absence and presence of 600 nM Lis1. Solid curves represent fitting to a two-exponential decay (decay time ± SE). **b**, Mean stall times of mtDDB and mtDDR in absence and presence of 600 nM Lis1 (± SEM). p values are calculated from a two-tailed t-test. In a and b, $n = 53, 27, 50$, and 39 from left to right, four independent experiments per condition.
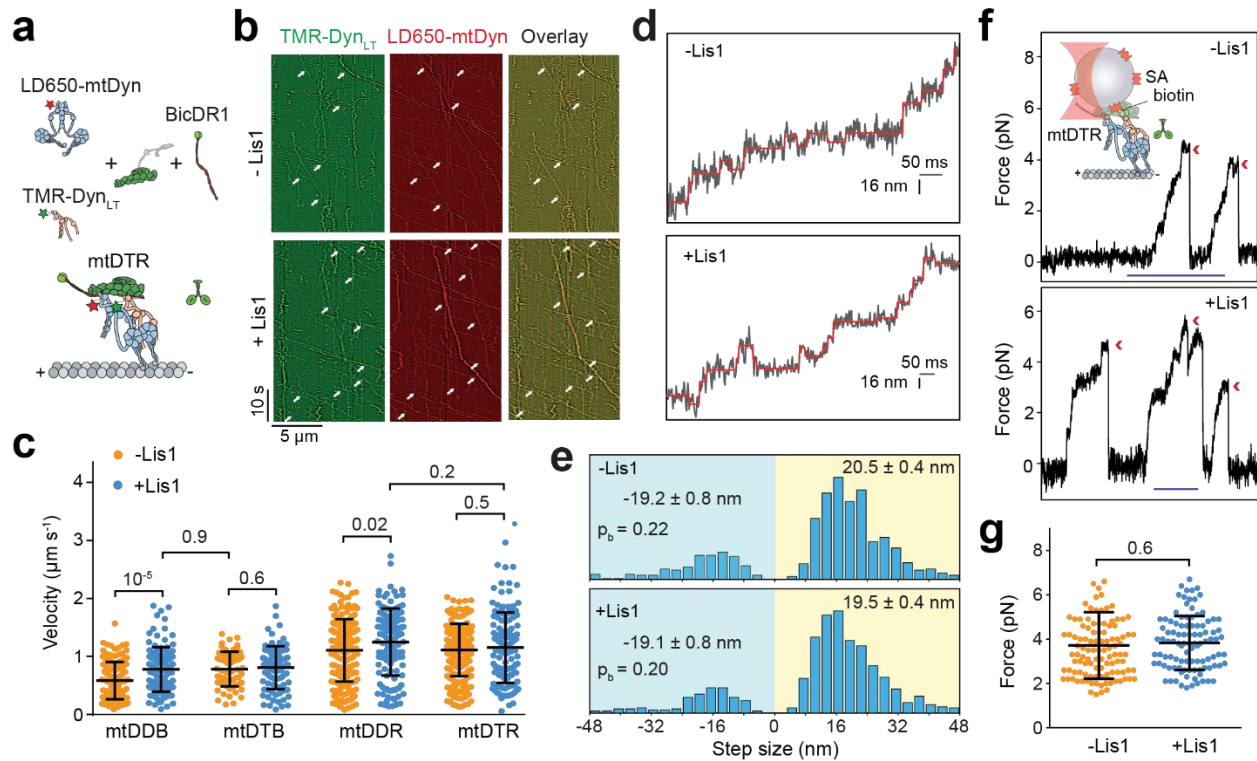
Figure 3.6: Lis1 does not affect the force generation and velocity of single dynein complexed to dynactin and a cargo adaptor. (**a**) Schematic depiction of the mtDTR complex. Full-length dynein and Dyn_{LT} are labeled with LD650 and TMR dyes, respectively. (**b**) Representative kymographs show the motility of mtDyn and Dyn_{LT}. Arrows represent the colocalization of TMR and LD650. (**c**) Velocity distribution of mtDDB, mtDTB, mtDDR and mtDTR in the presence and absence of 600 nM Lis1. The centerline and whiskers represent the mean and SD, respectively. From left to right, n = 144, 117, 65, 88, 209, 134, 213, and 126 and mean values are 584, 778, 783, 809, 1108, 1248, 1111, and 1154 nm s^{-1}. In b and c, three independent experiments were performed per condition. (**d**) Example traces of beads driven by mtDTR in the presence and absence of 600 nM Lis1 against 1 pN hindering force. The raw stepping data are shown in black and the steps fitting are in red. (**e**) Normalized histograms of mtDTR steps taken in the longitudinal direction. In d and e, n = 734 for -Lis1 and 724 for +Lis1 (three independent experiments per condition). Average sizes of steps taken in forward and backward directions (± SEM) and the probability of backward stepping in the presence and absence of Lis1 are indistinguishable (p = 0.6, two-tailed t-test). (**f**) (Top insert) Streptavidin (SA)-coated beads are sparsely decorated with biotin-Dyn_{LT} in the presence of mtDyn, dynactin, and BicDR1, and trapped with a focused laser beam. Traces represent typical stalls of beads driven by mtDTR in the absence and presence of 600 nM Lis1. Red arrowheads denote the detachment of the motor from the MT after the stall event. Scale bar is 1 s. (**g**) Distribution of mtDTR stall force. The centerline and whiskers represent the mean and SD, respectively. From left to right, n = 111 stalls from 23 beads and 101 stalls from 21 beads, and mean values are 3.7 and 3.8 pN. In f and g, three independent experiments were performed per condition. In c and g, p-values are calculated from a two-tailed t-test.
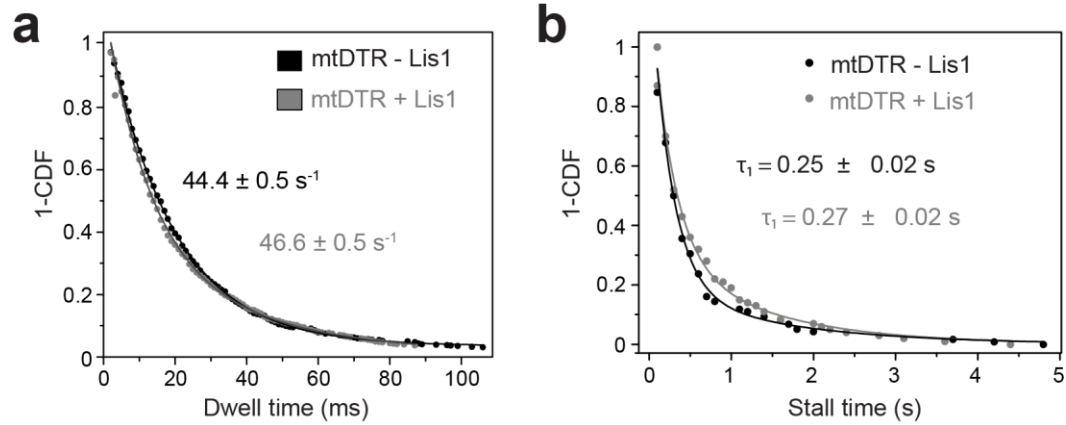
Figure 3.7: Lis1 does not affect stall time and stepping rate of single dynein bound to dynactin. a, Distribution of dwell times between consecutive steps along the longitudinal axis of the MT. A fit to an exponential decay reveals the decay rate (rate ± SE, $n = 734$ for mtDTR-Lis1 and 724 for mtDTR+Lis1). **b**, Inverse cumulative distribution of stall durations of mtDTR in the presence and absence of 600 nM Lis1. Solid curves represent fitting to a two-exponential decay (decay time ± SE, $n = 118$ for mtDTR-Lis1 and 100 for mtDTR+Lis1, three independent experiments).
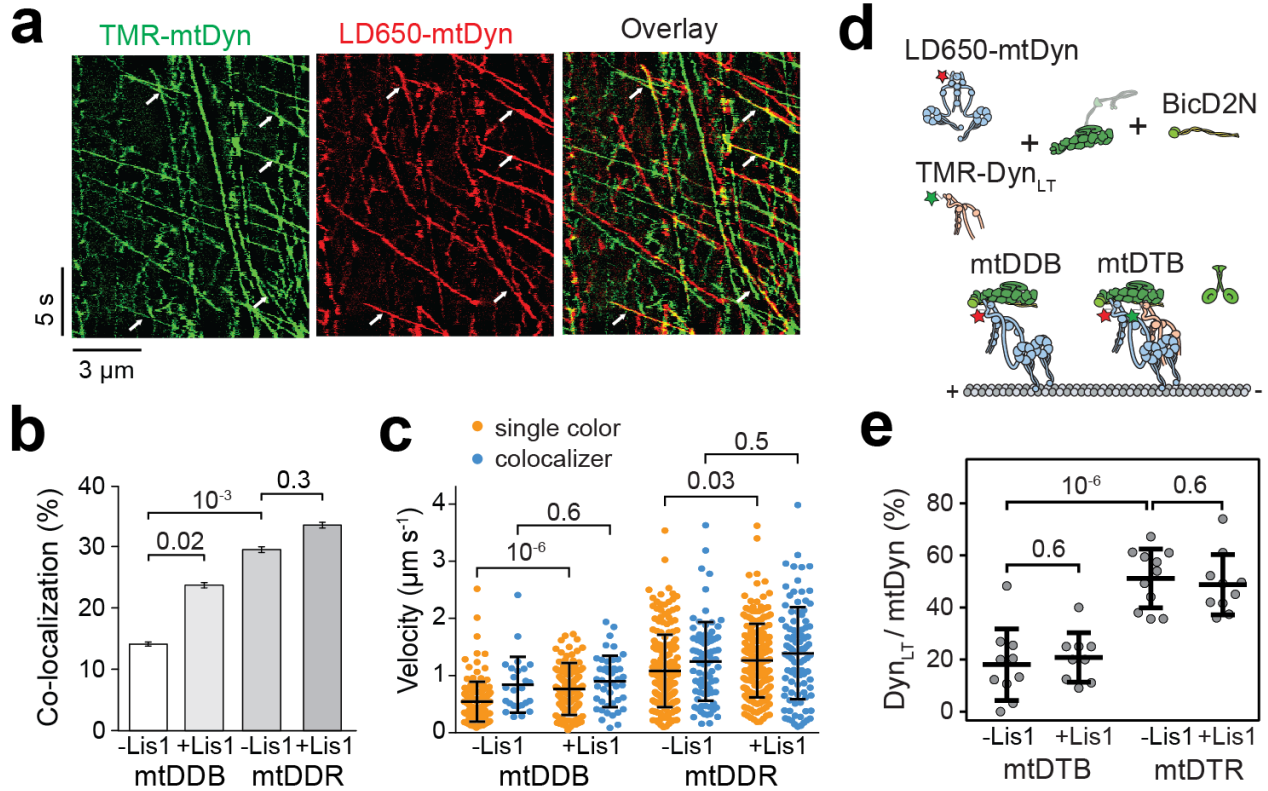
Figure 3.8: Lis1 favors the recruitment of two dyneins to dynactin. (a) Representative kymographs show the motility of LD650- and TMR-labeled dynein in the presence of dynactin, BicD2N, and 600 nM Lis1. Arrows represent TMR and LD650 colocalization. **(b)** The percentage of processive complexes that contain both TMR and LD650 signals (mean ± SEM, $n = 178$, 190, 289, 290 from left to right). Error bars represent SE calculated from multinomial distribution and p-values are calculated from a two-tailed z-test. **(c)** Velocity distribution of single-colored and dual-colored complexes of DDB and DDR in the presence and absence of Lis1. The line and whiskers represent the mean and SD, respectively. From left to right, $n = 153$, 25, 145, 45, 204, 85, 193, and 97 and mean values are 544, 840, 766, 899, 1082, 1248, 1263, and 1390 nm s^{-1}. p-values are calculated from a two-tailed t-test. In a-c, four independent experiments were performed per condition. **(d)** Schematic shows the assembly of mtDDB and mtDTB complexes using TMR-Dyn$_{LT}$, LD650-mtDyn, dynactin, and BicD2N. **(e)** The ratio of processive runs by TMR-Dyn$_{LT}$ to LD650-mtDyn on individual MTs in the presence and absence of Lis1. The line and whiskers represent the mean and SD, respectively ($n = 10$, 9, 11, and 10 MTs from left to right, three independent experiments). p values are calculated from a two-tailed t-test.
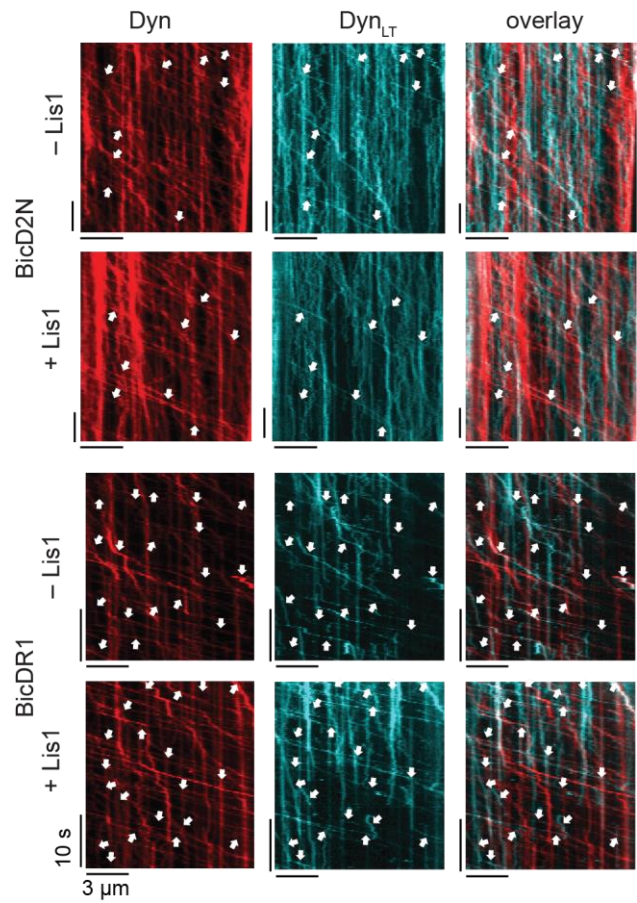
Figure 3.9: Lis1 does not stimulate the recruitment of dynein tail to dynactin. Representative kymographs show the motility of LD650-Dyn and TMR-Dyn$_{LT}$ assembled with BicD2N or BicDR1 in the presence and absence of 600 nM Lis1. White arrows point to complexes that contain both LD650-mtDyn and TMR-Dyn$_{LT}$ (three independent experiments were performed per condition).
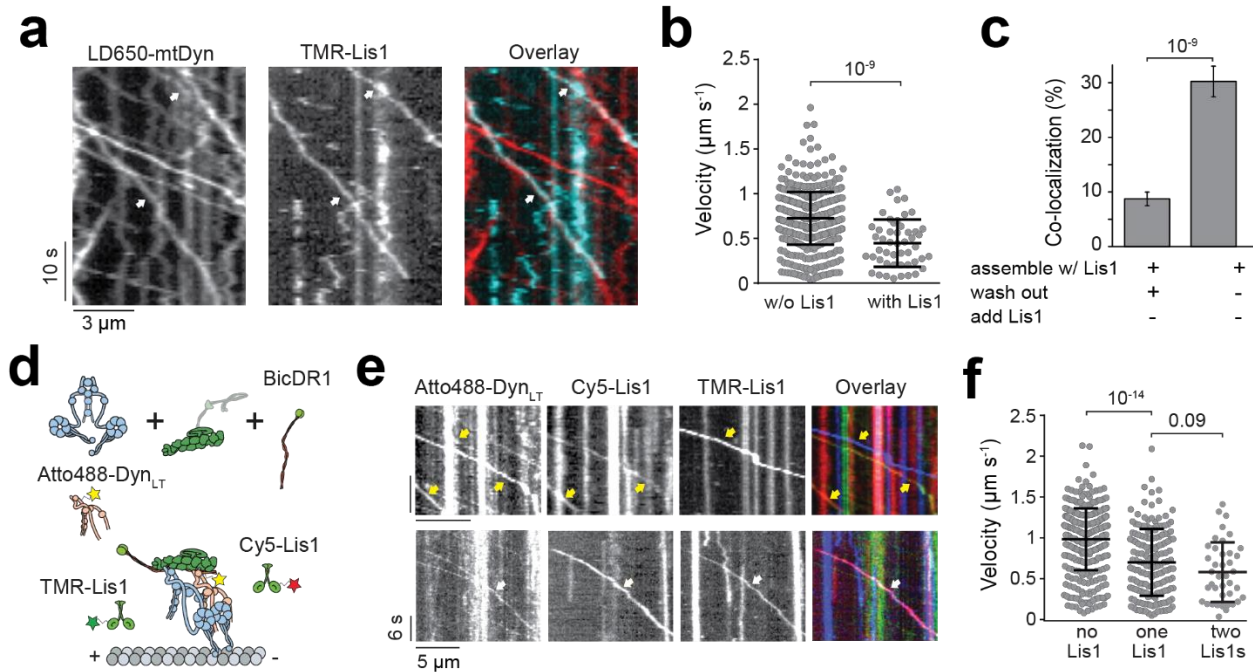
Figure 3.10: Lis1 binding decreases the velocity of dynein/dynactin. (a) Representative kymographs show the motility of mtDDB and Lis1 on MTs. White arrows represent the colocalization of LD650-Dyn (red) and TMR-Lis1 (cyan). **(b)** Velocity distribution of mtDDB and mtDDB-Lis1 assemblies. The centerline and whiskers represent the mean and SD, respectively. From left to right, n = 512, and 49 from left to right and mean values are 726 and 447 nm s^{-1}. The p-value is calculated from a two-tailed t-test. In a and b, four independent experiments were performed per condition. **(c)** The percentage of processive complexes that contain both LD650-mtDyn and Lis1-TMR signals using different assembly conditions (see Methods; mean ± SEM, n = 561 and 387 from left to right). Error bars represent SE calculated from multinomial distribution and p-values are calculated from a two-tailed z-test. **(d)** Schematic depiction of mtDTR complex assembled in the presence of 50 nM TMR- and Cy5-Lis1. **(e)** Representative kymographs show the motility of mtDTR and Lis1 on MTs. Yellow arrows represent the colocalization of Dyn$_{LT}$ (green) and one color of Lis1. White arrows represent the colocalization of Dyn$_{LT}$ with Cy5-Lis1 (red), and TMR-Lis1 (cyan). **(f)** Velocity distribution of mtDTR that colocalizes with zero, one and two colors of Lis1. The centerline and whiskers represent the mean and SD, respectively. From left to right, n = 357, 172, and 40 and mean values are 985, 701, and 582 nm s^{-1}. In e and f, three independent experiments were performed per condition. p-values are calculated from a two-tailed t-test.
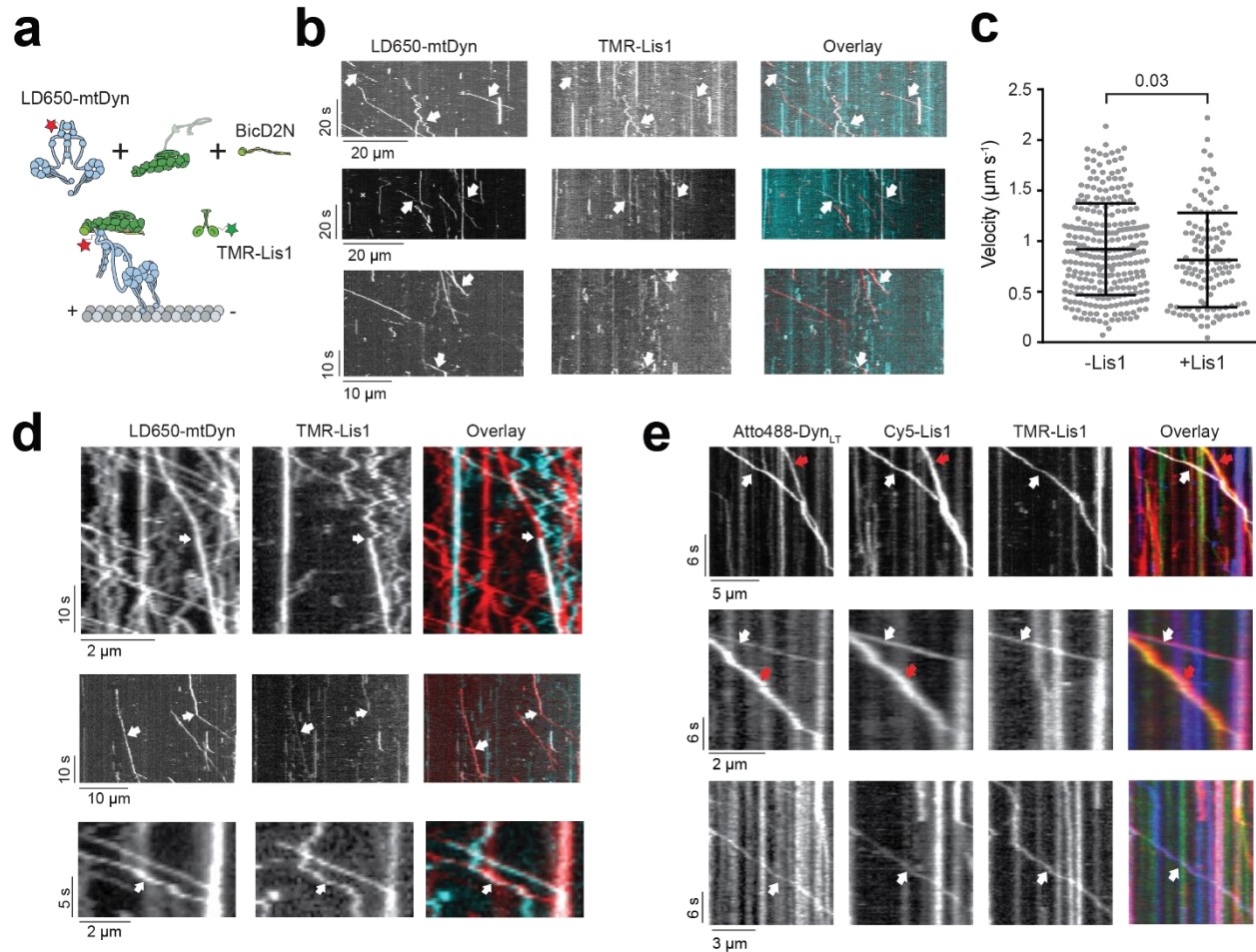
Figure 3.11: Additional examples of binding events of Lis1 to mtDDB and mtDTR during processive movement. a, Schematic depiction of mtDDB complex assembled in the presence of TMR-Lis1. **b**, Representative kymographs show binding of Lis1 to motile mtDDB complexes assembled by mixing 1 nM LD650-mtDDB and 75 nM TMR-Lis1 and immediately recording motility with free proteins in solution (see methods). White arrows represent colocalization of LD650-Dyn (red) and Lis1-TMR (cyan). **c**, Velocity distribution of mtDDB complexes not bound to Lis1 moves faster than complexes that are bound to Lis1 during single-molecule motility. The line and whiskers represent the mean and SD, respectively. From left to right, $n = 270$ and 117 and mean values are 921 and 813 nm s^{-1}. In b and c, three independent experiments were performed per condition. The p-value is calculated from a two-tailed t-test. **d**, Rare events of dynamic binding of Lis1 to dynein as mtDDB walks along an MT assembled in the presence of 50 nM Lis1. White arrows represent the colocalization of LD650-Dyn (red) and TMR-Lis1 (cyan). In the top kymograph, Lis1 initially diffuses on an MT and then binds to mtDDB during processive movement. Lis1 binding reduces the velocity of the complex. In the middle kymograph, dissociation of Lis1 during mtDDB motility increases the velocity. In the bottom kymograph, a diffusing Lis1 initially binds and later dissociates from mtDDB, without affecting the velocity of the complex (four independent experiments). **e**, Additional kymographs show single- and dual Lis1 binding to motile mtDTR complexes assembled in the presence of 50 nM Lis1. Red arrows represent the colocalization of Atto488-Dyn$_{LT}$ (green) and Cy5-Lis1 (red). White arrows represent the colocalization of Atto488-Dyn$_{LT}$ (green) with both Cy5-Lis1 (red), and TMR-Lis1 (cyan). Three independent experiments were performed per condition.
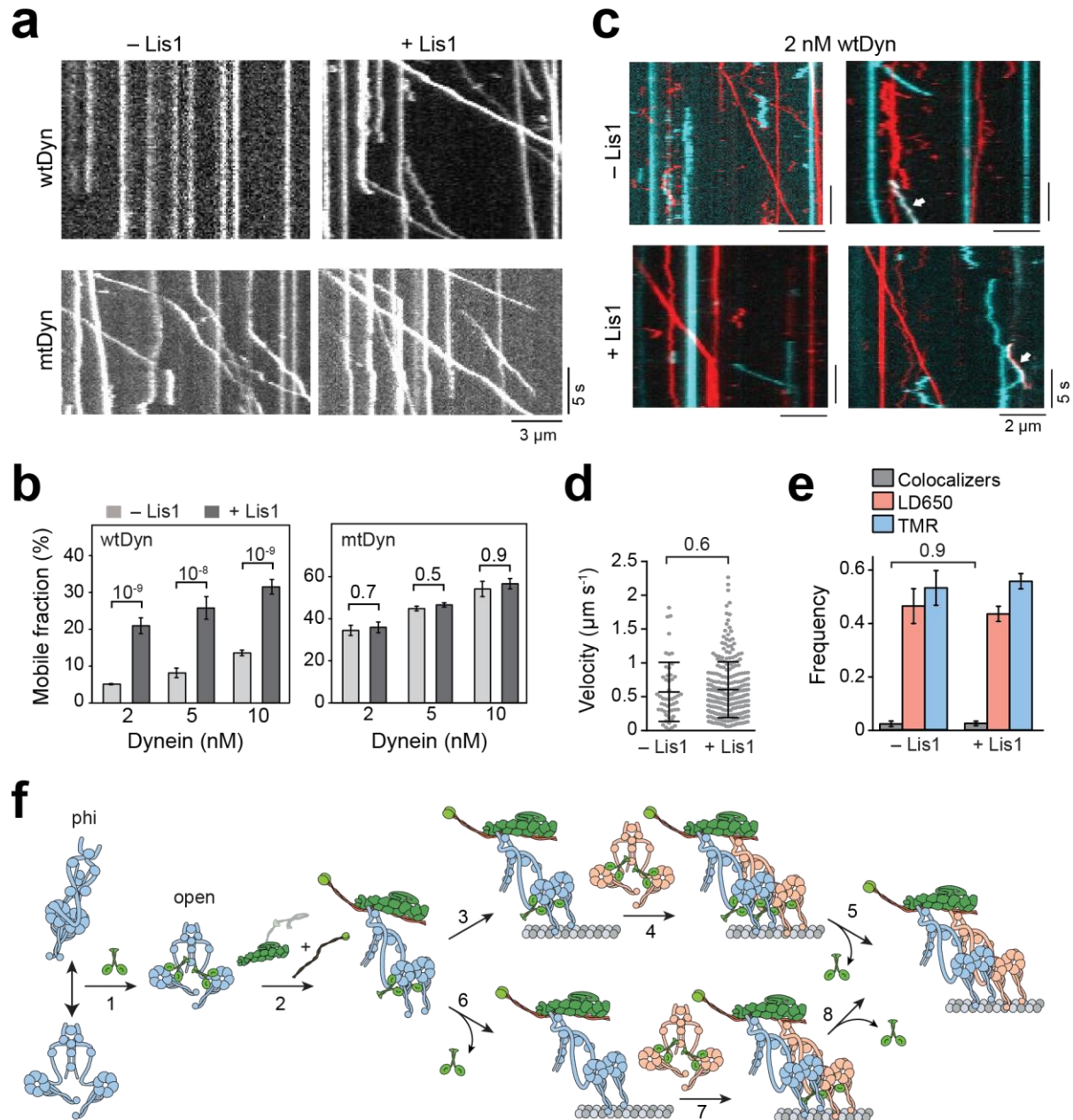
Figure 3.12: Lis1 promotes assembly of the dynein transport machinery. (a) Representative kymographs show the motility of DDB at 5 nM concentration of dynein in the absence and presence of 600 nM Lis1. **(b)** Ratio comparison of the number of processive runs by DDB to the total number of landed motors on MT (mean ± SEM). From left to right, n = 508, 355, 491, 262, 1244, and 392 for wtDyn, and 234, 459, 426, 1352, 457, and 859 for mtDyn. In a and b, three independent experiments were performed per condition. Error bars represent SE calculated from multinomial distribution and p values are calculated from a two-tailed z-test. **(c)** Representative kymographs show the motility of LD650- (red) and TMR- (cyan) wtDDB at 2 nM concentration of dynein in the absence and presence of 600 nM Lis1. Left kymographs show single-colored runs and right kymographs show rare events of TMR-LD650 colocalization (white arrows). **(d)** Velocity distribution of wtDDB motility assembled at 5 nM dynein concentration in the absence and presence of 600 nM Lis1. The centerline and whiskers represent the mean and SD, respectively. From left to right, n = 51 and 257, and mean values are 572 and 604 nm s^{-1}. In c and d, three independent experiments were performed per condition. **(e)** Fraction of processive complexes that contain TMR, LD650, and TMR-LD650 colocalizers (mean ± SEM, n = 59 for -Lis1 and 303 for + Lis1). The p values are calculated from a two-tailed t-test in d and a two-tailed z test in e. **(f)** A model for Lis1-mediated assembly of the dynein-dynactin complex. (1) Lis1 binds to the open-conformation of dynein with one Lis1 dimer for each dynein motor domain. (2) Lis1 binding prevents transitions of the open conformation to the phi conformation, which increases the affinity of dynein to dynactin. This mechanism also favors the

31

recruitment of second dynein to the complex resulting in higher force production and faster movement. Lis1 dissociates from active dynein-dynactin-cargo adaptor motors, either after pairing of two dyneins with dynactin (3-5) or during the assembly of the complex (6-8).
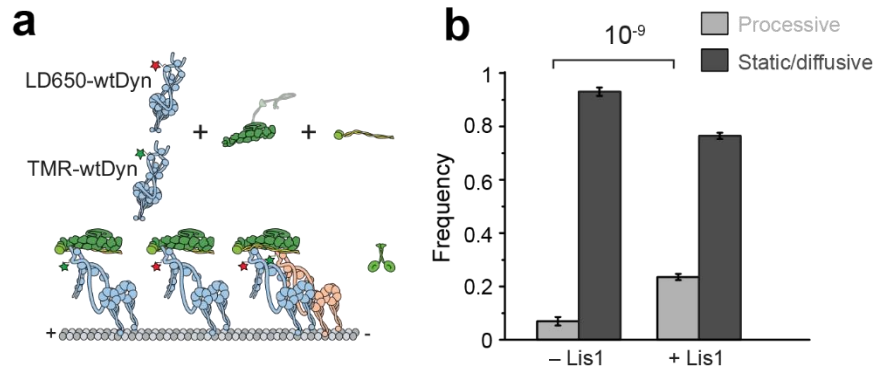
Figure 3.13: At limiting dynein concentration, Lis1 recruits single dynein to dynactin and BicD2N. a, Schematic depiction of wtDDB assembly using 5 nM LD650-wtDyn and TMR-wtDyn in the absence and presence of 600 nM Lis1. **b**, Fraction of processive and static/diffusive wtDDB complexes on MTs (mean ± SEM, n = 59, 788, 303 and 984 from left to right, three independent experiments).

Methods

Protein expression, labeling, and purification

Human SNAPf-wtDyn, SNAPf-mtDyn, SNAPf-Dyn$_{LT}$ (containing residues 1-1,074 of the heavy chain), BicD2N-GFP (containing residues 1-400), BicDR1-GFP, and Lis1-SNAPf were expressed in *Sf9* cells and purified using IgG affinity chromatography (using a cleavable ZZ tag), as described previously[32,38]. *Sf9* cells were regularly tested for mycoplasma infection and no positive results were found. SNAP-tagged proteins were labeled with BG-functionalized biotin, TMR, Atto488 (NEB) or LD650 probes, and purified as described previously[38]. Dynactin was purified from pig brains using the large-scale SP-sepharose and MiniQ protocol[31]. Western blotting and mass spectrometry show no detectable levels of Lis1 in dynactin preps (V. Madan and S.L.B., in preparation). Human Kinesin-1(1-560)-SNAPf-GFP was expressed in BL21DE3 cells and purified using Ni-NTA affinity chromatography, as described previously[110]. Concentration of isolated proteins was quantified using the Bradford colorimetric assay.

Motility assays

Biotinylated MTs were prepared by mixing 190 µM of 2% biotin-labeled biotin with 0.9 mM of unlabeled pig brain tubulin in BRB80 buffer (80 mM PIPES pH 6.8, 1mM MgCl$_2$, 1 mM EGTA), followed by the addition of equal volume of polymerization buffer (2x BRB80 supplemented with 2 mM GTP and 20% anhydrous Dimethyl sulfoxide (DMSO)). Tubulin was allowed to polymerize by incubation for 40 mins at 37°C, followed by the addition of 10 nM taxol and incubation for another 40 mins. Taxol-stabilized MTs were then pelleted at 20,000 g for 12 min and resuspended in BRB80 buffer containing 10 nM taxol and 1 mM Dithiothreitol (DTT).

The glass surface of motility chambers was first passivated by BSA and functionalized with biotin by flowing 1 mg/ml BSA-biotin (Sigma), followed by washing the chamber with 40 µl dynein buffer (DB: 30 mM HEPES pH 7.0, 5 mM MgSO$_4$, 1 mM EGTA, 1 mM TCEP (tris(2-carboxyethyl)phosphine) supplemented with 1.25 mg/ml casein (DB-C) . To immobilize biotinylated MTs on the functionalized surface, the chamber was incubated with 1 mg/ml SA (NEB) and washed with DB-C.

For DDB, DDR, and DTR motility, 70 nM LD650-dynein was mixed with 150 nM dynactin, and 700 nM cargo adaptor (BicD2N-GFP or BicDR1-GFP) in 10 µl DB supplemented with 1 mg/ml Bovine Serum Albumin (BSA). For DTR experiments, 300 nM TMR-dynein tail was added to the mixture. For dynein co-localization experiments, 70 nM TMR-dynein was additionally included in the motility mix. The complexes were incubated on ice for 10 mins, diluted in DB-C, and flowed into the chamber. The motility mix was kept for 2 mins and then washed with 40 µl DB-C. To record motility, 20 µl dynein motility buffer (DMB: DB-C supplemented with 1 mM Mg.ATP, 2.5 mM PCA (protocatechuic acid), 35 µg/ml PCD (protocatechuate-3,4-dioxygenase)) was introduced into the chamber and the sample immediately imaged for 3 mins at 23°C. Unless otherwise indicated, experiments with unlabeled Lis1 were performed by mixing Lis1-SNAPf with DDB and introducing the reaction mixture into the chamber. The chamber was then washed with 40 µl DB-C, and Lis1-SNAPf was then reintroduced at the same concentration into the chamber with DMB before recording the motility. In Figure 3.10a-b, 50 nM TMR-Lis1 was added to the diluted motility mix (~ 1 nM LD650-mtDDB) and introduced into the motility chamber. The chamber was then washed with 40 µl DB-C and motility was recorded in the absence of free Lis1 in DMB. In Figure 3.10e-f, 50 nM TMR-Lis1 and 70 nM Cy5-Lis1 were

incubated with 1 nM Atto488-mtDTR before introducing the mixture into the flow chamber. After washing out unbound proteins from the chamber with 40 µl DB-C, motility was recorded in the absence of free Lis1 in DMB. In Figure 3.1e, the role of Lis1 in DDB assembly and motility was tested by introducing and removing Lis1 in different stages of the sample preparation. In Extended Data Figure 3.12b-c 1 nM LD650-mtDDB and 75 nM TMR-Lis1 were introduced into the chamber in DMB containing 75 mM KOAC and motility was recorded without washing excess TMR-Lis1 in solution. Although Lis1 has a weak affinity to MTs, this has not affected the velocity of dynein-dynactin motility (Fig. 3.1d).

Single-molecule imaging was performed using a custom-built TIRF microscope equipped with a 100x 1.49 N.A. apochromatic oil-immersion objective (Nikon) and a perfect focusing system on an inverted microscopy body (Nikon Ti-Eclipse). The fluorescence signal was detected using an electron-multiplied charge-coupled device (EM-CCD) camera (Andor, Ixon EM+). The sample that contained LD650 was excited with a 0.05 kW cm^{-2} 633 laser beam (Coherent), and the emission signal was filtered using a 655/40 nm bandpass emission filter (Semrock). Movies were recorded using an effective pixel size of 160 nm at 300 ms per frame. For two- and three-color fluorescence assays, imaging was performed on a multi-color TIRF microscope (Nikon) using alternating excitation and time-sharing mode of emission collection. Atto488-, TMR- and LD650-labeled samples were excited using 0.05 kW cm^{-2} 488, 532, and 633 nm laser beams (Coherent), and fluorescence signals were detected on an ImagEM X2 EM-CCD camera (Hamamatsu). Movies were recorded at 150 ms per frame per color for two-color and 100 ms per frame per color for three-color fluorescence assays. The effective pixel size was 108 nm.

Kymographs were generated from movies in ImageJ. Processive movement and velocity were then defined and measured, as described previously[62]. Briefly, kymographs were created by plotting segmented lines along each MT using ImageJ and individual runs were manually scored. Complexes that were static, diffusive, or run shorter than 5 pixels (750 nm) along the MT were excluded from the analysis. In trajectories that exhibit pauses longer than 30 s, only the segments with unidirectional motility were analyzed. Pauses shorter than 30 s were included in the analysis. For two-color imaging, the two channels were overlaid using the merge function. The resulting kymographs were then manually scored for processive events that show co-localization between the two channels. In Figures 3.6b and 3.8a, kymographs were post-processed using the fast Fourier transform function of ImageJ for clarity. Labeling efficiency of dynein and Lis1 with at least one dye was 96% and 95% respectively, as determined by spectrophotometry. The fractions of the complexes containing two dyneins or Lis1s were calculated using the colocalization measurements, after accounting for unlabeled complexes, and complexes assembled with two dyneins that are labeled with the same color[38].

High-resolution fluorescence-tracking assays
QDs were functionalized with benzyl guanine by mixing 8 µM amino (PEG) QDs emitting at 655 nm (ThermoFisher) with 20 mM BG-GLA-NHS (NEB) in 100 mM sodium borate buffer, pH 8.0 for 40 min at room temperature. To remove excess BG-GLA-NHS, functionalized QDs were concentrated through five consecutive spins through 100,000 MWCO centrifugal filter units (Amicon). Finally, spin-concentrated QDs were suspended in 100 µl DB and stored at 4ºC.

For tracking the motility of individual dynein complexes, 70 nM SNAPf-dynein was mixed with 150 nM dynactin, and 700 nM BicD2N-GFP, and 600 nM Lis1-SNAPf in DB supplemented with 1 mg/ml BSA. The complex was incubated on ice for 10 mins followed by the addition of 50 nM

BG-functionalized QDs for another 10 mins in ice. The mixture was then diluted in DB-C and flowed into the motility chamber for 2 mins, followed by washing with 80 µl DB-C. Movies were recorded immediately after washing the chamber with 20 µl DMB containing 2 µM Mg.ATP. For tracking the stepping of dynein in the presence of Lis1, 600 nM Lis1-SNAPf was included in DMB. The sample was excited with a 1 kW cm^{-2} 488 nm beam (Coherent) and movies were recorded at 30 ms per frame on Ixon EM+ EM-CCD camera (Andor). For stepping analysis, fluorescence spots of QDs were localized using a 2-dimensional Gaussian fitting and the resulting trajectories fitted into steps using a custom-written algorithm based on Schwartz Information Criterion [50,55].

Tug-of-war assays
To prepare a DNA tether between DDB and kinesin, two complementary DNA strands were first functionalized with benzyl guanine as described previously. Briefly, 25 µM DNA oligos containing an amino group modification at their 5'ends were mixed with 5 mM BG-GLA-NHS (NEB) in 50 mM HEPES buffer containing 50% anhydrous DMSO, pH 8.5. The reaction was kept overnight at room temperature. The excess unreacted ligand was removed and the BG-functionalized oligos were purified by ethanol precipitation of DNA. Finally, isolated DNA was dissolved in DB and stored at 4°C. The concentration of BG-DNA was estimated from the absorbance at 260 nm.

BicD2N-SNAPf and kinesin-SNAPf-GFP were labeled with BG-functionalized oligos by mixing protein with DNA in DB for 1 hr at 4°C. DNA and protein concentrations were optimized to yield ~ 30% efficiency of protein labeling to ensure that the likelihood of dual-labeling of a single dimeric protein with two DNA oligos was minimized (<9%). The labeling efficiency was quantified by comparing the intensities of labeled to unlabeled bands on 4-12% Bis-Tris SDS-PAGE (Invitrogen). Excess unreacted DNA was removed from BicD2N-SNAPf using a TSKgel G4000SWXL size exclusion column (Tosoh). In the case of kinesin, a 10-fold molar excess of BG-GLA-TMR (NEB) was added to the motor-DNA mixture and the sample was incubated for an additional 30 min at 4°C. Excess DNA and dye were removed by an MT bind and release assay.

In tug-of-war experiments, 200 nM DNA-labeled BicD2N-SNAPf was mixed with 70 nM LD650-labeled dynein and 150 nM dynactin in 10 µl DB supplemented with 1 mg/ml BSA. For experiments with Lis1, 600 nM Lis1-SNAPf was added to the mixture. The mixture was incubated on ice for 10 mins, followed by the addition of 150 mM NaCl and 200 nM DNA- and TMR- labeled kinesin-SNAPf-GFP, and incubation on ice for a further 20 mins. Proteins were then diluted in DB-C and flowed into the chamber, followed by washing with DB-C and imaging in DMB. The buffer was supplemented with 600 nM Lis1-SNAPf in case of Lis1 experiments.

Optical trapping assays
For DDB and DDR experiments, complexes assembled with SNAPf-dynein, dynactin, and BicD2N-GFP or BicDR1-GFP were mixed with 860 nm diameter anti-GFP coated latex beads in ice for 10 mins. This assay geometry ensures that beads are driven by active dynein motors assembled to cargo adaptors and eliminates the possibility of cargo adaptor multimerization. Carboxyl latex beads (860 nm-diameter, Life Technologies) were washed and resuspended in activation buffer (10 mM MES, 100 mM NaCl, pH 6.0). The beads were coated by mixing with ~ 2 mg of custom-made polyclonal rabbit anti-GFP antibodies (BioLegend, previously Covance, catalog# MMS-118P) in activation buffer supplemented with 1 mg each of N-

36

hydroxysulfosuccinimide (Sulfo-NHS) and 1-Ethyl-3-(3-dimethylaminopropyl) carbodiimide (EDC) crosslinkers (Pierce) dissolved in dimethylformamide (DMF)[47]. The beads were passivated with BSA, washed and stored in phosphate-buffered saline (PBS) supplemented with 0.5 mg/ml BSA and 0.1% sodium azide at 4 °C. For DTR experiments, SNAPf-Dyn$_{LT}$ was labeled with biotin; and biotin-Dyn$_{LT}$, mtDyn, dynactin, and BicDR1 were incubated with 800 nm diameter SA-coated beads (Spherotech) in ice for 10 mins. The protein-coated beads were then diluted in DB-C and flowed into the motility chamber in DMB. The protein concentration in the mixture was gradually reduced in assays until less than 30% of the tested beads exhibited motility activity in contact with Cy5-labeled axonemes to ensure that >95% of the beads are driven by a single complex. For force measurements in the presence of Lis1, 600 nM Lis1-SNAPf was added to the bead-protein mixture and also later added to DMB.

Force measurements were performed on a custom-built optical trap on a Nikon Ti-Eclipse microscope body consisting of a 2 W 1,064 nm continuous wave laser beam (Coherent) and a 100 x 1.49 NA Plan-Apo objective (Nikon), as described previously [47]. Beads were trapped by the laser beam steered by two computer-controlled perpendicular acousto-optical deflectors (AA Electronics). The sample was excited with a 633 nm laser (Coherent) and Cy5-labeled axonemes were imaged using a monochrome camera (The Imaging Source). To detect the bead position relative to the center of the trap, a position-sensitive detector (First Sensor Inc.) was placed at the back focal plane of a 1.4 N.A. oil-immersion condenser (Nikon). Trap stiffness was derived by fitting the power spectrum of a trapped bead that was rapidly raster-scanned in both x and y directions using the acousto-optical deflectors to a Lorentzian spectrum. The typical spring constant used in these experiments was ~ 0.04 pN/nm to allow motors to travel 100-150 nm before stalling. The PSD data were recorded at 20 kHz during calibration and the resulting curve was fit to a cubic polynomial to calibrate the response of the PSD in each sample. For fixed trap assays, PSD data were collected at 5 kHz and downsampled to 500 Hz for ease of visualization. To qualify as a stall event, the bead position should remain stationary for at least 100 ms before rapid (<2 ms) jumping towards the trap center, implicating release of the motor from the MT. Stall force histograms are then generated from individual stall events that were manually scored. For force-clamps assays, the PSD signal was acquired at 5 kHz and position feedback was performed at 100 Hz. Beads that walked for at least 100 nm were subjected to force feedback and resulting runs were downsampled to 500 Hz and fit to a step-finding algorithm as described previously[47]. Force-clamp runs that are shorter than 200 nm or included instant jumps larger than 50 nm were excluded from the analysis.

Statistics and reproducibility
At least three independent experiments were performed. Independent experiments showed similar results. The exact number of replicates (n) of every dataset is given at the corresponding figure legends. Statistical analysis methods are stated in the main text or the figure legend.

Chapter 4: Lis1 binding regulates force-induced detachment of cytoplasmic dynein from microtubules

The work presented in this chapter was published in the following preprint: "Lis1 binding regulates force-induced detachment of cytoplasmic dynein from microtubules" written by Emre Kusakci, Zaw Min Htet, John P. Gillies, Samara L. Reck-Peterson, Ahmet Yildiz. **bioRxiv (2022)**

Abstract

Cytoplasmic dynein-1 (dynein) is an AAA+ motor that transports intracellular cargos towards the microtubule minus end. Lissencephaly-1 (Lis1) binds to the AAA+ ring and stalk of dynein's motor domain and promotes the assembly of active dynein complexes. Because Lis1 slows motility when it remains bound to dynein, dissociation of Lis1 may be a key step in the initiation of dynein-mediated transport. Using single-molecule and optical trapping assays, we investigated how Lis1 binding affects the motility and force generation of yeast dynein in vitro. We showed that Lis1 does not slow dynein motility by serving as a roadblock or tethering dynein to microtubules. Lis1 binding also does not affect the forces that stall dynein movement, but it induces prolonged stalls and reduces the asymmetry in force-induced detachment of dynein from microtubules. Mutagenesis of the Lis1 binding sites on dynein's stalk partially recovers this asymmetry but does not restore dynein velocity. We propose that Lis1 binding slows dynein motility by disrupting nucleotide-induced rearrangements within the AAA+ ring and that Lis1's interaction with dynein's stalk slows force-induced detachment of dynein from microtubules.

Introduction

Cytoplasmic dynein-1 (dynein hereafter) is the primary motor responsible for motility and force generation towards the minus ends of microtubules[12]. Dynein transports membranous organelles, vesicles, mRNA, and unfolded proteins towards the nucleus, drives retrograde transport in neurons, and plays crucial roles in cell division[3]. Mutations that impair dynein function are linked to severe neurodegenerative and developmental disorders[10].

The dynein complex consists of the dynein heavy chain (DHC) and associated subunits (Fig. 4.1a). The tail domain of the DHC facilitates dimerization and recruits other subunits. The motor domain forms a catalytic AAA+ ring that connects to the tail via the linker domain and to the microtubule via a coiled-coil stalk[13,14] (Fig. 4.1a). ATP hydrolysis in the AAA+ ring is coupled to the swinging motion of the linker at the surface of the ring, which powers minus-end-directed motility and generates force[58]. Nucleotide hydrolysis also controls the binding and release of the motor from the microtubule by altering the registry of the stalk coiled coils[22]. Isolated dynein adopts an autoinhibited "phi" conformation and exhibits diffusive or nonprocessive motility on microtubules[25,30,111]. Processive motility is activated when dynein forms the dynein-dynactin-adaptor complex with its cofactor dynactin and the coiled-coil domain of adaptor proteins that link dynein to its many cargos[32,81].

Dynein-mediated transport also requires Lis1, which is the only known regulatory protein that directly binds to the dynein motor domain[85]. Heterozygous mutations in the *LIS1* gene lead to

neuronal migration deficiency during embryonic brain development and cause severe neurodevelopmental disease, lissencephaly[112]. Lis1 consists of an amino-terminal dimerization domain and a carboxy-terminal WD40 β-propeller domain that binds to dynein's motor domain at two sites, one on dynein's AAA+ ring and the other on dynein's stalk (Fig. 4.1a)[49,85,113]. Studies in live cells showed that Lis1 is a required cofactor for recruitment of dynein to kinetochores, the nuclear envelope, and the cell cortex, and the initiation of dynein-mediated transport of a wide variety of cargos, including Rab6-vesicles, lysosomes, and ribonucleoprotein complexes (reviewed in[114]). However, Lis1 has been reported to be absent from moving dynein cargos[86,90,115,116], suggesting that it is not required for dynein motility.

Recent in vitro and in vivo studies have proposed that Lis1 facilitates the assembly of active dynein-dynactin-adaptor complexes by preventing dynein from adopting the phi conformation[106,117-119]. Unlike dynactin, Lis1 is not required for subsequent dynein motility, and it appears to dissociate from most dynein complexes during or after the activation of processive motility[117,118]. Dissociation of Lis1 may be a key step in dynein activation because the comigration of Lis1 substantially reduces the velocity of dynein complexes in vitro[117], and enhancing the affinity of dynein for Lis1 leads to defects in nuclear migration in the budding yeast, *S. cerevisiae*[97]. Several models have been proposed to explain how Lis1 binding pauses or slows down dynein motility. In vitro studies reported that Lis1 binding increases dynein's microtubule-binding affinity[45,85,120,121]. Cryo-electron microscopy of Lis1-bound to dynein at the AAA+ site suggested that Lis1 clamps multiple AAA subunits together, trapping dynein in a conformation with high microtubule binding affinity, and possibly preventing rearrangements of the AAA subunits needed to switch to the low affinity conformation[113]. In addition, Lis1 binding to dynein has been proposed to inhibit or slow dynein motility by blocking the powerstroke of its linker domain[45], or by tethering dynein to the microtubule[119]. Lis1 was also shown to interact with the coiled-coil stalk of dynein when the AAA3 site is trapped in the ATP-bound state, and this interaction induces a lower microtubule affinity state[49]. Structure-guided mutations showed that the Lis1-stalk interaction is important for the localization of dynein to the cortex of yeast cells[49,113]. However, it remains to be determined how the Lis1-stalk interaction affects the mechanism of dynein motility.

In this study, we used single-molecule imaging and optical trapping to investigate how Lis1 binding affects the motility and force generation of *S. cerevisiae* cytoplasmic dynein. Similar to mammalian dynein, Pac1 (the Lis1 homolog in *S. cerevisiae*, "Lis1" hereafter) binding to yeast dynein prevents it from adopting the phi confirmation, and mutants that cannot form the phi conformation partially rescue dynein function in yeast lacking Lis1[119]. Unlike mammalian dynein, yeast dynein is processive in the absence of dynactin and a cargo adaptor[26], and it has similar stepping and force generation properties to active mammalian dynein-dynactin-adaptor complexes[39,47,50,51,62]. Therefore, yeast dynein serves as a simpler model to investigate how Lis1 binding affects the intrinsic motility and force generation properties of dynein. Consistent with previous observations[45,85,120,121], here we find that Lis1 binding slows dynein motility, induces longer run times on microtubules in unloaded conditions, and results in slower microtubule detachment of dynein under hindering forces. We find that Lis1 weakly interacts with the microtubule lattice, but that this interaction does not slow dynein motility. Our optical trapping measurements show that Lis1 does not reduce the dynein stall force, but rather decreases the asymmetry in velocity of dynein from the microtubule under force. Mutations that disrupt Lis1's interactions with dynein's stalk partially restore the asymmetric detachment of dynein from

microtubules in the presence of Lis1. These observations provide new insight into the mechanism of dynein regulation by Lis1.

Results

Lis1 binding stoichiometrically slows down dynein motility

We expressed the full-length DHC (*DYN1*) with an amino-terminal GFP tag and a carboxy-terminal HaloTag from its endogenous locus in an *S. cerevisiae* strain lacking the genes encoding Lis1 (*PAC1*), the Lis binding protein, NudEL (*NDL1*), and the p150 subunit of dynactin (*NIP100*, Table 4.1). The DHC co-purified with the endogenous dynein light intermediate chain (Dyn3), light chain (Dyn2), and intermediate chain (Pac11)[26]. We monitored the motility of this endogenously expressed complex (hereafter dynein) on surface-immobilized microtubules in the presence and absence of Lis1 using total-internal reflection fluorescence (TIRF) microscopy (Fig. 4.1a). Consistent with a previous report[85], GFP-dynein moved at 112 ± 5 nm s^{-1} (mean $\pm$ s.e.m.) in the absence of Lis1, and unlabeled Lis1 slowed dynein motility by 77% with a dissociation constant (K_D) of 17.9 ± 2.5 nM ($\pm$s.e., Fig. 4.1b,c). Lis1 also increased the run time of individual motors, indicating that Lis1 increases the microtubule-binding affinity of dynein (Fig. 4.1d).

To determine how many Lis1 dimers can bind to a dynein dimer, we separately labeled two different batches of Lis1 with TMR and LD655 dyes. We then monitored the colocalization of TMR-Lis1 and LD655-Lis1 with moving GFP-dynein in a three-color TIRF assay. In this assay, colocalization of dynein with a single color of Lis1 might be due to one or two Lis1 dimers bound per dynein, whereas colocalization of both dyes with the GFP signal would ensure that two Lis1 dimers are bound to dynein. We observed either LD655-Lis1 or TMR-Lis1 translocating together with dynein on microtubules at similar colocalization percentages (14% each; Fig. 4.1e). A small fraction (1%) of GFP-dynein motors colocalized with LD655- and TMR-Lis1 simultaneously, suggesting that a single dynein motor can recruit two Lis1 dimers (Fig. 4.1e,f), but this occurred rarely in our assay conditions[99]. Similar to mammalian dynein-dynactin-adaptor complexes[117,118], yeast dynein motors that colocalized with a single color of Lis1 moved slower (41 ± 1 nm s^{-1}) than motors that did not colocalize with Lis1 (110 ± 1 nm s^{-1}). When dynein co-localized with two Lis1 dimers, its velocity was further reduced (21 ± 4 nm s^{-1}) and its run time was further increased (Fig. 4.1f, Fig. 4.2a). We also observed that transient binding of Lis1 paused or slowed dynein, whereas unbinding of Lis1 restored dynein's velocity (Fig. 4.1g, Fig. 4.2b). The velocity of dynein motors not colocalizing with Lis1 was similar to the dynein velocity when there was no Lis1 in the chamber (Fig. 4.1h). Therefore, Lis1 slows dynein motility only when it is directly bound to the motor, and the presence of excess Lis1 in the chamber does not affect dynein movement.

Previously, we showed that human Lis1 facilitates the recruitment of two dyneins to the dynactin-adaptor complex by opening dynein's autoinhibited phi-conformation[117,118]. It is also possible that a Lis1 dimer can simultaneously bind to the motor domains of two dynein dimers (Fig. 4.1i) and recruit them together to the dynactin-adaptor complex. To test whether yeast Lis1 can simultaneously bind two dynein dimers, we differentially labeled two batches of dynein with LD555 and LD655 dyes and monitored their comigration on microtubules in the presence or absence of Lis1. Because the yeast strain we purify endogenous dynein from lacks the *NIP100*

gene, a functional dynactin complex should not be present in our assays, and colocalization of two dyneins could only be mediated by Lis1. In the absence of Lis1, we observed less than 1% colocalization between dynein labeled with LD555 and LD655. The presence of Lis1 led to a marginal increase in colocalization between the differentially labeled dyneins, but these events were extremely rare (2%, Fig. 4.1i), suggesting that Lis1 does not effectively crossbridge two dyneins.

Lis1's interaction with the microtubule does not affect dynein velocity

Unlike mammalian Lis1[117,118], yeast Lis1 has been reported to interact with microtubules[119]. Because the concentration of Lis1 scaled with Lis1's ability to reduce dynein velocity, the authors proposed that yeast Lis1 slows dynein by binding both dynein and the microtubule[119]. This tethering model requires that 1) either one Lis1 β-propeller in a Lis1 dimer interacts with dynein and the other with the microtubule, or 2) a single Lis1 β-propeller interacts simultaneously with both dynein and microtubule (Fig. 4.3a). The first model predicts that Lis1 monomers would not affect dynein's velocity. To test this, we measured the velocity of dynein in the presence of either wild-type Lis1 dimer (Lis1^{WT}) or monomeric Lis1 lacking its amino-terminal dimerization domain (Lis1^{monomer})[85]. We observed that both dimers and monomers of Lis1 slowed dynein motility in a dose-dependent manner[85] (Fig. 4.3b). Thus, if Lis1 crosslinks dynein to microtubules, it must do so in the context of a monomer, with one face of Lis1 interacting with dynein and a different one interacting with microtubules.

The second model predicts that mutants that disrupt Lis1 binding to dynein would not disrupt Lis1 microtubule binding as the interfaces involved must be different. To test this, we characterized how Lis1 interacts with microtubules in vitro. As previously reported[119], Lis1^{WT} decorates microtubules in 50 mM KAc (Fig. 4.3c). Lis1 maintained microtubule-binding when the carboxy-terminal tails of tubulin were cleaved by subtilisin treatment (Fig. 4.3d, Fig. 4.4a). However, there was little to no microtubule decoration of Lis1 at a physiologically relevant salt concentration (150 mM KAc; Fig. 4.3c). We next used Lis1 mutants where a single (Lis1^{R378A}) or five (Lis1^{5A}) positively charged residues in Lis1's β-propeller domain were mutated to alanine. These mutations disrupt Lis1's binding to dynein's AAA+ ring (Fig. 4.3b)[45]. Unlike Lis1^{WT}, Lis1^{R378A} and Lis1^{5A} were unable to decorate microtubules in 50 mM KAc (Fig. 4.3e, Fig. 4.4c-f). Lis1^{5A} also did not bind to microtubules in microtubule pelleting assays (Fig. 4.4g), indicating that a Lis1 monomer would not be capable of crosslinking dynein to microtubules. We conclude that Lis1 interacts with the microtubule lattice primarily through electrostatic interactions between negatively charged microtubules and basic amino acids at the dynein-interacting surface of Lis1's β-propeller domain. However, this interaction is not strong enough to sustain microtubule binding in physiologically-relevant salt concentrations, consistent with the lack of microtubule colocalization of Lis1 in yeast cells[97].

Unlike our observations (Fig. 4.1h), Marzo et al. reported that the presence of Lis1 is sufficient to reduce the velocity of dynein motors that do not comigrate with Lis1[119]. This observation is inconsistent with the tethering model, which requires the comigration of Lis1 to slow dynein motility. Alternatively, Lis1 may serve as a static obstacle against dynein motility on the microtubule surface, akin to microtubule-associated proteins (MAPs)[122]. Because all dyneins would encounter microtubule-bound Lis1, this model predicts a similar reduction in velocity for dyneins that comigrate with Lis1 and those that are not bound to Lis1[119]. We pre-decorated

microtubules with excess Lis1 with no added salt and washed away free Lis1 from the chamber (Fig. 4.4h). The velocity of dynein on Lis1-decorated microtubules was similar to its velocity on undecorated microtubules (Fig. 4.3f), demonstrating that microtubule decoration of Lis1 does not substantially slow dynein motility along these tracks.

To understand how Lis1 might slow motility without comigrating with dynein, we purified dynein from the *S. cerevisiae* strain used by Marzo et al.[119], which overexpresses DHC and each of its associated chains under the galactose promoter (hereafter dynein$_{Gal}$). Similar to dynein expressed using the endogenous promoter (Fig. 4.1), dynein$_{Gal}$ had an increased run length and run time when colocalized with Lis1 (Figs. 4.5-4.7). However, dynein$_{Gal}$ motors moved significantly slower whether or not they colocalized with Lis1 in the chamber (Fig. 4.6d), as reported[119]. The reduction in dynein$_{Gal}$ velocity was not due to decoration of the microtubule surface by Lis1, because Lis1 addition slowed dynein$_{Gal}$ even when it did not decorate microtubules under physiological salt (150 mM; Fig. 4.5). We next introduced or removed Lis1 from the chamber while recording dynein$_{Gal}$ motility. Introducing Lis1 into the chamber did not alter the velocity of dynein$_{Gal}$ motors that were already moving along the microtubule at the time Lis1 was added (Fig. 4.8a-c). Likewise, the removal of free Lis1 from the chamber failed to recover dynein$_{Gal}$ velocity (Fig. 4.8c). While the underlying mechanism remains unclear, the differences between the Lis1-mediated regulation of dynein subunits expressed under their endogenous promoters and dynein$_{Gal}$ may be related to different stoichiometries of the dynein-associated chains in purified complexes or the tendency of dynein$_{Gal}$ to aggregate after purification[119].

Lis1 does not affect dynein stall force

We next investigated whether Lis1 binding slows dynein motility by interfering with the swinging motion of the linker at the surface of the ring, as previously proposed[45]. Because the linker drives the force-generating powerstroke of dynein, this model predicts that Lis1 binding reduces the ability of dynein to walk against hindering forces. To test this possibility, we returned to using the full-length dynein complex expressed under endogenous promoters and measured the stall force of GFP-dynein in the presence and absence of excess (300 nM) Lis1 using an optical trap (Fig. 4.9a). In the absence of Lis1, dynein stalled at 3.8 ± 0.1 pN (mean $\pm$ s.e.m., N = 116 stalls) and remained attached to the microtubule for 14.6 ± 0.8 s (mean $\pm$ s.e.m.) before the bead snapped back to the trap center[47] (Fig. 4.9b,c). The stall force was unaltered by Lis1 addition (3.8 ± 0.1 pN, N = 126 stalls; Fig. 4.9b,c), suggesting that Lis1 does not disrupt the force-generating powerstroke of the linker. However, the Lis1 addition resulted in a 70% increase in the duration of the stalls (24.7 ± 0.9 s, p = 0.018, Kolmogorov-Smirnov test), indicating that Lis1 reduces the microtubule detachment rate of dynein under hindering forces (Fig. 4.9d). Unlike full-length dynein, Lis1 binding reduced the stall force of tail-truncated GST-dimerized dynein (GFP-GST-Dyn$_{331kDa}$ and GFP-GST-Dyn$_{314kDa}$) constructs[47,123], suggesting that artificial dimerization of the linkers at the exit of the ring introduces a steric obstacle against their swinging motion when Lis1 is present on the outer surface of the ring (Fig. 4.10). However, Lis1 binding does not affect the force generation of full-length dynein, presumably because the longer length of the full-length dynein tails has greater flexibility compared to the truncated dynein constructs used by Toropova et al.[45].

Lis1 reduces the asymmetry in force-induced detachment of dynein

Because Lis1 increases the microtubule affinity of dynein (Fig. 4.1)[49,85,113], we also tested whether Lis1 binding slows dynein motility by altering the detachment kinetics of dynein from the microtubule. Nucleotide hydrolysis in dynein's AAA+ ring controls its microtubule affinity by altering the registry of the stalk coiled coils[54,63,64]. The stalk sliding mechanism is also sensitive to external forces, such that dynein releases quickly from the microtubule and moves substantially faster when it is pulled in the assisting direction (towards the minus-end of microtubules), but it strongly resists backward movement when pulled in the hindering direction[47,54]. If Lis1 binding interferes with this mechanism, we anticipated that the addition of Lis1 would reduce the asymmetry in the force-induced velocity of dynein. To test this prediction, we measured the velocity of dynein motors when they were subjected to constant forces in assisting and hindering directions using a force-feedback controlled trap. Dynein responded asymmetrically to external forces in the absence of Lis1 and its force-velocity (F-V) behavior in 2 mM ATP could be explained by the asymmetric potential barrier for the release of the motor from the microtubule[63] (Fig. 4.11a). The addition of 300 nM Lis1 reduced dynein velocity when the motor was being pulled in both directions (Fig. 4.11b). The velocity was reduced more substantially under assisting forces than under hindering forces (Fig. 4.11c,d), resulting in a reduced asymmetry in the F-V behavior of dynein in the presence of Lis1.

We reasoned that Lis1 binding may reduce the asymmetry in F-V by interfering with either the linker swing or the stalk sliding mechanisms of the dynein motor domain. To distinguish between these possibilities, we repeated the F-V measurements in the absence of ATP. The swinging motion of the linker is strictly coupled to the ATP hydrolysis cycle, whereas the registry of the stalk coiled-coils can be altered by external force even in the absence of ATP[64]. Similar to the ATP condition, Lis1 addition decreased dynein velocity when the motor was pulled in both directions and the decrease in velocity was more substantial when the motor was pulled in the assisting direction in the absence of ATP (Fig. 4.12a,b). These results suggest that Lis1 binding slows the detachment of dynein from microtubules by interfering with the stalk sliding mechanism.

Recently, we have shown that Lis1 stably interacts with a second binding site at the base of dynein's stalk when the AAA3 site of dynein is trapped in the ATP-bound state[49]. To test whether this Lis1-stalk interaction might be responsible for Lis1's ability to reduce the asymmetry in force-induced detachment of dynein from microtubules, we performed F-V measurements using a dynein mutant, in which three Lis1-interacting residues on its stalk were replaced with alanine (dynein[EQN], purified from yeast expressing dynein and its subunits from their endogenous promoters)[49]. We first confirmed that dynein[EQN] motility is slowed down by Lis1, albeit with a ~3-fold higher K_D (54 ±10 nM, ±s.e.) compared to that for wild-type (WT) dynein[49] (Fig. 4.13a,b). Similar to WT dynein, the binding of two Lis1 dimers further slowed dynein[EQN] motility (Fig. 4.13c,d). In the absence of Lis1, dynein[EQN] also had similar stall force, but lower stall durations relative to WT dynein (p = 0.03, Kolmogorov-Smirnov test, Fig. 4.13E-F). To determine how Lis1 affects stall force and F-V behavior of dynein[EQN], we used higher concentrations of Lis1 (900 nM) to compensate for dynein[EQN]'s lower affinity for Lis1[49]. The addition of Lis1 resulted in only minor changes in the stall force and stall time of dynein[EQN] (Fig. 4.13e-g). Thus, the mutagenesis of the stalk interaction site of Lis1 does not abrogate its ability to induce a high microtubule affinity for dynein. However, unlike WT dynein, the addition of

Lis1 did not reduce the asymmetry of dynein[EQN]'s F-V behavior (Fig. 4.14 and Fig. 4.15). Collectively, these results show that the Lis1-ring interaction is primarily responsible for the reduction of dynein velocity in Lis1-bound dynein and that the Lis1-stalk interaction reduces the asymmetry in force-induced detachment of dynein from the microtubule.

Discussion

Lis1 is a required cofactor for the initiation of dynein-mediated transport, but it needs to dissociate from the dynein complex to enable rapid transport of intracellular cargos[117-119]. In this study, we used single-molecule imaging to test the models that describe how Lis1 slows dynein motility when it remains bound to the dynein motor domain[45,85,95,119]. We also performed optical trapping studies of active dynein complexes in the presence of Lis1 to understand how Lis1 binding affects force generation and force response of dynein. We showed that Lis1 binding does not affect the dynein stall force, indicating that the linker can perform its force-generating powerstroke when Lis1 is bound to the AAA+ ring. This result is consistent with the ability of dynein motors to walk processively, albeit at lower speeds, when colocalized with Lis1[117], whereas disrupting the linker swing mechanism fully abrogates the motility[24,55]. We also showed that Lis1's interaction with the microtubule at low salt is not primarily responsible for slower motility, because Lis1 does not bind microtubules but still slows down dynein motility under physiological salt. Furthermore, decoration of the microtubule surface with Lis1 does not serve as an efficient obstacle against dynein motility, because dynein motors walk on these microtubules at full speed.

We observed that dynein moves slowly and runs on microtubules for a longer time when it colocalizes with a single Lis1, and its velocity decreases while its run time increases further when colocalized with two Lis1s. Lis1-bound dynein also persists against microtubule detachment for longer durations under hindering forces and moves slower under both assisting and hindering forces. Consistent with previous reports[49,85,113], these results indicate that Lis1 binding increases the microtubule binding affinity of dynein. Mutagenesis of the Lis1 interaction site on dynein's stalk in dynein[EQN] did not recover dynein velocity, demonstrating that Lis1's interaction with the AAA+ ring is primarily responsible for slower movement[49,113]. These results are consistent with a model in which Lis1 binding to the AAA+ ring prevents nucleotide-induced rigid body motions of the AAA+ subunits and traps the AAA+ ring in the high microtubule affinity conformation[49], resulting in a slower velocity.

Our optical trapping measurements provide evidence that Lis1 restricts the registry shift of the stalk coiled coils under external forces. Without Lis1, the dynein stalk switches from the strongly-bound to the weakly-bound registry when dynein is subjected to assisting forces but remains in a strongly-bound registry under hindering forces[64]. Lis1 binding slows WT dynein speed in both assisting and hindering forces, but it has a more profound effect in limiting the acceleration of dynein under assisting forces. These results indicate that Lis1 binding may prevent dynein's stalk switching from the α registry to a registry with lower affinity. The Lis1 binding to dynein's stalk may restrict the registry shift of the coiled coils because Lis1 is less effective in reducing the speed of dynein motility under assisting forces when the stalk residues that interact with Lis1 were replaced with alanine.

We previously showed that Lis1 stably interacts with dynein's stalk and reduces microtubule affinity when the AAA3 site of dynein is unable to hydrolyze ATP and trapped at the ATP-bound state[49]. If the Lis1-stalk interaction also reduces microtubule affinity when the AAA3 site freely binds and hydrolyzes ATP, mutagenesis of the Lis1 interaction site on dynein's stalk would result in a more substantial reduction in velocity in the presence of external force. However, we observed that Lis1 is less effective in reducing the speed of dynein[EQN] velocity under assisting forces, indicating that the Lis1-stalk interactions lead to an overall increase in microtubule affinity of WT dynein as it walks along the microtubule. Future structural and mechanistic work will be required to investigate whether Lis1 interacts with the stalk at different states of the dynein mechanochemical cycle and how these interactions regulate the microtubule affinity of the motor.

Recent studies in fungi showed that Lis1-mediated activation is required for dynein function[106,119]. However, the dynein mutant that cannot adopt the phi conformation fails to fully rescue the deletion of Lis1 in *Aspergillus nidulans*[106], indicating that Lis1 may have additional regulatory roles, such as trapping the stalk coiled-coils in the high-affinity state when it remains bound to the motor domain. Lis1 may promote a high microtubule affinity state when dynein anchors large organelles to the microtubule network or pulls on astral microtubules during cell division[98-100]. Alternatively, a Lis1-mediated increase in microtubule affinity may contribute to the proper assembly of dynein with dynactin and an activating adaptor on the microtubule. In this scheme, Lis1 remains bound until an activating adaptor triggers its release from dynein during or after the assembly of the complex[96,98], its dissociation initiates dynein-driven transport. Future studies are required to determine whether the association and dissociation of Lis1 from dynein are regulated in different cellular contexts.

Figures and Tables
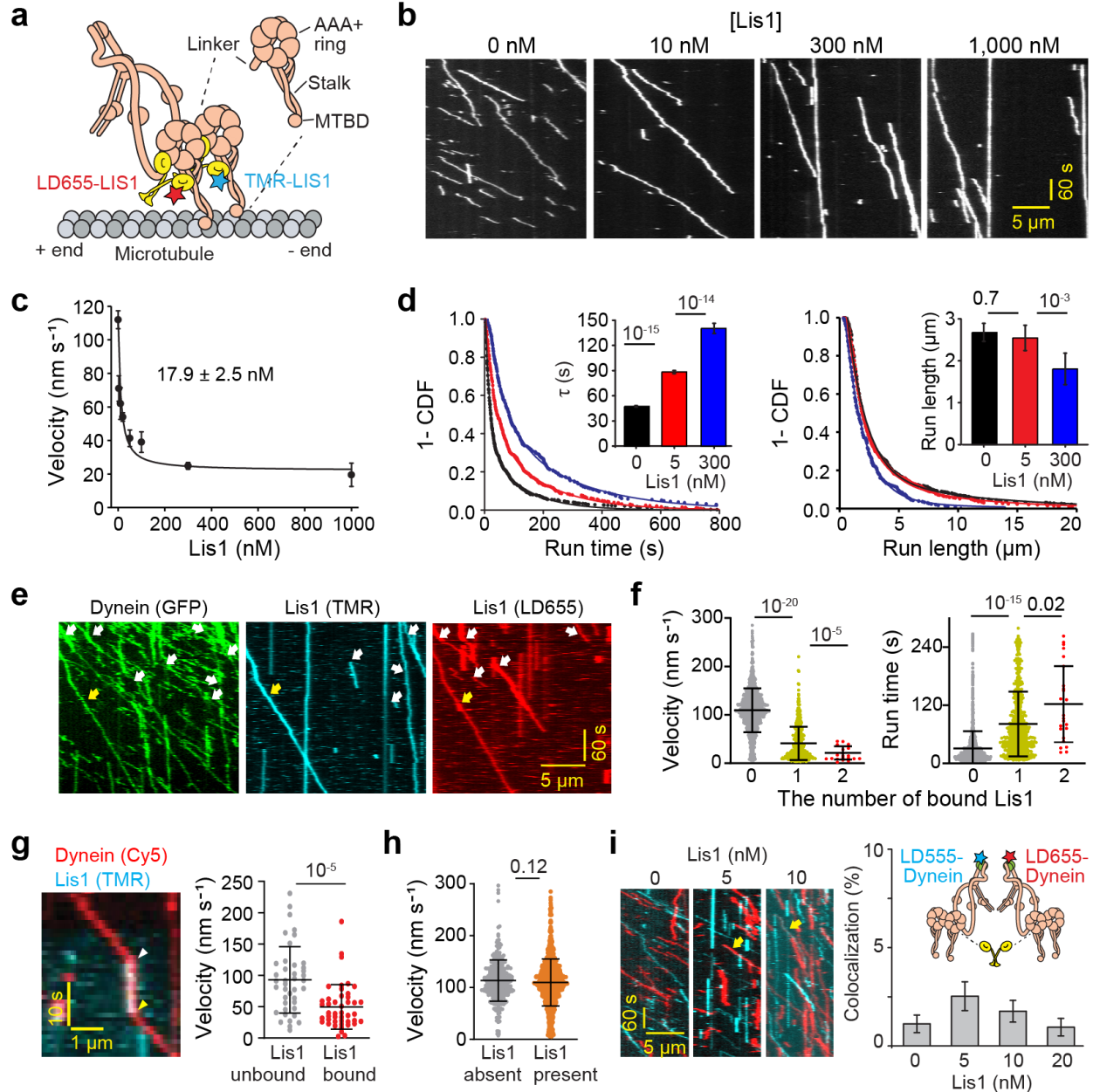
Figure 4.1: Lis1 binding reduces the velocity while increasing the microtubule residence time of dynein. a) Schematic of the single-molecule motility of yeast cytoplasmic dynein in the presence of fluorescently-labeled Lis1. **b**) Representative kymographs of dynein with increasing concentrations of unlabeled Lis1. **c**) The velocity of dynein under different Lis1 concentrations in 50 mM KAc, respectively (mean ± s.e.m.; N = 861, 534, 233, 352, 278, 312, 131 for 0, 5, 10, 20, 50, 100, 300, and 1,000 nM Lis1; three biological replicates). The fit of the velocity data (solid curve) reveals K_D (±s.e., see Methods). **d**) The inverse cumulative distribution function (1-CDF) of run time and run length under different Lis1 concentrations. Fits to a double exponential decay (solid curves) reveal average run time and run length in each condition (bar graphs, ± s.e.; N = 861, 534, 312 from left to right). **e**) A representative kymograph of GFP-dynein in the presence of 2 nM LD655- and 2 nM TMR-labeled Lis1. Arrows highlight processive motors colocalized with single (white) and two (yellow) colors of Lis1. **f**) The velocity and run time of dynein motors colocalized with 0, 1, and 2 Lis1s (mean ± s.d., N = 1706, 671, and 24 from left to right). **g**) (Left) A representative trace of transient binding (white arrowhead) and unbinding (yellow arrowhead) of Lis1 from processively walking dynein. (Right) The velocity of Lis1 unbound and bound sections of individual dynein trajectories (mean ± s.d., N = 41 and 45). **h**) The velocity distribution in the absence of Lis1 compared to the motors that do not colocalize with Lis1 when fluorescently-

46

labeled Lis1 is present in the chamber (N = 361 and 1534, from left to right). **i)** (Insert) Schematic shows whether a single Lis1 dimer can crossbridge two dynein dimers labeled with different dyes. (Left) Example kymographs 5 nM LD555-dynein (cyan) and 5 nM LD655-dynein (red) in the presence of different Lis1 concentrations. Yellow arrows show colocalization between LD555 and LD655 dyes. (Right) The percentage of dynein trajectories that exhibit colocalization between LD555 and LD655 dyes (N = 408, 378, 426, and 208 from left to right, three independent experiments). In **f**, **g**, and **h**, the centerline and whiskers represent the mean and s.d., respectively. In **d**, **f**, **g**, and **h**, P-values were calculated by a two-tailed t-test with Welch correction for velocity and by Kolmogorov-Smirnov test for run time and run length.
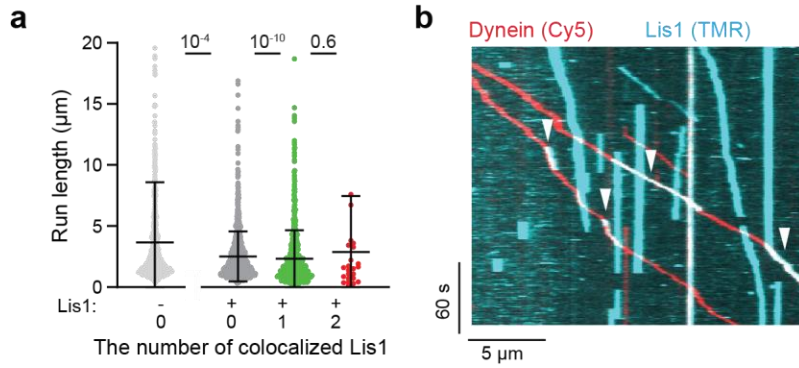
Figure 4.2: Transient binding of Lis1 slows down motility whereas Lis1 unbinding restores the velocity. a) The run length of dynein in the absence and presence of Lis1. In the presence of Lis1, run lengths were separately calculated for motors that colocalize with 0, 1, and 2 colors of Lis1. The center line and whiskers represent the mean and s.d., respectively. P-values were calculated by a Kolmogorov-Smirnov test. **b)** A representative kymograph shows that transient binding of Lis1 slows down whereas the subsequent release of Lis1 restores the velocity (arrowheads).
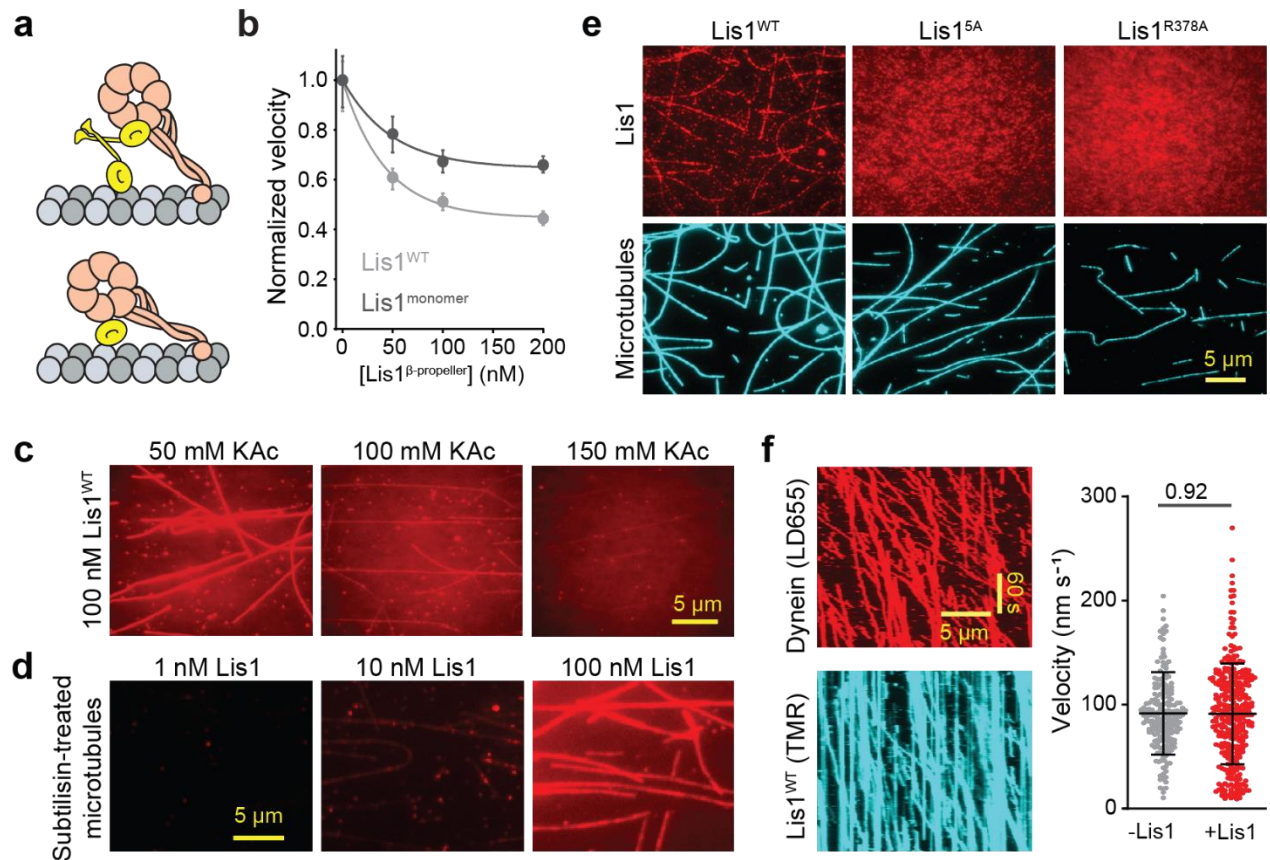
Figure 4.3: Lis1's interaction with microtubules does not slow down dynein motility. a) Models of dynein tethered to a microtubule via a Lis1 dimer with one Lis1 ß-propeller docked to dynein and the other on the microtubule (top) or one Lis1 ß-propeller simultaneously interacts with dynein and the microtubule (bottom). **b)** Single-molecule velocity of dynein with increasing concentrations of Lis1^{WT} or Lis1^{monomer}. The median and interquartile ranges are shown. Data were normalized to a velocity in the absence of Lis1. At least 400 single molecule events were measured per condition. **c)** Lis1 binding to surface-immobilized microtubules under different salt concentrations. **d)** Lis1 decorates subtilisin-treated microtubules in the presence of 50 mM KAc. **e**) Two-color imaging of Cy3-labeled microtubules and LD655-labeled Lis1^{WT}, Lis1^{5A}, or Lis1^{R378A}. Lis1 concentration was set to 100 nM and the assays were performed in a buffer containing 50 mM KAc. **f)** (Left) A representative kymograph of dynein motility on Lis1-decorated microtubules. Runs in the Lis1 channel colocalize with dynein. (Right) Velocities of dynein motors on undecorated (-Lis1) and Lis1-decorated (+Lis1) microtubules. (N= 208 and 329, from left to right). The center line and whiskers represent the mean and s.d., respectively. The P-value was calculated by a two-tailed t-test with Welch correction.

49
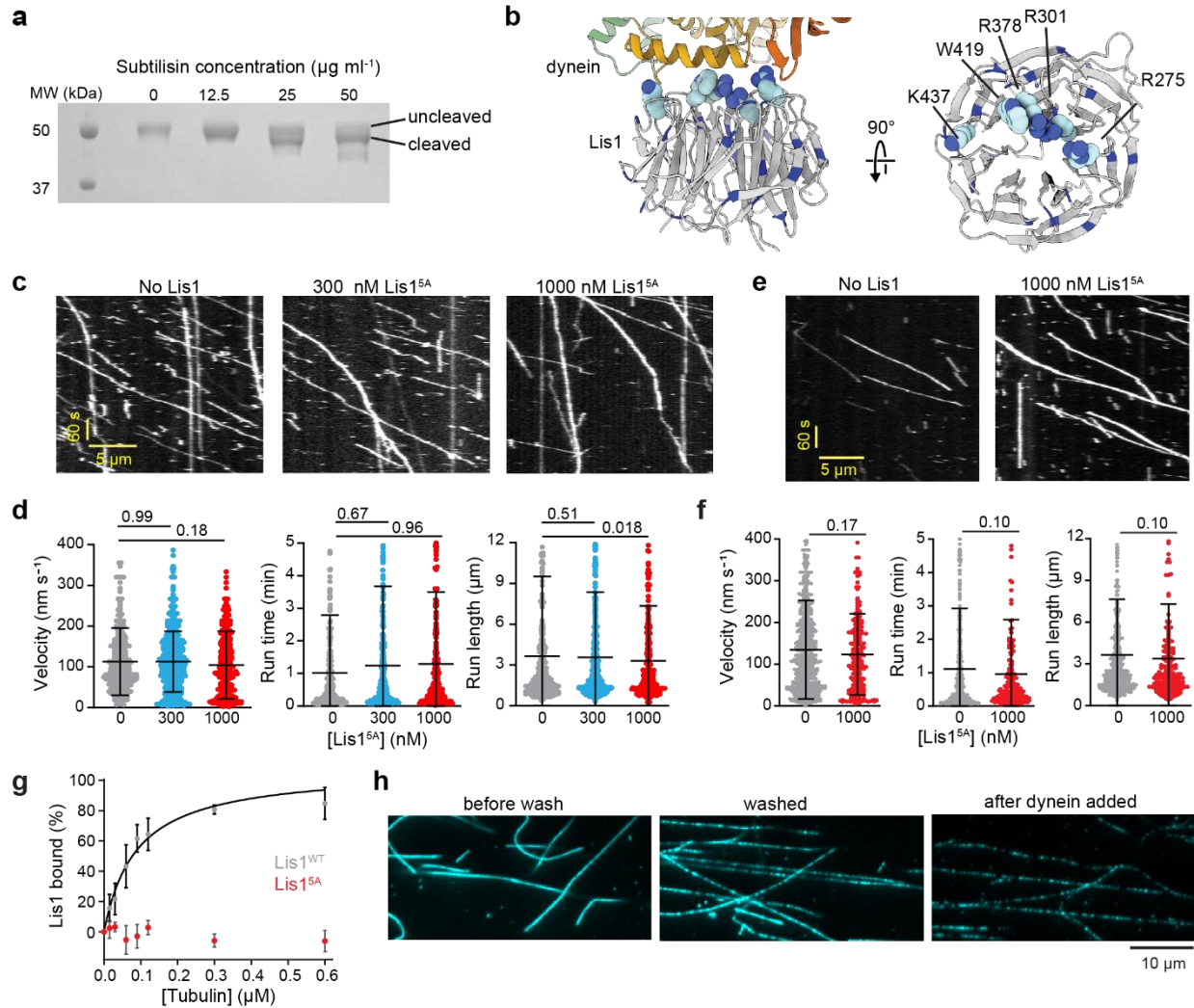
Figure 4.4: Lis1 interacts with the microtubule lattice through its dynein binding site in vitro. a) The subtilisin treatment of microtubules reduces the molecular weight of tubulin in a denaturing gel. **b**) The structure of Lis1 bound to the AAA ring with the five residues mutated in Lis1[5A] are shown as spheres and all lysine and arginine residues are in blue. **c**) Representative kymographs of dynein in the presence and absence of Lis1[5A]. **d**) The velocity, run time, and run length of dynein in the presence and absence of Lis1[5A] (N = 326, 534, 336 from left to right). **e**) Representative kymographs of dynein[Gal] in the presence or absence of 1 μM unlabeled Lis1[5A]. **f**) The velocity, run time, and run-length of dynein[Gal] in the presence or absence of 1 μM Lis1[5A] (N = 610 and 209 from left to right). **g**) Microtubule co-pelleting assay with Lis1[WT] and Lis1[5A] (mean ±s.e.m., three replicates per condition). Statistical analysis was performed using an extra sum-of-squares F test; p<0.0001. **h**) Surface-immobilized microtubules were decorated by 100 nM TMR-Lis1 before and after removing unbound Lis1 in the channel. In **c-f**, assays were performed in 50 mM KAc. Assays in **h** were performed in the absence of added salt to maximize the Lis1-microtubule interaction. In **d** and **f**, the center line and whiskers represent the mean and s.d., respectively. P values were calculated by a two-tailed t-test with Welch correction for velocity and by Kolmogorov-Smirnov test for run time and run length.
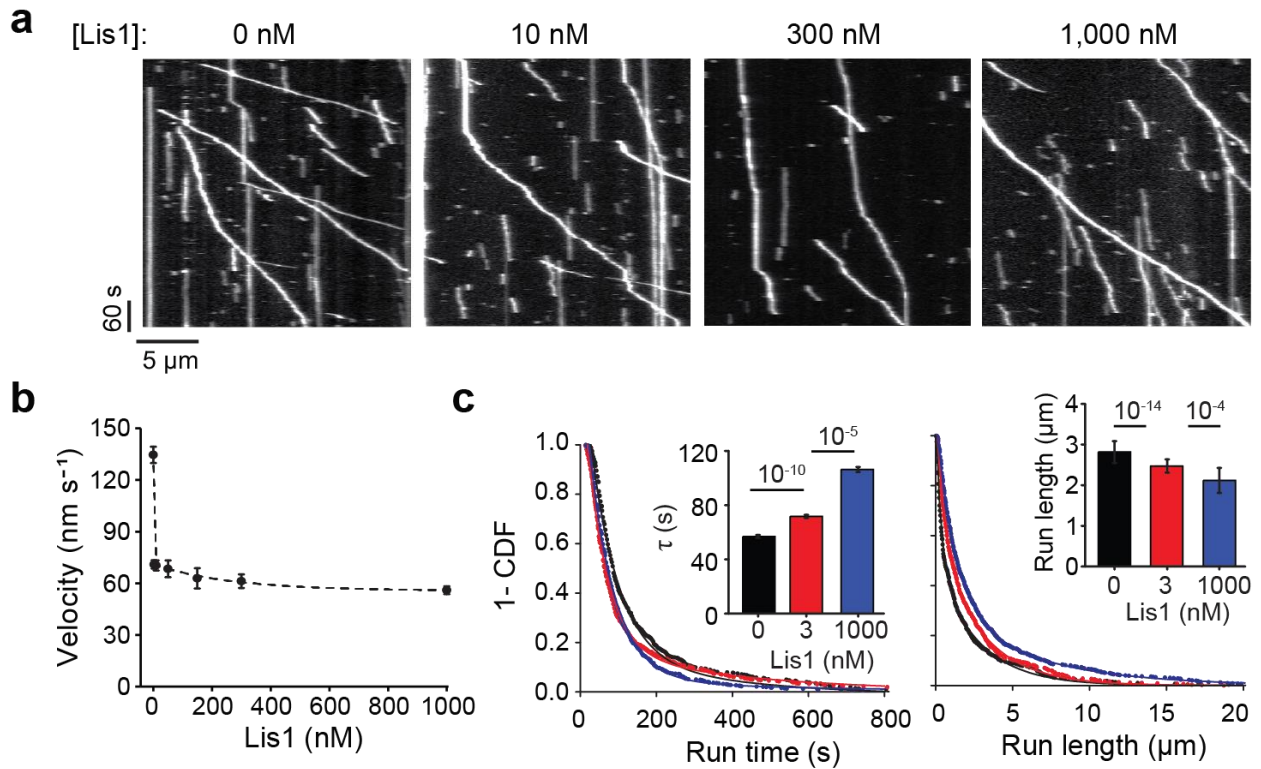
Figure 4.5: Motility of dynein_Gal in the presence of unlabeled Lis1. a) Representative kymographs of dynein_Gal with increasing concentrations of unlabeled Lis1. **b)** The velocity of dynein_Gal under different Lis1 concentrations in 150 mM KAC (mean ± s.e.m.; N = 611, 694, 604, 230, 260, 251, 852 for 0, 3, 10, 50, 150, 300, and 1,000 nM Lis1, respectively; two biological replicates). **c)** The inverse cumulative distribution function of run time and run-length of dynein_Gal under different Lis1 concentrations. Fits to a double exponential decay (solid curves) reveal the average run time and run length of the motor in each condition (bar graphs, ± s.e.; N = 611, 694, 251 from left to right).
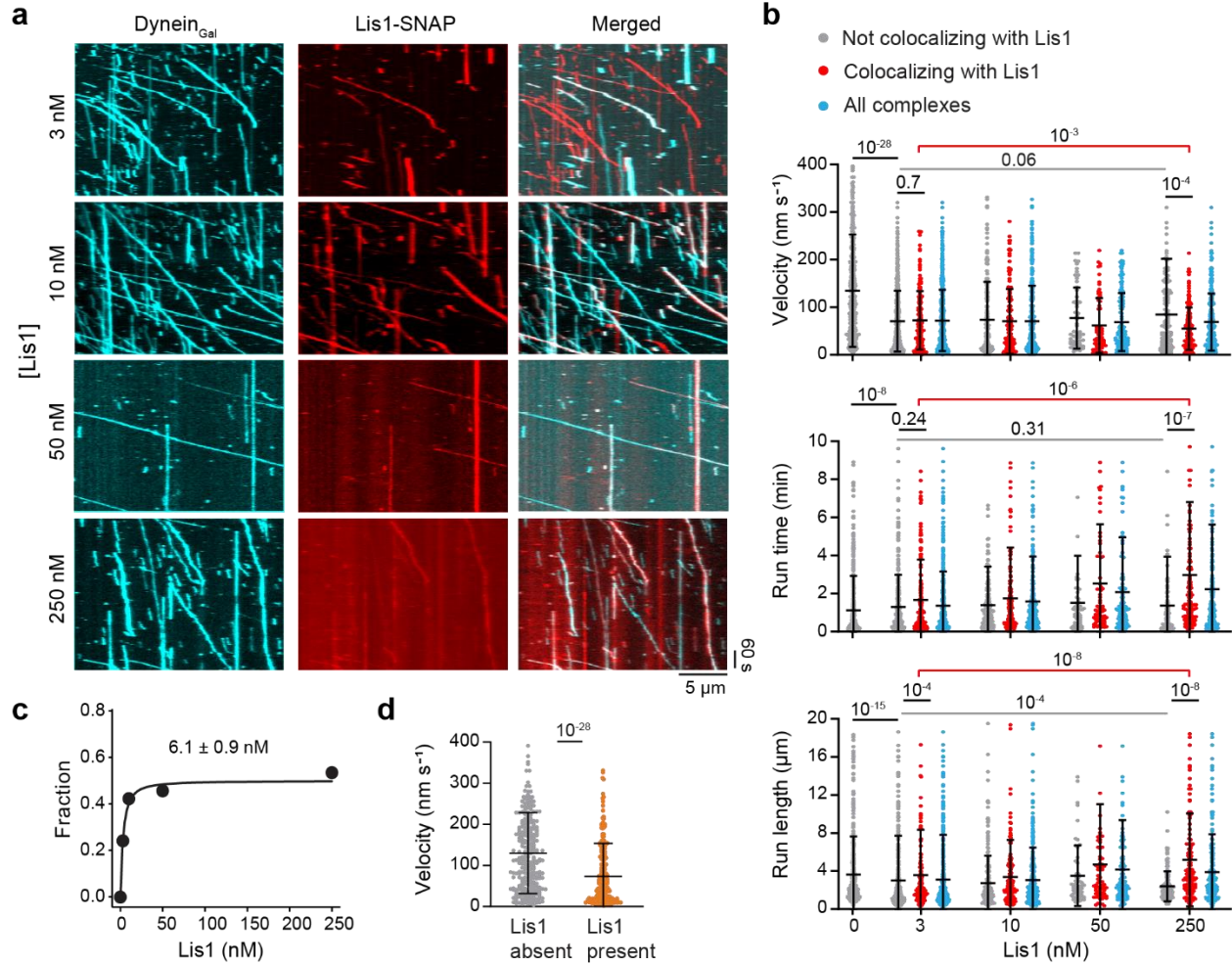
Figure 4.6: Motility of dynein_Gal in the presence of fluorescently-labeled Lis1. a) Representative kymographs of two-color imaging of LD655-labeled dynein_Gal and LD555-labeled Lis1 under different Lis1 concentrations. **b)** The velocity, run time, and run length distributions of dynein complexes under different concentrations of Lis1 (N = 611, 526, 168, 694, 233, 175, 408, 55, 69, 124,126, 145, 271 from left to right). **c)** The fraction of LD655-dynein complexes that colocalize with LD555-Lis1 under different Lis1 concentrations. A fit to a binding isotherm function (solid curve, see Methods) reveals K_D (±s.e.). **d)** The velocity distribution of dynein_Gal in the absence of Lis1 compared to the motors that do not colocalize with Lis1 when fluorescently-labeled Lis1 is present in the chamber (N = 611 and 233 from left to right). In **b** and **d**, the centerline and whiskers represent the mean and s.d., respectively. P-values were calculated by a two-tailed t-test with Welch correction for velocity and by Kolmogorov-Smirnov test for run time and run length.
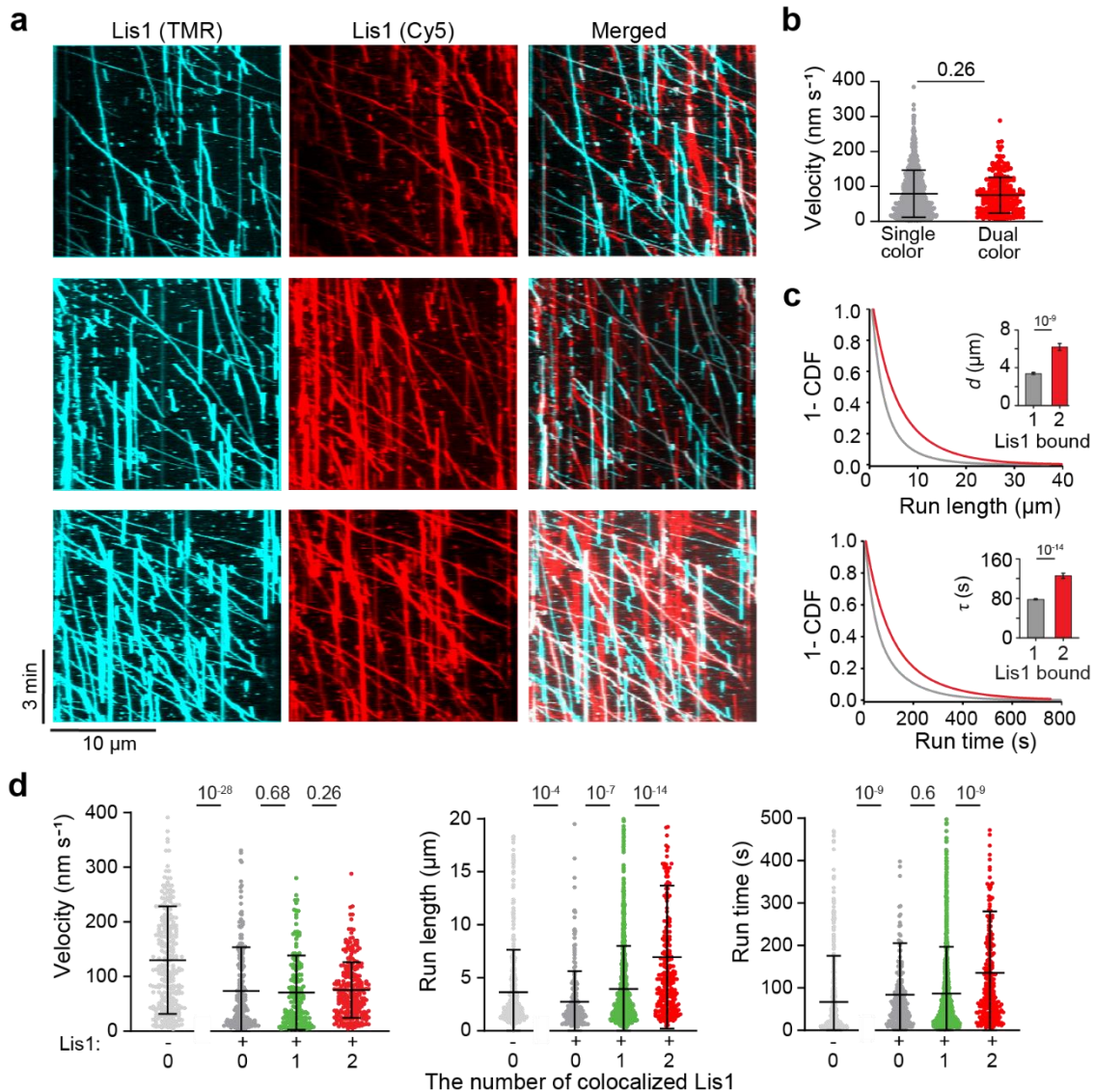
Figure 4.7: Binding of two Lis1s further increases the run time and run length, but not the velocity of dynein$_{Gal}$. a) Representative kymographs show colocalization of TMR- (5 nM) and Cy5-labeled (5 nM) Lis1 to unlabeled dynein$_{Gal}$. **b)** The velocity distribution of the trajectories that contain single (N = 811) or both (N = 216) colors of Lis1. The binding of second Lis1 to dynein$_{Gal}$ does not significantly reduce the velocity. **c)** Run length and run time of dynein$_{Gal}$ that colocalize with single (gray, N = 811) or both (red, N = 216) colors of Lis1. The binding of second Lis1 increases the run time and run length. Inserts show calculated run length and run time values (mean ± s.e.) from a fit to a double exponential decay (solid curves). P values were calculated by a Kolmogorov-Smirnov test. **d)** Velocity, run length, and run time distributions of dynein$_{Gal}$ in the absence and presence of Lis1 in the channel (N = 287, 233, 175, 274, from left to right). Dynein$_{Gal}$ motors that colocalize with 0, 1, or 2 colors of Lis1 were analyzed separately. In **b**, **c**, and **d**, the center line and whiskers represent the mean and s.d., respectively. P values were calculated by two-tailed t-tests with Welch correction for velocity and by Kolmogorov-Smirnov test for run time and run-length measurements.

53
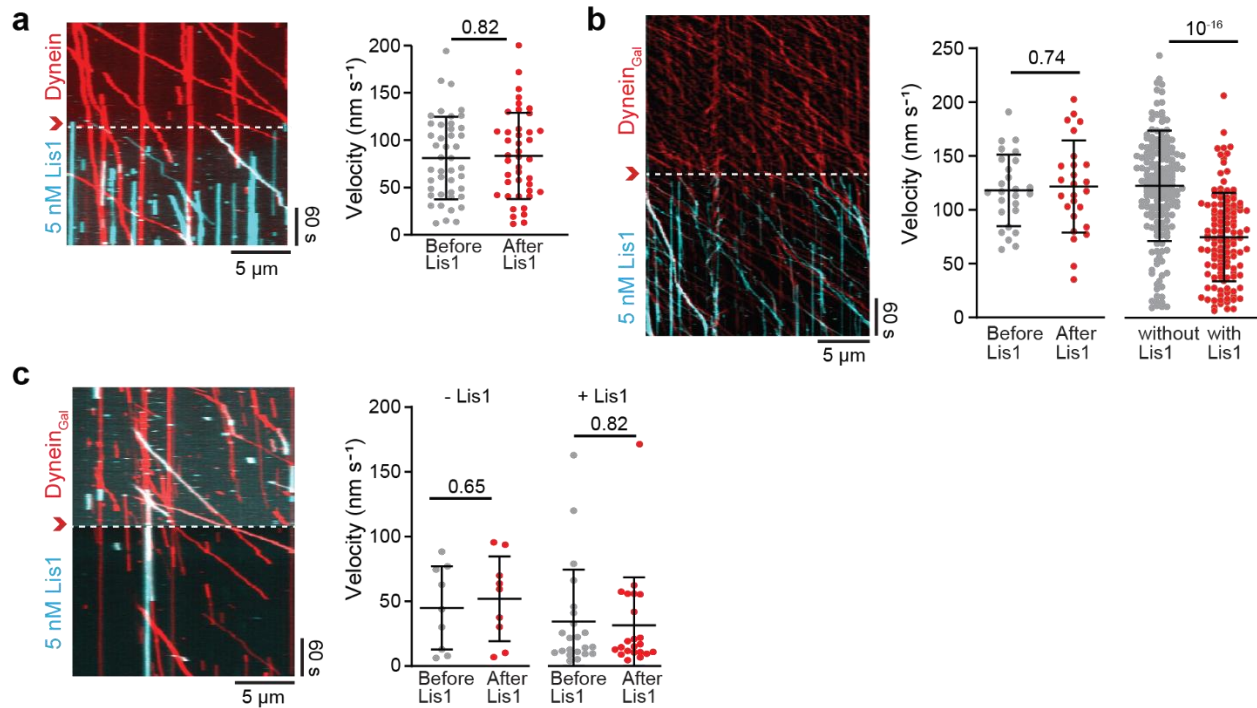
Figure 4.8: The addition and removal of Lis1 whilst recording dynein motility. a) A kymograph (left) and velocity (right) of dynein before and after Lis1 was flown into the flow chamber (N = 44 and 42 from left to right). **b)** A kymograph of dynein$_{Gal}$ when Lis1 was flown into the channel. (Middle) The velocity of the complexes that walk on the microtubules during Lis1 addition before and after flowing Lis1 (N = 26 and 26 from left to right). (Right) The velocity of the complexes that colocalize or do not colocalize with Lis1 after Lis1 addition (N = 122 and 84 from left to right). **c)** A kymograph (left) and velocity (right) of dynein$_{Gal}$ before and after washing excess Lis1 from the flow chamber. Complexes that colocalize (+Lis1) and not colocalize (-Lis1) with Lis1 were analyzed separately (N = 9, 9, 22, 22 from left to right). Assays were performed in 50 mM KAc. The center line and whiskers represent the mean and s.d., respectively. P-values were calculated by a two-tailed t-test with Welch correction.
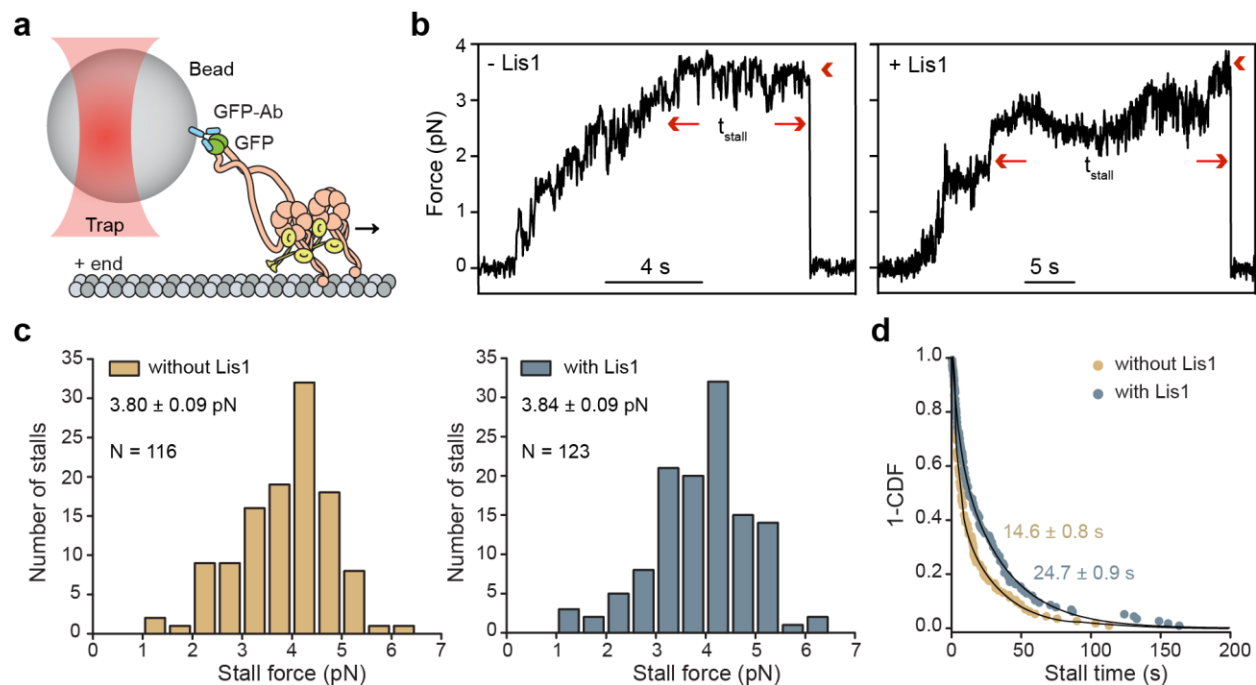
Figure 4.9: Lis1 does not affect the stall force of dynein. a) The schematic shows stall force measurements of GFP-dynein in the presence of unlabeled Lis1 using a fixed-beam optical trap. **b)** Sample trajectories of beads driven by single dynein motors with and without 300 nM Lis1. The arrows show the beginning and the end of a stalling event (t_{stall}: stall duration). The arrowheads indicate the detachment of the motor from the microtubule and the snapping of the bead to the trap center. **c)** The stall force histogram of dynein in the presence and absence of 300 nM Lis1 (mean ±s.e.m.; p = 0.77, two-tailed t-test). **d)** Stall durations of dynein with and without 300 nM Lis1. Fit to a double exponential decay (solid curves) reveals the average stall duration (±s.e.).
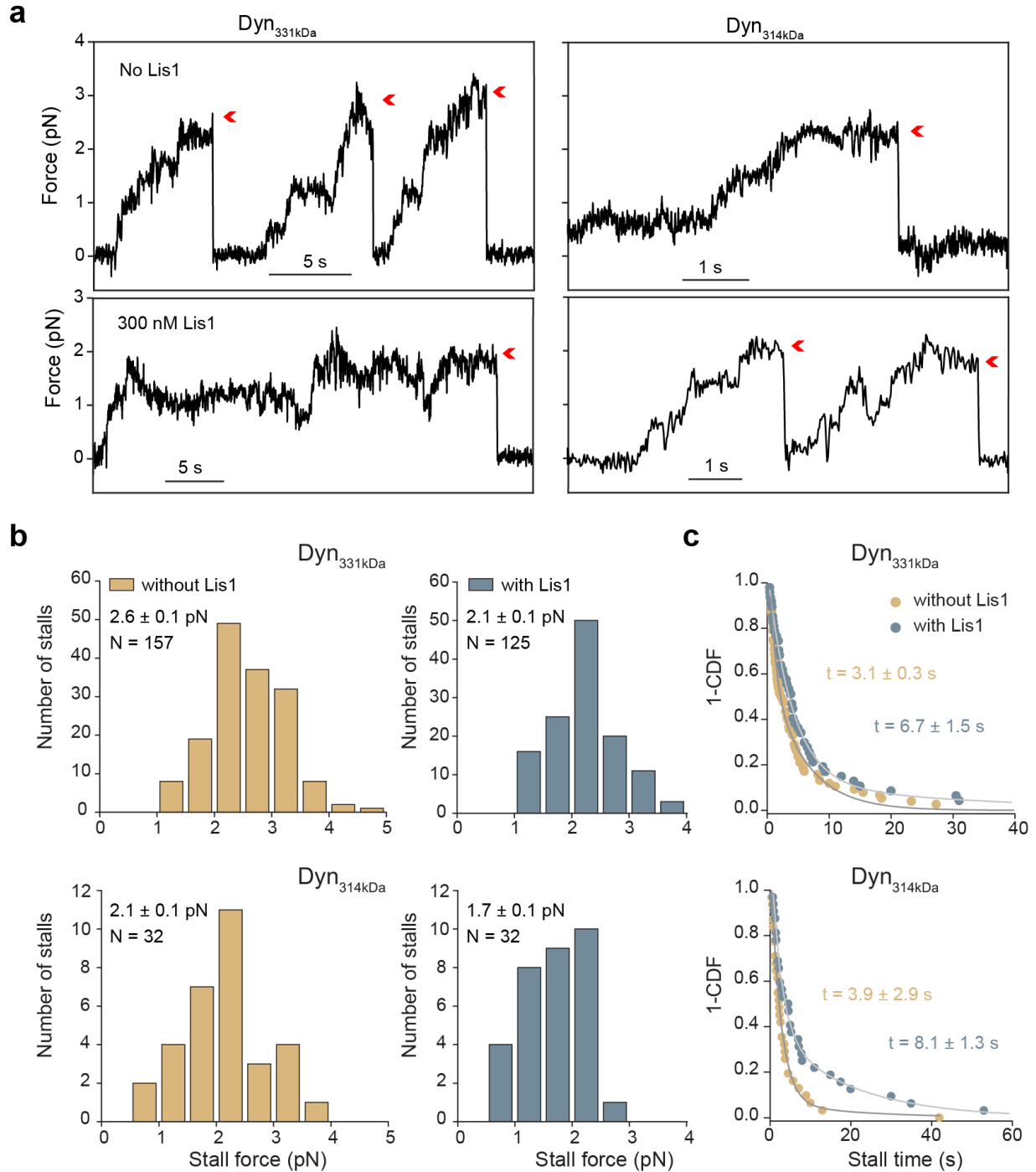
Figure 4.10: Lis1 reduces the stall force of the tail-truncated dynein. a) Representative trajectories of beads driven by GFP-GST-Dyn$_{331kDa}$ and GFP-GST-Dyn$_{314kDa}$ in the presence and absence of 300 nM Lis1. Red arrowheads represent the detachment of the motor from the microtubule followed by the snapping back of the bead to the trap center. **b)** Stall force histograms of Dyn$_{331kDa}$ and Dyn$_{314kDa}$ in the presence and absence of 300 nM Lis1 (mean ± s.e.m.; p = 2x10^{-7} for Dyn$_{331kDa}$ and 0.006 for Dyn$_{314kDa}$, two-tailed t-test). **c)** Stall durations of Dyn$_{331kDa}$ and Dyn$_{314kDa}$ in the presence and absence of 300 nM Lis1 (p = 0.22 and p = 0.1, respectively, Kolmogorov-Smirnov test). Fit to a double exponential decay (solid curves) reveals the average stall time (±s.e.).
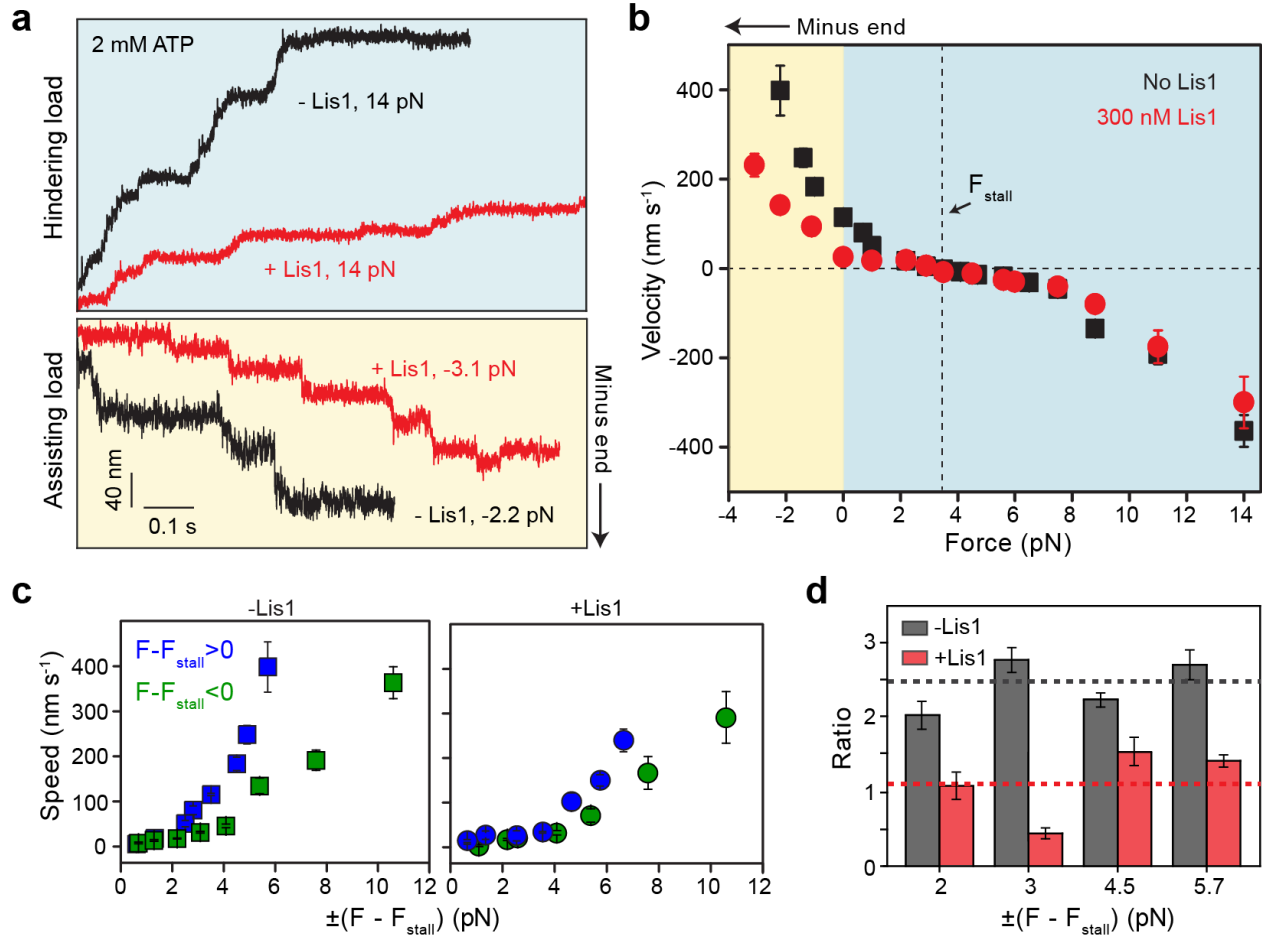
Figure 4.11: Lis1 reduces the asymmetry in the F-V behavior of dynein. a) Representative traces of dynein-driven beads under assisting and hindering loads with and without 300 nM Lis1. Assays were performed in 1 mM ATP and 50 mM KAc. **b)** F-V measurements of dynein in the presence and absence of 300 nM Lis1 (mean ±s.e.m., from left to right, N = 41, 38, 37, 861, 27, 52, 106, 28, 51, 60, 89, 115, 124, 62, 23, 38, 40 without Lis1 and 34, 52, 25, 312, 33, 42, 49, 37 62, 47 33 42, 36, 29, 18 with Lis1). **c)** The speed of dynein-driven beads (mean ± s.e.m.) under the same magnitude of forces (F) in assisting and hindering directions relative to the stall force (F_{stall}). **d)** The ratios of the dynein speeds under the same magnitude of forces in assisting and hindering directions relative to F_{stall}. The dashed lines represent the average of the asymmetry ratios measured under different forces. The error bars represent s.e.m.
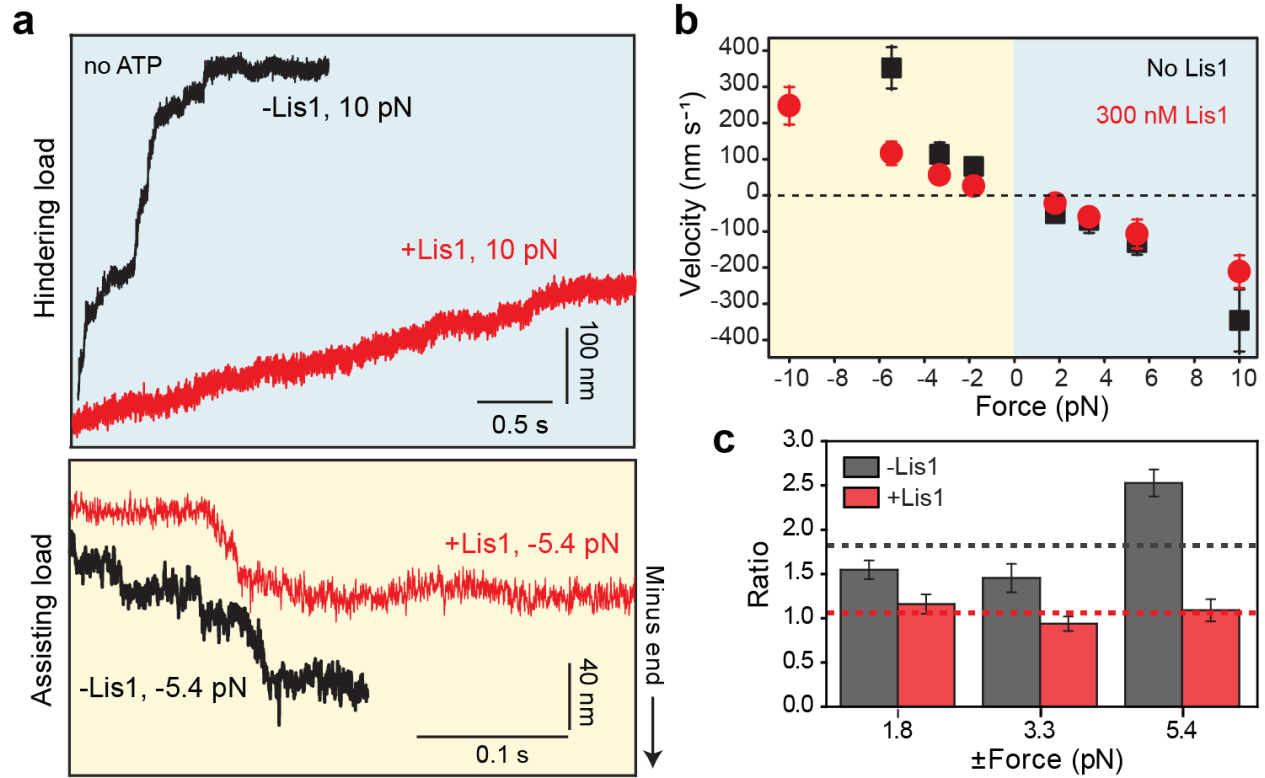
Figure 4.12: Lis1-induced reduction of the asymmetry in the F-V behavior of dynein is independent of ATP. a) Representative traces of dynein-driven beads under assisting and hindering loads with and without 300 nM Lis1. Assays were performed in 50 mM KAc and without ATP. **b)** F-V measurements of dynein in the absence and presence of 300 nM Lis1 (mean ± s.e.m.; N = 42, 29, 65, 51, 38, 62, 15 without Lis1 and 36, 35, 34, 28, 21, 25, 20, 19 with Lis1 from left to right). **c)** The ratios of the velocities under the same magnitude of forces in assisting and hindering directions. The dashed lines represent the average of the asymmetry ratios measured under different forces. The error bars represent s.e.m.
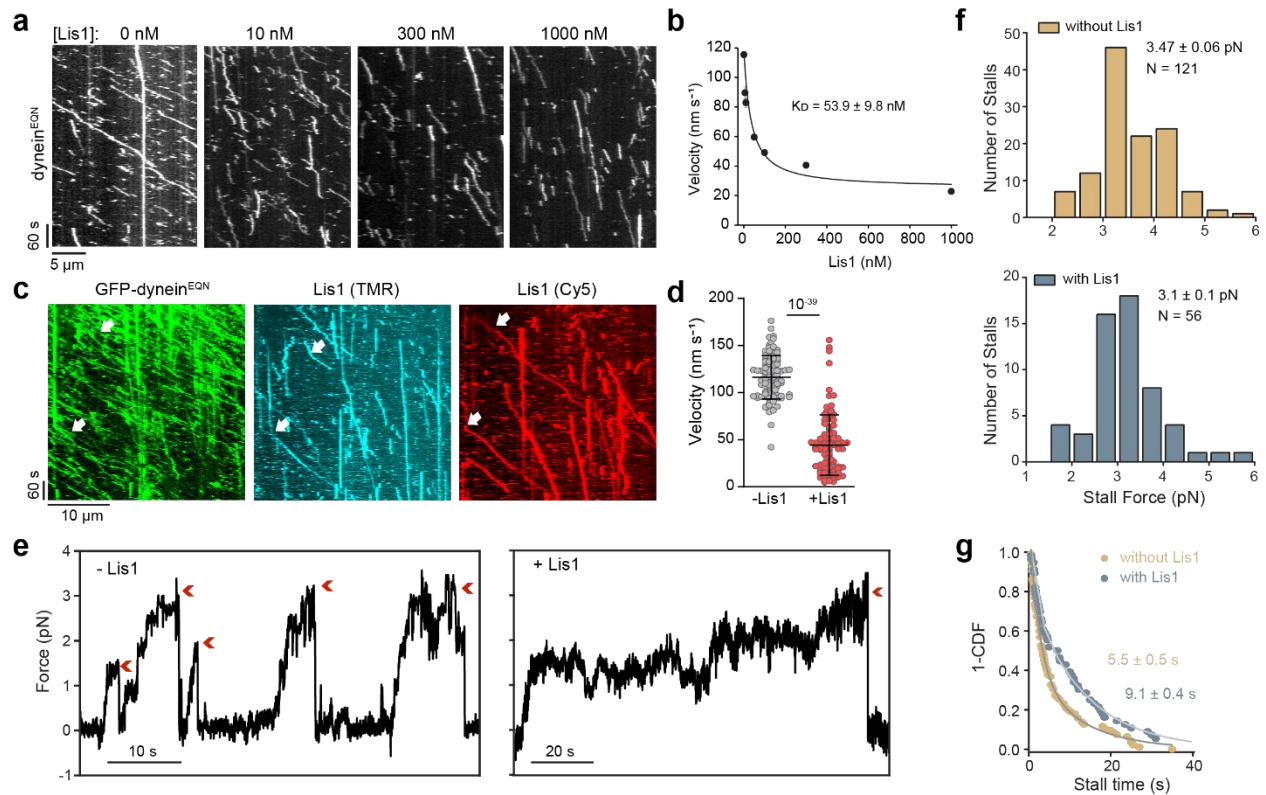
Figure 4.13: Lis1 binding to dynein's stalk is not required to slow down dynein motility. a) Representative kymographs of dynein^{EQN} motility under different concentrations of unlabeled Lis1. **b)** The velocity of dynein^{EQN} motility under different concentrations of unlabeled Lis1 (mean ± s.e.m.; N = 659, 283, 482, 484, 487, 610, 132 from left to right). The fit of the dynein^{EQN} velocity data (solid curve) reveals K_D (±s.e., see Methods). **c)** A representative kymograph of a three-color imaging assay shows two Lis1s to bind to the same dynein^{EQN} motor (white arrows). **d)** The velocities of dynein^{EQN} motors not colocalizing (-Lis1) or colocalizing (+Lis1) with Lis1 (N = 98 and 92 from left to right). The center line and whiskers represent the mean and s.d., respectively. The P-value was calculated by a two-tailed t-test with Welch correction. **e)** Representative trajectories of beads driven by dynein^{EQN} in the presence or absence of 900 nM Lis1. Red arrowheads represent the detachment of the motor from the microtubule followed by the snapping back of the bead to the trap center. **f)** Stall force histograms of dynein^{EQN} in the presence and absence of 900 nM Lis1 (mean ± s.e.m.; p = 10^{-3}, two-tailed t-test). **g)** Stall durations of dynein^{EQN} in the presence and absence of 900 nM Lis1. Fit to a double exponential decay (solid curves) reveals the average stall time (±s.e.).
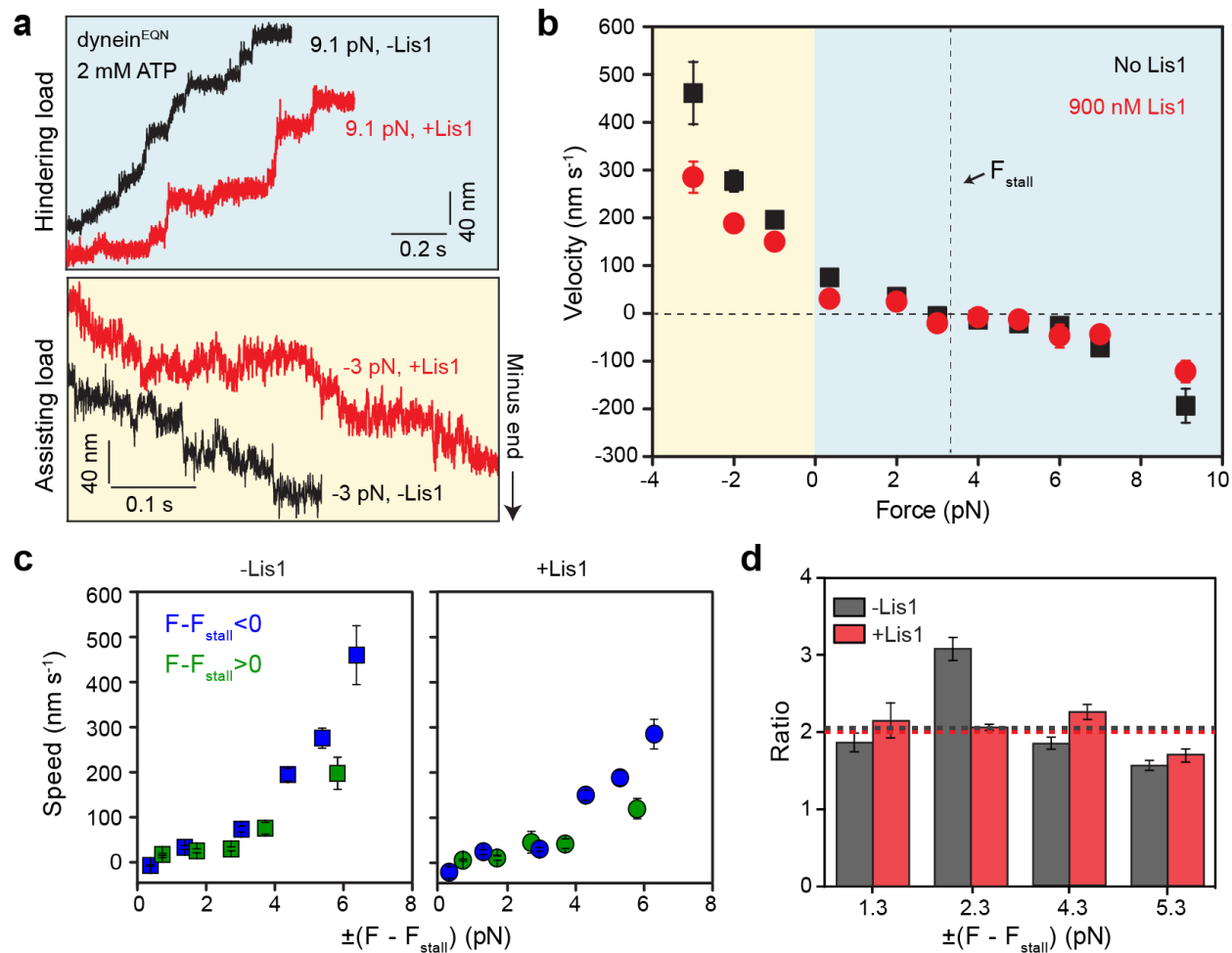
Figure 4.14: Mutagenesis of the Lis1 binding site on the stalk recovers the asymmetry in the F-V behavior of dynein. a) Representative traces of dynein[EQN]-driven beads under assisting and hindering loads with and without 900 nM Lis1. Assays were performed in 1 mM ATP and 50 mM KAc. **b)** F-V measurements of dynein[EQN] with and without 900 nM Lis1 (mean ± s.e.m.; from left to right N = 31, 66, 62, 48, 47, 26, 42, 39, 23, 45, 33 without Lis1 and 54, 36, 61, 31, 37, 17, 54, 14, 19, 38, 26 with Lis1). **c)** The speed of dynein[EQN]-driven beads (mean ± s.e.m.) under the same magnitude of forces in assisting and hindering directions relative to the dynein[EQN] stall force (3.3 pN). **d)** The ratios of the velocities under the same magnitude of forces in assisting and hindering directions relative to the stall force. The dashed lines represent the average of the asymmetry ratios measured under different forces. The error bars represent s.e.m.
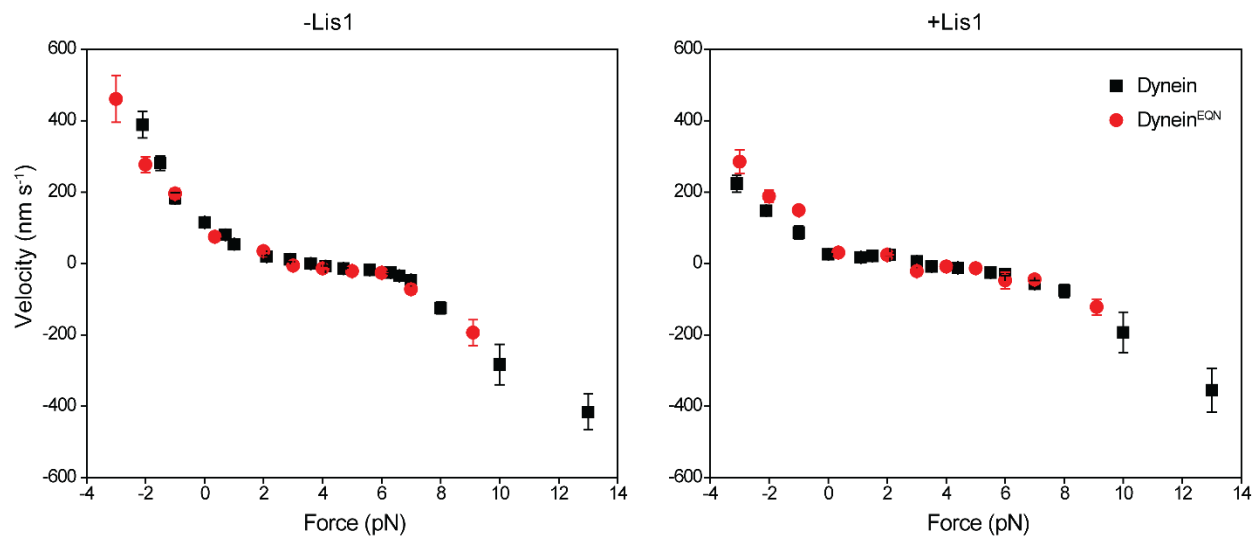
Figure 4.15: The comparison of the F-V behavior of dynein and dynein^{EQN} in the presence and absence of Lis1. (Left) F-V measurements of dynein and dynein^{EQN} in the absence of Lis1 (mean ±s.e.m., from left to right, N = 41, 38, 37, 861, 27, 52, 106, 28, 51, 60, 89, 115, 124, 62, 23, 38, 40 for dynein and N = 31, 66, 62, 48, 47, 26, 42, 39, 23, 45, 33 for dynein^{EQN}). (Right) F-V measurements of dynein in 300 nM Lis1 compared to F-V of dynein^{EQN} in 900 nM Lis1 (mean ±s.e.m., from left to right, N = 34, 52, 25, 312, 33, 42, 49, 37 62, 47 33 42, 36, 29, 18 for dynein; and N = 54, 36, 61, 31, 37, 17, 54, 14, 19, 38, 26 for dynein^{EQN}).

Strain	Construct	Genotype	Ref	Figures
RPY1732	GFP-dynein-DHA	MATa; *his3-11,15*; *ura3-1*; *leu2-3,112*; *ade2-1*; *trp1-1*; *pep4Δ::HIS5*; prb1Δ; ZZ-Tev-GFP-3XHA-*DYN1*-gs-DHA-Kan^R; nip100Δ; ndl1Δ::cgLEU2; pac1Δ::Hygro^R	This work	Fig. 1e-i, 2a,b,f, 3a-d, 4a-d, 5a-c, ED1a,b,ED2c,d, ED6a, ED9
RPY1736	GFP-dynein^{EQN}-DHA	MATa; *his3-11,15*; *ura3-1*; *leu2-3,112*; *ade2-1*; *trp1-1*; *pep4Δ::HIS5*; prb1Δ; ZZ-TEV-GFP-3XHA-*DYN1(E3012A, Q3014A, N3018A)*-gs-DHA-Kan^R; nip100Δ; ndl1Δ::cgLEU2; pac1Δ::Hygro^R	This work	Fig. 6a-d, ED8a-g, ED9
SM2344	HALO-dynein$_{gal}$	MATa; *nip100Δ::LEU2; ura3-1*::GAL1p-*DYN2*:GAL1p-*DYN3*:GAL1p-*PAC11*:GAL1p-8xHis-ZZ-2XTEV-HALO-*DYN1::URA3*; *his3-11,15*; *ura3-1*; *leu2-3,112*; *ade2-1*; *trp-1*; *pep4Δ::HIS5*; prb1Δ	119	ED2e,f, ED3a-c, ED4a-d, ED5a-d, ED6b,c
RPY1167	GFP-GST-Dyn$_{331kDa}$-DHA	MATa; *his3-11,15*; *ura3-1*; *leu2-3,112*; *ade2-1*; *trp1-1*; *pep4Δ::HIS5*; *prb1Δ*; P$_{GAL1}$-ZZ-Tev-GFP-3XHA-GST-*DYN1(331kDa)*-gs-DHA-Kan^R; *pac1Δ*; *ndl1Δ::cgLEU2*	49	ED7a-c
RPY228	GFP-GST-Dyn$_{314kDa}$-DHA	MATa; *his3-11,15*; *ura3-1*; *leu2-3,112*; *ade2-1*; *trp1-1*; *pep4Δ::HIS5*; prb1Δ; P$_{GAL1}$-ZZ-Tev-GFP-3xHA-GST-*DYN1(314kDa)*-gs-DHA	26	ED7a-c
RPY799	SNAP-Lis1	MATa*; his3-11,15*; *ura3-1*; *leu2-3,112*; *ade2-1*; *trp1-1*; *pep4Δ::HIS5*; *prb1Δ*; *dyn1Δ::cgLEU2*; P$_{GAL1}$-8HIS-ZZ-SNAP-gs-*PAC1*	49	Fig. 1e-h, 2c-f , ED1a,b, ED2h, ED4a-d, ED5a-d, ED6a-c, ED8c-d
RPY816	Lis1^{WT}	MATa*; his3-11,15*; *ura3-1*; *leu2-3,112*; *ade2-1*; *trp1-1*; *pep4Δ::HIS5*; *prb1Δ*; P$_{GAL1}$-8HIS-ZZ-Tev-*PAC1*; *dyn1Δ::cgLEU2*; *ndl1Δ::*Hygro^R	45	Fig. 1b-d,i, 3b-d, 4a-d, 5a-c, 6a-d, ED2c-g, ED3a-c, ED7a-c, ED8a,b,e-g, ED9
RPY1042	Lis1^{monomer}	MATa; *pep4D::HIS5; prb1D; GAL1-8HIS-ZZ-Tev-PAC1(aa 3-129 delete)-g-1XFLAG-gaSNAP-kanR; dyn1D::CgLEU2; ndl1D::HPH*	85	Fig 2b
RPY1544	Lis1^{R378A}	MATa*; his3-11,15*; *ura3-1*; *leu2-3,112*; *ade2-1*; *trp1-1*; *pep4Δ::HIS5*; *prb1Δ*; P$_{GAL1}$-8HIS-ZZ-Tev-*PAC1(R378A)*; *dyn1Δ::cgLEU2*; *ndl1Δ::*Hygro^R	45	Fig. 2e
RPY1547	Lis1^{5A}	MATa*; his3-11,15*; *ura3-1*; *leu2-3,112*; *ade2-1*; *trp1-1*; *pep4Δ::HIS5*; *prb1Δ*; P$_{GAL1}$-8HIS-ZZ-Tev-*PAC1(R275A, R301A, R378A, W419A, K437A)*; *dyn1Δ::cgLEU2*; *ndl1Δ::*Hygro^R	45	Fig. 2e, ED2b-g

Table 4.1: The list of *S. cerevisiae* strains used in this study. SNAP, DHA, and HALO are genetic tags used for labeling the protein with a fluorescent dye. Lis1 constructs that are not tagged with SNAP were labeled with maleimide reactive probes. TEV indicates a Tev protease cleavage site. P_{GAL1} denotes the galactose promoter, which was used for inducing strong expression of Lis1 and dynein motor domain constructs. Amino acid spacers are indicated by g (glycine) and gs (glycine-serine). (Ref: Reference, ED: Extended Data Figure).

Methods

Protein purification and labeling

The endogenous genomic copies of *S. cerevisiae* dynein heavy chain (*DYN1*) and Lis1 (*PAC1*) were modified or deleted using homologous recombination[26]. The list of strains used in this study is shown in Table 4.1. *S. cerevisiae* strains that express dynein, dynein$_{Gal}$, and Lis1 constructs were grown in 2 L YPA-galactose media (1% yeast extract, 1% peptone, % 0.004 adenine sulfate, 2% galactose) until OD$_{600}$ reaches 2.0. The cells were pelleted at 6,000 *g* for 15 min, resuspended in phosphate buffer saline (PBS), and frozen in liquid nitrogen. For purification of dynein and dynein$_{Gal}$, cell pellets were grinded and then dissolved in the lysis buffer (30 mM HEPES pH 7.4, 50 mM KAc, 2 mM Mg(Ac)$_2$, 1 mM EGTA, 10% glycerol, 1 mM DTT, 0.1 mM ATP, 1 mM phenylmethylsulfonyl fluoride (PMSF), 0.1% Triton) at 37°C. The lysate was centrifuged at 500,000 *g* for 45 min and the supernatant was incubated with 300 µL IgG beads for 1 h at 4 °C. The mixture was then applied to Qiagen columns, washed with 30 mL lysis buffer supplemented with 250 mM KAc, and then with 20 mL TEV buffer (10 mM Tris-HCl pH 8.0, 150 mM KCl, 10% glycerol, 1 mM DTT, 0.1 mM ATP, 0.25 mM PMSF) at 4 °C. The mixture was then incubated with 10 µL 2 mg mL^{-1} TEV protease for 1 h at 4 °C. The eluted protein was separated from the beads by centrifuging the mixture in Amicon Ultra Free MC tubes at 21,000 *g* for 2 min, flash-frozen in liquid nitrogen, and stored at -80 °C. A similar procedure was used to purify Lis1, except cells were lysed in a hi-salt phosphate lysis buffer (50 mM potassium phosphate pH = 8.0, 150 mM KAc, 2 mM Mg(Ac)$_2$, 10% glycerol, 10 mM Imidazole, 150 mM NaCl, 50 mM 2-Mercaptoethanol (BME), 1 mM PMSF, 0.2% Triton) and protein was eluted in nu-TEV buffer (50 mM Tris-HCl pH 8.0, 1 mM EGTA, 150 mM KAc, 150 mM NaCl, 2 mM Mg(Ac)$_2$, 10% glycerol, 1 mM DTT, 0.5 mM PMSF). The protein concentration was determined by both 280 nm absorbance and the Bradford assay.

Proteins were labeled with fluorescent dyes after resuspending the lysate with beads and before adding TEV protease. 10 nanomoles of a fluorescent dye were well mixed with the protein-bead mixture and incubated for 1 h at 4 °C. The column was then washed with 100 mL TEV buffer to remove excess dye before eluting the protein from beads. The labeling percentage was determined by measuring the protein concentration in Bradford assays and the absorbance under 555 nm and 655 nm excitation for TMR/LD555 and Cy5/LD655 dyes, respectively. The probability, *p* of each SNAP-Lis1 monomer labeled with TMR and LD655 dyes derivatized with benzyl guanine was 72% and 80% per Lis1 monomer, respectively. The probabilities of a SNAP-Lis1 dimer to be labeled with at least one TMR or LD655 dyes (calculated as $2p - p^2$) were 92% and 96%, respectively.

Microtubule Polymerization and Subtilisin Treatment

Tubulin was purified from pig brains in 1 M PIPES buffer. 60 ng unlabeled tubulin, 60 ng biotinylated tubulin, and 1 ng fluorescently-labeled tubulin were diluted to 1 mg ml^{-1} in 120 µL BRB80 buffer (80 mM PIPES pH = 6.8, 2 mM MgCl$_2$, 1 mM EGTA) supplemented with 1x polymerization mixture (1mM GTP, 10% DMSO) and polymerized at 37 °C for 40 min and another 40 min after supplementing the mixture with 1 mM taxol. The mixture was centrifuged at 21,000 *g* for 13 min at room temperature and resuspended in 30 µL BRB80 buffer

supplemented with 10 mM taxol and 1 mM DTT. Microtubules were stored in dark at room temperature and used within seven days.

For subtilisin treatment, polymerized microtubules were stored in dark for 1 day for elongation and then incubated with a 1:100 (w/w) subtilisin to tubulin ratio for 2 h at a 37 °C bath. The proteolytic cleavage was stopped with the addition of 2 mM PMSF. The microtubules were centrifuged at 21,000 g for 13 min at room temperature and the pellet was resuspended in BRB80 supplemented with 10 mM taxol.

Single-molecule motility assays

Flow channels were prepared by placing a multichannel parafilm in between a microscope slide and a cover glass functionalized with PEG/PEG-biotin (Microsurfaces Inc.). The channel was incubated with 20 µL of 2 mg mL^{-1} streptavidin for 2 min and excess streptavidin was removed by washing the channel with 60 µl DP buffer (DLB with 10% glycerol, 2% pluronic acid, 1 mM taxol, 1 mM tris(2-carboxyethyl)phosphine (TCEP)). The channel was then incubated with 20 µl of 2 mg mL^{-1} biotinylated microtubules in DP buffer for 2 min and unbound microtubules were removed by washing the channel with 60 µl DP buffer and then with 20 µl DM buffer (DLB supplemented with 10% glycerol, 0.4% pluronic, 1 mM taxol, 1 mM TCEP). After 3 min, the channel was then washed with 20 µL of stepping buffer (93% DM buffer, 2 mM ATP, gloxy (glucose oxidase and catalase), 0.5% dextrose, and 50 -150 mM KAc). Dynein and Lis1 were diluted in stepping buffer and incubated on ice for 10 min. 20 µL motor+Lis1 final mixture in stepping buffer was added to the channel and the sample was imaged immediately for 15 min.

Lis1-dynein colocalization experiments were performed by mixing fluorescently-labeled dynein and Lis1 into the final mixture, before flowing into the chamber. Colocalization between two differentially labeled dynein was performed by mixing 5 nM LD555 dynein with LD655-dynein and letting on ice for 10 min with or without Lis1. To maximize crosslinking efficiency with different colors of dyneins, dyneins were added to the mixture before Lis1. Dynein-Lis1 mixture was diluted in stepping buffer supplemented with 1 mM ATP and 50 mM KAc.

Single-molecule imaging was performed using a custom-built objective-type TIRF microscope equipped with an inverted microscopy body (Nikon Ti-Eclipse), 100× magnification 1.49 numerical aperture (N.A.) plan-apochromat oil-immersion objective (Nikon), and a perfect focusing system. The fluorescence signal was detected using an electron-multiplied charge-coupled device (EM-CCD) camera (Andor, Ixon). The effective pixel size after magnification was 108 nm. Samples labeled with GFP, TMR/LD555, and Cy5/LD655 were excited using 0.04 kW cm^{-2} 488, 532, and 633 nm laser beams (Coherent), and the emission signal was detected using bandpass emission filters (Semrock). For two- and three-color fluorescence assays, imaging was performed using alternating excitation and the time-sharing mode. Single color movies were recorded at 1 Hz, whereas multi-color movies were recorded with 0.5 s per frame per color using the time-sharing mode. To introduce or remove Lis1 from the channel during imaging, two 0.5 mm diameter holes were drilled on a glass slide at both ends of the flow channel. The region of interest in the channel was imaged for 1 min before introducing Lis1 or washing the free Lis1 from the channel while imaging dynein motility in real-time.

Data Analysis

Movies were analyzed in ImageJ to create kymographs. Motors that are stationary, exhibit diffusional movement, or move less than 3 pixels were excluded from the analysis. The results of the data analysis were plotted in Prism and Origin. Data fitting was performed in Origin. Cumulative distribution functions (CDFs) of the run length and run-time data were fitted to a double exponential decay, $y = A_1 e^{-t/\tau_1} + A_2 e^{-t/\tau_2}$ where A_1 and A_2 are the amplitudes and τ_1 and τ_2 are the decay constants. The weighted average of the decay constants, $\tau_{av} = \frac{A_1\tau_1 + A_2\tau_2}{A_1 + A_2}$ was reported as the decay constant.

The average velocities of motors that colocalize with 0 (V_0), 1 (V_1), and 2 (V_2) colors of Lis1 were determined from two- and three-color TIRF assays. To determine K_D of Lis1, the average dynein velocity under different Lis1 concentrations, V ($[Lis1]$) was fitted to $(1 - p_b)^2 V_0 + 2p_b(1 - p_b)V_1 + (p_b)^2 V_2$ where $p_b = \frac{1}{1 + \frac{K_D}{[Lis1]}}$ is the binding probability of Lis1 to a dynein monomer. The probability of Lis1 colocalization to dynein$_{Gal}$ in Figure 4.6c was fitted to a binding isotherm function, defined as $C(2p_b - (p_b)^2)$, where C is less than 1 due to incomplete labeling of Lis1 and the limited single-molecule detection ability due to the presence of excess labeled Lis1 in solution.

Microtubule co-pelleting assays

Unlabeled taxol-stabilized microtubules were polymerized as above and free tubulin was removed by centrifugation through a 60% glycerol gradient in BRB80 (80 mM PIPES-KOH pH 6.8, 1 mM magnesium chloride, 1 mM EGTA, 1 mM DTT, 20 µM Taxol) for 15min at 100,000xg and 37 °C. The microtubule pellet was resuspended in DLB supplemented with 20 µM taxol. Microtubules (0-600nM tubulin) were incubated with 100 nM Lis1 for 10 min before being pelleted for 15 min at 100,000xg and 25 °C. The supernatant was analyzed via SDS-PAGE and depletion was determined using densitometry in ImageJ. Binding curves were fit in Prism8 (GraphPad) with a nonlinear regression for one site binding with B$_{max}$ set to 1.

Optical trapping assays

Optical trapping experiments were performed on a custom-built optical trap using a Nikon Ti-E microscope body and a 100× 1.49 NA plan-apochromat oil immersion objective, as previously described[47]. The beads were trapped with a 2W 1,064 nm laser (IPG Photonics) and the trap was steered with a two-axis acousto-optical deflector (AA Electronics). The trap stiffness was calculated from the Lorentzian fit to the power spectrum of a trapped bead. For stall force measurements, the trap stiffness was adjusted to allow the motor to walk 100 nm away from the trap center before the bead comes to stall. The position of the bead from the center of the fixed trap was recorded for at least 90 s at 5 kHz.

For fixed trap measurements, 0.8 µm diameter carboxylated latex beads (Life Technologies) were functionalized with rabbit polyclonal GFP antibody (BioLegend, no. MMS-118P), as previously described[47]. The 2 µL of the bead stock were diluted in 8 µL DLB. 2 µL of diluted beads were sonicated for 8 s. To ensure that more than 90% of the beads are driven by single motors, GFP-dynein concentration was diluted in the stepping buffer (93% DLBM buffer (DLB supplemented with 10% glycerol, 0.25 mM casein, 1 mM taxol, 1 mM TCEP), 2 mM ATP, 1%

gloxy, 0.5% dextrose, and 50 mM KAc) to desired concentrations such that less than 30% of the beads exhibit motility when brought on top of a surface-immobilized axoneme. The mixture was sonicated for 8 s and 2 µL of diluted beads were mixed with 2 µL of GFP-dynein, 1.5 µL Lis1, and 2 µL stepping buffer, and incubated on ice for 10 min. For the no Lis1 condition, an equal volume of stepping buffer was added to the mixture instead of Lis1.

Cy5-labeled sea urchin axonemes were nonspecifically adsorbed to the channel surface. After 30 s, the channel was washed with 60 µL DLBC buffer (DLB with 10% glycerol, 2 mM casein, 1 mM taxol, and 1 mM TCEP) to remove the unbound axoneme. After 3 min, the channel was washed with 60 µL DLBM buffer and then with 20 µL stepping buffer. 7.5 µL of the dynein-Lis1-bead mixture was diluted in 20 µL stepping buffer and the KAc concentration was adjusted to 50 mM before being flown into the channel. The channel was sealed with nail polish to prevent evaporation during data acquisition.

Optical trap data were analyzed with a custom-written MATLAB script. The data were downsampled to 500 Hz via median filtering before analysis. Stall events were manually scored when the velocity of the bead movement was reduced to ~0 nm s^{-1} under hindering load and terminated with a sudden (<4 ms) snapping of the bead to the trap center. Events that occur within 25 nm distance to the trap center, last shorter than 0.4 s, or terminate with backward movement, multiple-step detachment, or slow (>4 ms) return of the bead to the trap center were excluded from the analysis. Stall forces were calculated as the average force value of the plateau where the bead is nearly immobile before detaching from the axoneme. Stall time was defined as the time the bead spends at the 30% margin of the stall force before it detaches from an axoneme. CDFs of stall times were fitted to a double exponential decay and the weighted average of two decay constants from the fit was reported as the decay constant.

F-V measurements

Similar sample preparation procedures were used for F-V measurements using an optical trap. After the bead movement reached half of the measured stall force of the motor, the trapping beam repositioned itself and maintained a 100 nm distance from the bead via a force-feedback mechanism. To determine the microtubule polarity in the no-ATP condition, unlabeled axonemes were immobilized to the channel and LD655-labeled GST-Dyn$_{331kDA}$ motors (without a GFP tag) were flown into the channel in a stepping buffer supplemented with 30 µM ATP. The motors were allowed to walk on and accumulate at the minus-end of surface-immobilized axonemes for 4 mins. The channel was then washed with 40 µl with DLBM buffer, followed by 20 µl stepping buffer supplemented with 0.5 U ml^{-1} apyrase instead of ATP to deplete residual ATP in the channel. 0.5 U ml^{-1} apyrase was also included in the bead-dynein-Lis1 mixture to remove residual ATP from protein preparations. During optical trapping, microtubule polarity was determined by the minus-end accumulation of the LD655 signal determined by an sCMOS camera (Hamamatsu, Orca Flash 4.0). Beads were pulled along the length of an axoneme at a constant velocity, and the beads that engaged with the axoneme were trapped by repositioning the trapping beam 100 nm away from the bead center along the direction of the applied force.

The bead position was recorded at 5 kHz and the data were downsampled to 500 Hz via median filtering. The slope of each trace was defined as the velocity of individual motors under an applied force. The traces that are shorter than 70 ms, show bidirectional motility under load, or

exhibit instantaneous jumps larger than 50 nm were excluded from data analysis. The asymmetry ratios were calculated by comparing the average velocities under forces equally larger or smaller than F_{stall}. Velocities at corresponding forces were either directly measured or calculated by linear regression of the measured velocities under the closest force measurements. The errors of asymmetry ratios were determined by error propagation of the compared velocities.

Statistical Analysis The p-values were calculated by the two-tailed t-test for stall force histograms, the two-tailed t-test with Welch corrections for velocity measurements, and the Kolmogorov-Smirnov test for run length and run time measurements in Prism and Origin. CDFs were calculated in MATLAB.

Chapter 5: Conclusion and Future directions

Lis1 is required in most, if not all, of the dynein-related roles in the cytoplasm[36,86,91,116,124-128]. Deciphering the details of molecular interaction between Lis1 and dynein will provide us with a clearer understanding of the regulation of dynein motility and the many cellular processes in which they are involved. Many studies focused on distinct parts of this regulation using different biophysical techniques and model systems. Previous in vitro studies on yeast dynein identified Lis1 as an inhibitor of dynein motility when it remains bound to dynein[49,85,92,120,121]. On the other hand, more recent studies using mammalian dynein showed that Lis1 has an activating role in dynein motility[98-100,117-119]. These observations were seemingly at odds with each other and the mechanism of Lis1-mediated dynein regulation was not well understood.

My thesis work has significantly contributed to understanding both the molecular interaction and cellular roles of Lis1 using in-vitro biophysical techniques. Lis1 relieves dynein from autoinhibition by opening up its φ conformation[105,117,118], which is the initial key step for forming an active DDX complex. In the meantime, dynein needs to stay on the MT plus end before forming a complex with dynactin and a cargo adaptor. Lis1 increases dynein's MT binding affinity so that the motor remains on MTs longer times. This may provide enough time to form a full complex with dynactin and a cargo adaptor so that DDX can start cargo transportation from the plus end of MTs.

By using both mammalian DDX and yeast dynein, I have shown that Lis1 colocalized dynein (or DDX complexes) walks slower. I tested the models that explain why Lis1-bound dynein is moving slower. My results are inconsistent with the currently proposed models of MT-tethering[105] and clutch mechanisms[45]. Instead, the results of my studies support the model that Lis1's binding to the ring is sufficient to disrupt the transduction of the conformational changes due to ATP hydrolysis on the ring. Moreover, Lis1's interaction with the dynein stalk changes its asymmetric release from microtubules, decreasing its detachment more in the forward direction. The loss of asymmetry in the MT detachment of Lis1-bound dynein can be critical for its plus end recruitment, or for retaining dynein for longer times at the plus end until the DDX complex assembles. In Chapter 2, I have explained that Z-force may affect the motor's detachment from MTs[65,66]. I note that, in future studies, eliminating the Z-force in optical trapping may result in a more striking asymmetry in dynein's detachment rate and higher relative loss of asymmetry due to Lis1 binding than I found using the standard single-bead assays.

The role of NudE in dynein-mediated transport

Lis1 appears as a puncta at the plus tips of MTs. The precise point localization of Lis1 at the MT plus tip indicates that Lis1's binding and unbinding happens at the tip. Moreover, the lack of evidence about Lis1's moving together with cargoes carried by dynein in cells[86,90,115,116] indicates that Lis1 needs to dissociate from such complexes before the initiation of transport. How Lis1 binds and why it dissociates needs to be studied further. A possible candidate to mediate Lis1 binding to dynein is NudE[129,130]. NudE contains one long and one short coiled-coil which has binding sites for both the dynein intermediate chain (DIC) and Lis1[131-135]. NudE also competes with dynactin for the binding site on DIC[108,136,137]. A possible scenario is that NudE binds dynein and recruits Lis1, which switches dynein to open conformation and keeps it stably bound to MTs. Dynactin's binding to dynein may kick off NudE from DIC, which can also trigger Lis1's

dissociation from dynein leading to processive cargo transportation.

Lis1 and NudE work together and it is known that mutations in these genes cause severe neurodevelopmental diseases known as Lissencephaly[112,138-141] and microcephaly[142,143], respectively. In the future, it is critical to investigate how Lis1-NudE together affects dynein motility to understand the underlying mechanism of this regulation. In order to determine the order of events that leads to activation of DDX complexes, association-dissociation of Lis1-NudE vs dynactin-cargo adapter from dynein needs to be monitored in real-time using multi-color TIRF assays. Further research on the *in vivo* imaging of the plus end recruitment and initiation of dynein-driven transport and their relative interaction with Lis1-NudE pairs will provide critical insight into the molecular basis of Lis1- and NudE-related diseases.

References

1   Paschal, B. M., Shpetner, H. S. & Vallee, R. B. MAP 1C is a microtubule-activated ATPase which translocates microtubules in vitro and has dynein-like properties. *J Cell Biol* **105**, 1273-1282 (1987).

2   Schroer, T. A., Steuer, E. R. & Sheetz, M. P. Cytoplasmic dynein is a minus end-directed motor for membranous organelles. *Cell* **56**, 937-946 (1989).

3   Reck-Peterson, S. L., Redwine, W. B., Vale, R. D. & Carter, A. P. The cytoplasmic dynein transport machinery and its many cargoes. *Nat Rev Mol Cell Biol* **19**, 382-398, doi:10.1038/s41580-018-0004-3 (2018).

4   Roberts, A. J., Kon, T., Knight, P. J., Sutoh, K. & Burgess, S. A. Functions and mechanics of dynein motor proteins. *Nat Rev Mol Cell Biol* **14**, 713-726, doi:10.1038/nrm3667 (2013).

5   Pazour, G. J., Dickert, B. L. & Witman, G. B. The DHC1b (DHC2) isoform of cytoplasmic dynein is required for flagellar assembly. *J Cell Biol* **144**, 473-481 (1999).

6   Sharp, D. J., Rogers, G. C. & Scholey, J. M. Microtubule motors in mitosis. *Nature* **407**, 41-47 (2000).

7   Ishikawa, T. Axoneme Structure from Motile Cilia. *Cold Spring Harb Perspect Biol* **9**, doi:10.1101/cshperspect.a028076 (2017).

8   Viswanadha, R., Sale, W. S. & Porter, M. E. Ciliary Motility: Regulation of Axonemal Dynein Motors. *Cold Spring Harb Perspect Biol* **9**, doi:10.1101/cshperspect.a018325 (2017).

9   El-Kadi, A. M., Soura, V. & Hafezparast, M. Defective axonal transport in motor neuron disease. *J Neurosci Res* **85**, 2557-2566, doi:10.1002/jnr.21188 (2007).

10   Guedes-Dias, P. & Holzbaur, E. L. F. Axonal transport: Driving synaptic function. *Science* **366**, doi:10.1126/science.aaw9997 (2019).

11   Lipka, J., Kuijpers, M., Jaworski, J. & Hoogenraad, C. C. Mutations in cytoplasmic dynein and its regulators cause malformations of cortical development and neurodegenerative diseases. *Biochem Soc Trans* **41**, 1605-1612, doi:10.1042/BST20130188 (2013).

12   Canty, J. T., Tan, R., Kusakci, E., Fernandes, J. & Yildiz, A. Structure and Mechanics of Dynein Motors. *Annu Rev Biophys* **50**, 549-574, doi:10.1146/annurev-biophys-111020-101511 (2021).

13   Carter, A. P., Cho, C., Jin, L. & Vale, R. D. Crystal structure of the dynein motor domain. *Science* **331**, 1159-1165, doi:10.1126/science.1202393 (2011).

14   Kon, T. *et al.* The 2.8 A crystal structure of the dynein motor domain. *Nature* **484**, 345-350, doi:10.1038/nature10955 (2012).

15   Schmidt, H., Gleave, E. S. & Carter, A. P. Insights into dynein motor domain function from a 3.3-A crystal structure. *Nat Struct Mol Biol* **19**, 492-497, S491, doi:10.1038/nsmb.2272 (2012).

16   Cho, C., Reck-Peterson, S. L. & Vale, R. D. Regulatory ATPase sites of cytoplasmic dynein affect processivity and force generation. *J Biol Chem* **283**, 25839-25845, doi:10.1074/jbc.M802951200 (2008).

17   Kon, T., Nishiura, M., Ohkura, R., Toyoshima, Y. Y. & Sutoh, K. Distinct functions of nucleotide-binding/hydrolysis sites in the four AAA modules of cytoplasmic dynein. *Biochemistry* **43**, 11266-11274, doi:10.1021/bi048985a (2004).

18   Schmidt, H., Zalyte, R., Urnavicius, L. & Carter, A. P. Structure of human cytoplasmic dynein-2 primed for its power stroke. *Nature* **518**, 435-438, doi:10.1038/nature14023 (2015).

19   DeWitt, M. A., Cypranowska, C. A., Cleary, F. B., Belyy, V. & Yildiz, A. The AAA3 domain of cytoplasmic dynein acts as a switch to facilitate microtubule release. *Nat Struct Mol Biol* **22**, 73-80, doi:10.1038/nsmb.2930 (2015).

20   Gee, M. A., Heuser, J. E. & Vallee, R. B. An extended microtubule-binding structure within the dynein motor domain. *Nature* **390**, 636-639, doi:10.1038/37663 (1997).

21   Gibbons, I. R. *et al.* The affinity of the dynein microtubule-binding domain is modulated by the conformation of its coiled-coil stalk. *J Biol Chem* **280**, 23960-23965, doi:10.1074/jbc.M501636200 (2005).

22   Kon, T. *et al.* Helix sliding in the stalk coiled coil of dynein couples ATPase and microtubule binding. *Nat Struct Mol Biol* **16**, 325-333, doi:10.1038/nsmb.1555 (2009).

23   Burgess, S. A., Walker, M. L., Sakakibara, H., Knight, P. J. & Oiwa, K. Dynein structure and power stroke. *Nature* **421**, 715-718 (2003).

24   Kon, T., Mogami, T., Ohkura, R., Nishiura, M. & Sutoh, K. ATP hydrolysis cycle-dependent tail motions in cytoplasmic dynein. *Nat Struct Mol Biol* **12**, 513-519, doi:10.1038/nsmb930 (2005).

25   Zhang, K. *et al.* Cryo-EM Reveals How Human Cytoplasmic Dynein Is Auto-inhibited and Activated. *Cell* **169**, 1303-1314 e1318, doi:10.1016/j.cell.2017.05.025 (2017).

26   Reck-Peterson, S. L. *et al.* Single-molecule analysis of dynein processivity and stepping behavior. *Cell* **126**, 335-348, doi:10.1016/j.cell.2006.05.046 (2006).

27   Amos, L. A. Brain dynein crossbridges microtubules into bundles. *J Cell Sci* **93 (Pt 1)**, 19-28 (1989).

28   Dixit, R., Ross, J. L., Goldman, Y. E. & Holzbaur, E. L. Differential regulation of dynein and kinesin motor proteins by tau. *Science* **319**, 1086-1089, doi:10.1126/science.1152993 (2008).

29   Mallik, R., Carter, B. C., Lex, S. A., King, S. J. & Gross, S. P. Cytoplasmic dynein functions as a gear in response to load. *Nature* **427**, 649-652, doi:10.1038/nature02293 (2004).

30   Torisawa, T. *et al.* Autoinhibition and cooperative activation mechanisms of cytoplasmic dynein. *Nat Cell Biol* **16**, 1118-1124, doi:10.1038/ncb3048 (2014).

31   Urnavicius, L. *et al.* The structure of the dynactin complex and its interaction with dynein. *Science* **347**, 1441-1446, doi:10.1126/science.aaa4080 (2015).

32   Schlager, M. A., Hoang, H. T., Urnavicius, L., Bullock, S. L. & Carter, A. P. In vitro reconstitution of a highly processive recombinant human dynein complex. *EMBO J* **33**, 1855-1868, doi:10.15252/embj.201488792 (2014).

33   Gill, S. R. *et al.* Dynactin, a conserved, ubiquitously expressed component of an activator of vesicle motility mediated by cytoplasmic dynein. *J Cell Biol* **115**, 1639-1650 (1991).

34   Bielska, E. *et al.* Hook is an adapter that coordinates kinesin-3 and dynein cargo attachment on early endosomes. *J Cell Biol* **204**, 989-1007, doi:10.1083/jcb.201309022 (2014).

35   Schlager, M. A. *et al.* Pericentrosomal targeting of Rab6 secretory vesicles by Bicaudal-D-related protein 1 (BICDR-1) regulates neuritogenesis. *EMBO J* **29**, 1637-1651, doi:10.1038/emboj.2010.51 (2010).

36   Splinter, D. *et al.* BICD2, dynactin, and LIS1 cooperate in regulating dynein recruitment to cellular structures. *Mol Biol Cell* **23**, 4226-4241, doi:10.1091/mbc.E12-03-0210 (2012).

37   Grotjahn, D. A. *et al.* Cryo-electron tomography reveals that dynactin recruits a team of dyneins for processive motility. *Nat Struct Mol Biol* **25**, 203-207, doi:10.1038/s41594-018-0027-7 (2018).

38   Urnavicius, L. *et al.* Cryo-EM shows how dynactin recruits two dyneins for faster movement. *Nature* **554**, 202-206, doi:10.1038/nature25462 (2018).

39   Elshenawy, M. M. *et al.* Cargo adaptors regulate stepping and force generation of mammalian dynein-dynactin. *Nat Chem Biol* **15**, 1093-1101, doi:10.1038/s41589-019-0352-0 (2019).

40   Bhabha, G. *et al.* Allosteric communication in the dynein motor domain. *Cell* **159**, 857-868, doi:10.1016/j.cell.2014.10.018 (2014).

41   Kon, T., Sutoh, K. & Kurisu, G. X-ray structure of a functional full-length dynein motor domain. *Nat Struct Mol Biol* **18**, 638-642, doi:10.1038/nsmb.2074 (2011).

42   Roberts, A. J. *et al.* ATP-driven remodeling of the linker domain in the dynein motor. *Structure* **20**, 1670-1680, doi:10.1016/j.str.2012.07.003 (2012).

43   Nishida, N. *et al.* Structural basis for two-way communication between dynein and microtubules. *Nat Commun* **11**, 1038, doi:10.1038/s41467-020-14842-8 (2020).

44 Lin, J., Okada, K., Raytchev, M., Smith, M. C. & Nicastro, D. Structural mechanism of the dynein power stroke. *Nat Cell Biol* **16**, 479-485, doi:10.1038/ncb2939 (2014).

45 Toropova, K. *et al.* Lis1 regulates dynein by sterically blocking its mechanochemical cycle. *Elife* **3**, doi:10.7554/eLife.03372 (2014).

46 Uchimura, S. *et al.* A flipped ion pair at the dynein-microtubule interface is critical for dynein motility and ATPase activation. *J Cell Biol* **208**, 211-222, doi:10.1083/jcb.201407039 (2015).

47 Belyy, V., Hendel, N. L., Chien, A. & Yildiz, A. Cytoplasmic dynein transports cargos via load-sharing between the heads. *Nat Commun* **5**, 5544, doi:10.1038/ncomms6544 (2014).

48 Liu, X., Rao, L. & Gennerich, A. The regulatory function of the AAA4 ATPase domain of cytoplasmic dynein. *Nat Commun* **11**, 5952, doi:10.1038/s41467-020-19477-3 (2020).

49 DeSantis, M. E. *et al.* Lis1 Has Two Opposing Modes of Regulating Cytoplasmic Dynein. *Cell* **170**, 1197-1208 e1112, doi:10.1016/j.cell.2017.08.037 (2017).

50 DeWitt, M. A., Chang, A. Y., Combs, P. A. & Yildiz, A. Cytoplasmic dynein moves through uncoordinated stepping of the AAA+ ring domains. *Science* **335**, 221-225, doi:10.1126/science.1215804 (2012).

51 Qiu, W. *et al.* Dynein achieves processive motion using both stochastic and coordinated stepping. *Nat Struct Mol Biol* **19**, 193-200, doi:10.1038/nsmb.2205 (2012).

52 Ferro, L. S., Can, S., Turner, M. A., ElShenawy, M. M. & Yildiz, A. Kinesin and dynein use distinct mechanisms to bypass obstacles. *Elife* **8**, doi:10.7554/eLife.48629 (2019).

53 Leduc, C. *et al.* Molecular crowding creates traffic jams of kinesin motors on microtubules. *Proc Natl Acad Sci U S A* **109**, 6100-6105, doi:10.1073/pnas.1107281109 (2012).

54 Nicholas, M. P. *et al.* Cytoplasmic dynein regulates its attachment to microtubules via nucleotide state-switched mechanosensing at multiple AAA domains. *Proc Natl Acad Sci U S A* **112**, 6371-6376, doi:10.1073/pnas.1417422112 (2015).

55 Cleary, F. B. *et al.* Tension on the linker gates the ATP-dependent release of dynein from microtubules. *Nat Commun* **5**, 4587, doi:10.1038/ncomms5587 (2014).

56 Block, S. M. Kinesin motor mechanics: binding, stepping, tracking, gating, and limping. *Biophys J* **92**, 2986-2995, doi:10.1529/biophysj.106.100677 (2007).

57 Yildiz, A., Tomishige, M., Vale, R. D. & Selvin, P. R. Kinesin walks hand-over-hand. *Science* **303**, 676-678, doi:10.1126/science.1093753 (2004).

58 Can, S., Lacey, S., Gur, M., Carter, A. P. & Yildiz, A. Directionality of dynein is controlled by the angle and length of its stalk. *Nature* **566**, 407-410, doi:10.1038/s41586-019-0914-z (2019).

59 Carter, A. P. *et al.* Structure and functional role of dynein's microtubule-binding domain. *Science* **322**, 1691-1695, doi:10.1126/science.1164424 (2008).

60 Niekamp, S., Coudray, N., Zhang, N., Vale, R. D. & Bhabha, G. Coupling of ATPase activity, microtubule binding, and mechanics in the dynein motor domain. *EMBO J* **38**, e101414, doi:10.15252/embj.2018101414 (2019).

61 Svoboda, K., Schmidt, C. F., Schnapp, B. J. & Block, S. M. Direct observation of kinesin stepping by optical trapping interferometry. *Nature* **365**, 721-727 (1993).

62 Belyy, V. *et al.* The mammalian dynein-dynactin complex is a strong opponent to kinesin in a tug-of-war competition. *Nat Cell Biol* **18**, 1018-1024, doi:10.1038/ncb3393 (2016).

63 Ezber, Y., Belyy, V., Can, S. & Yildiz, A. Dynein harnesses active fluctuations of microtubules for faster movement. *Nature Physics* **16**, 312-316, doi:10.1038/s41567-019-0757-4 (2020).

64 Rao, L., Berger, F., Nicholas, M. P. & Gennerich, A. Molecular mechanism of cytoplasmic dynein tension sensing. *Nat Commun* **10**, 3332, doi:10.1038/s41467-019-11231-8 (2019).

65 Pyrpassopoulos, S., Shuman, H. & Ostap, E. M. Modulation of Kinesin's Load-Bearing Capacity by Force Geometry and the Microtubule Track. *Biophys J* **118**, 243-253, doi:10.1016/j.bpj.2019.10.045 (2020).

66   Sudhakar, S. *et al.* Germanium nanospheres for ultraresolution picotensiometry of kinesin motors. *Science* **371**, doi:10.1126/science.abd9944 (2021).

67   Cianfrocco, M. A., DeSantis, M. E., Leschziner, A. E. & Reck-Peterson, S. L. Mechanism and regulation of cytoplasmic dynein. *Annu Rev Cell Dev Biol* **31**, 83-108, doi:10.1146/annurev-cellbio-100814-125438 (2015).

68   Goshima, G., Nedelec, F. & Vale, R. D. Mechanisms for focusing mitotic spindle poles by minus end-directed motor proteins. *J Cell Biol* **171**, 229-240 (2005).

69   Carter, A. P., Diamant, A. G. & Urnavicius, L. How dynein and dynactin transport cargos: a structural perspective. *Curr Opin Struct Biol* **37**, 62-70, doi:10.1016/j.sbi.2015.12.003 (2016).

70   Hafezparast, M. *et al.* Mutations in dynein link motor neuron degeneration to defects in retrograde transport. *Science* **300**, 808-812, doi:10.1126/science.1083129 300/5620/808 [pii] (2003).

71   Merdes, A., Heald, R., Samejima, K., Earnshaw, W. C. & Cleveland, D. W. Formation of spindle poles by dynein/dynactin-dependent transport of NuMA. *J Cell Biol* **149**, 851-862 (2000).

72   Gerdes, J. M. & Katsanis, N. Microtubule transport defects in neurological and ciliary disease. *Cell Mol Life Sci* **62**, 1556-1570, doi:10.1007/s00018-005-5007-5 (2005).

73   Schiavo, G., Greensmith, L., Hafezparast, M. & Fisher, E. M. Cytoplasmic dynein heavy chain: the servant of many masters. *Trends Neurosci* **36**, 641-651, doi:10.1016/j.tins.2013.08.001 (2013).

74   Perrone, C. A. *et al.* A novel dynein light intermediate chain colocalizes with the retrograde motor for intraflagellar transport at sites of axoneme assembly in chlamydomonas and Mammalian cells. *Mol Biol Cell* **14**, 2041-2056, doi:10.1091/mbc.E02-10-0682 (2003).

75   Roberts, A. J. *et al.* AAA+ Ring and linker swing mechanism in the dynein motor. *Cell* **136**, 485-495, doi:10.1016/j.cell.2008.11.049 (2009).

76   Can, S., Lacey, S., Gur, M., Carter, A. P. & Yildiz, A. Directionality of dynein is controlled by the angle and length of its stalk. *Nature*, doi:10.1038/s41586-019-0914-z (2019).

77   Vallee, R. B., Williams, J. C., Varma, D. & Barnhart, L. E. Dynein: An ancient motor protein involved in multiple modes of transport. *J Neurobiol* **58**, 189-200, doi:10.1002/neu.10314 (2004).

78   Bingham, J. B., King, S. J. & Schroer, T. A. Purification of dynactin and dynein from brain tissue. *Methods Enzymol* **298**, 171-184 (1998).

79   Walter, W. J., Brenner, B. & Steffen, W. Cytoplasmic dynein is not a conventional processive motor. *J Struct Biol* **170**, 266-269, doi:10.1016/j.jsb.2009.11.011 (2010).

80   Schlager, M. A. *et al.* Bicaudal d family adaptor proteins control the velocity of Dynein-based movements. *Cell Rep* **8**, 1248-1256, doi:10.1016/j.celrep.2014.07.052 (2014).

81   McKenney, R. J., Huynh, W., Tanenbaum, M. E., Bhabha, G. & Vale, R. D. Activation of cytoplasmic dynein motility by dynactin-cargo adapter complexes. *Science* **345**, 337-341, doi:10.1126/science.1254198 (2014).

82   Ayloo, S. *et al.* Dynactin functions as both a dynamic tether and brake during dynein-driven motility. *Nat Commun* **5**, 4807, doi:10.1038/ncomms5807 (2014).

83   Carnes, S. K., Zhou, J. & Aiken, C. HIV-1 Engages a Dynein-Dynactin-BICD2 Complex for Infection and Transport to the Nucleus. *J Virol* **92**, doi:10.1128/JVI.00358-18 (2018).

84   Elshenawy, M. M. *et al.* Cargo adaptors regulate stepping and force generation of mammalian dynein-dynactin. *Nat Chem Biol*, doi:10.1038/s41589-019-0352-0 (2019).

85   Huang, J., Roberts, A. J., Leschziner, A. E. & Reck-Peterson, S. L. Lis1 acts as a "clutch" between the ATPase and microtubule-binding domains of the dynein motor. *Cell* **150**, 975-986, doi:10.1016/j.cell.2012.07.022 (2012).

86   Lenz, J. H., Schuchardt, I., Straube, A. & Steinberg, G. A dynein loading zone for retrograde endosome motility at microtubule plus-ends. *EMBO J* **25**, 2275-2286, doi:10.1038/sj.emboj.7601119 (2006).

87   Stehman, S. A., Chen, Y., McKenney, R. J. & Vallee, R. B. NudE and NudEL are required for mitotic progression and are involved in dynein recruitment to kinetochores. *J Cell Biol* **178**, 583-594, doi:10.1083/jcb.200610112 (2007).

88   Pandey, J. P. & Smith, D. S. A Cdk5-dependent switch regulates Lis1/Ndel1/dynein-driven organelle transport in adult axons. *J Neurosci* **31**, 17207-17219, doi:10.1523/JNEUROSCI.4108-11.2011 (2011).

89   Yi, J. Y. *et al.* High-resolution imaging reveals indirect coordination of opposite motors and a role for LIS1 in high-load axonal transport. *J Cell Biol* **195**, 193-201, doi:10.1083/jcb.201104076 (2011).

90   Egan, M. J., Tan, K. & Reck-Peterson, S. L. Lis1 is an initiation factor for dynein-driven organelle transport. *J Cell Biol* **197**, 971-982, doi:10.1083/jcb.201112101 (2012).

91   Dix, C. I. *et al.* Lissencephaly-1 promotes the recruitment of dynein and dynactin to transported mRNAs. *J Cell Biol* **202**, 479-494, doi:10.1083/jcb.201211052 (2013).

92   Wang, S. *et al.* Nudel/NudE and Lis1 promote dynein and dynactin interaction in the context of spindle morphogenesis. *Mol Biol Cell* **24**, 3522-3533, doi:10.1091/mbc.E13-05-0283 (2013).

93   Moughamian, A. J., Osborn, G. E., Lazarus, J. E., Maday, S. & Holzbaur, E. L. Ordered recruitment of dynactin to the microtubule plus-end is required for efficient initiation of retrograde axonal transport. *J Neurosci* **33**, 13190-13203, doi:10.1523/JNEUROSCI.0935-13.2013 (2013).

94   Moon, H. M. & Wynshaw-Boris, A. Cytoskeleton in action: lissencephaly, a neuronal migration disorder. *Wiley Interdiscip Rev Dev Biol* **2**, 229-245, doi:10.1002/wdev.67 (2013).

95   McKenney, R. J., Vershinin, M., Kunwar, A., Vallee, R. B. & Gross, S. P. LIS1 and NudE induce a persistent dynein force-producing state. *Cell* **141**, 304-314, doi:10.1016/j.cell.2010.02.035 (2010).

96   Lammers, L. G. & Markus, S. M. The dynein cortical anchor Num1 activates dynein motility by relieving Pac1/LIS1-mediated inhibition. *J Cell Biol* **211**, 309-322, doi:10.1083/jcb.201506119 (2015).

97   Markus, S. M. & Lee, W. L. Regulated offloading of cytoplasmic dynein from microtubule plus ends to the cortex. *Dev Cell* **20**, 639-651, doi:10.1016/j.devcel.2011.04.011 (2011).

98   Jha, R., Roostalu, J., Cade, N. I., Trokter, M. & Surrey, T. Combinatorial regulation of the balance between dynein microtubule end accumulation and initiation of directed motility. *EMBO J* **36**, 3387-3404, doi:10.15252/embj.201797077 (2017).

99   Gutierrez, P. A., Ackermann, B. E., Vershinin, M. & McKenney, R. J. Differential effects of the dynein-regulatory factor Lissencephaly-1 on processive dynein-dynactin motility. *J Biol Chem* **292**, 12245-12255, doi:10.1074/jbc.M117.790048 (2017).

100   Baumbach, J. *et al.* Lissencephaly-1 is a context-dependent regulator of the human dynein complex. *Elife* **6**, doi:10.7554/eLife.21768 (2017).

101   Andreasson, J. O. *et al.* Examining kinesin processivity within a general gating framework. *Elife* **4**, doi:10.7554/eLife.07403 (2015).

102   Smith, D. S. *et al.* Regulation of cytoplasmic dynein behaviour and microtubule organization by mammalian Lis1. *Nat Cell Biol* **2**, 767-775, doi:10.1038/35041000 (2000).

103   Tai, C. Y., Dujardin, D. L., Faulkner, N. E. & Vallee, R. B. Role of dynein, dynactin, and CLIP-170 interactions in LIS1 kinetochore function. *J Cell Biol* **156**, 959-968, doi:10.1083/jcb.200109046 (2002).

104   Htet, Z. M. *et al.* Lis1 promotes the formation of maximally activated cytoplasmic dynein-1 complexes. *biorXiv*, doi:https://doi.org/10.1101/683052 (2019).

105   Marzo, M. G., Griswold, J. M. & Markus, S. M. Pac1/LIS1 promotes an uninhibited conformation of dynein that coordinates its localization and activity. *biorXiv*, doi:https://doi.org/10.1101/684290 (2019).

106   Qiu, R., Zhang, J. & Xiang, X. LIS1 regulates cargo-adapter-mediated activation of dynein by overcoming its autoinhibition in vivo. *J Cell Biol*, doi:10.1083/jcb.201905178 (2019).

107   Suzuki, S. O. *et al.* Expression patterns of LIS1, dynein and their interaction partners dynactin, NudE, NudEL and NudC in human gliomas suggest roles in invasion and proliferation. *Acta Neuropathol* **113**, 591-599, doi:10.1007/s00401-006-0180-7 (2007).

108   McKenney, R. J., Weil, S. J., Scherer, J. & Vallee, R. B. Mutually exclusive cytoplasmic dynein regulation by NudE-Lis1 and dynactin. *J Biol Chem* **286**, 39615-39622, doi:10.1074/jbc.M111.289017 (2011).

109   Reddy, B. J. *et al.* Load-induced enhancement of Dynein force production by LIS1-NudE in vivo and in vitro. *Nat Commun* **7**, 12259, doi:10.1038/ncomms12259 (2016).

110   Dogan, M. Y., Can, S., Cleary, F. B., Purde, V. & Yildiz, A. Kinesin's front head is gated by the backward orientation of its neck linker. *Cell Rep* **10**, 1967-1973, doi:10.1016/j.celrep.2015.02.061 (2015).

111   Trokter, M., Mucke, N. & Surrey, T. Reconstitution of the human cytoplasmic dynein complex. *Proc Natl Acad Sci U S A* **109**, 20895-20900, doi:10.1073/pnas.1210573110 (2012).

112   Reiner, O. *et al.* Isolation of a Miller-Dieker lissencephaly gene containing G protein beta-subunit-like repeats. *Nature* **364**, 717-721, doi:10.1038/364717a0 (1993).

113   Gillies, J. P. *et al.* Structural basis for cytoplasmic dynein-1 regulation by Lis1. *eLife* **11**, doi:10.7554/eLife.71229 (2022).

114   Markus, S. M., Marzo, M. G. & McKenney, R. J. New insights into the mechanism of dynein motor regulation by lissencephaly-1. *Elife* **9**, doi:10.7554/eLife.59737 (2020).

115   Lee, W. L., Oberle, J. R. & Cooper, J. A. The role of the lissencephaly protein Pac1 during nuclear migration in budding yeast. *J Cell Biol* **160**, 355-364, doi:10.1083/jcb.200209022 (2003).

116   Markus, S. M. *et al.* Quantitative analysis of Pac1/LIS1-mediated dynein targeting: Implications for regulation of dynein activity in budding yeast. *Cytoskeleton (Hoboken)* **68**, 157-174, doi:10.1002/cm.20502 (2011).

117   Elshenawy, M. M. *et al.* Lis1 activates dynein motility by modulating its pairing with dynactin. *Nat Cell Biol* **22**, 570-578, doi:10.1038/s41556-020-0501-4 (2020).

118   Htet, Z. M. *et al.* LIS1 promotes the formation of activated cytoplasmic dynein-1 complexes. *Nat Cell Biol* **22**, 518-525, doi:10.1038/s41556-020-0506-z (2020).

119   Marzo, M. G., Griswold, J. M. & Markus, S. M. Pac1/LIS1 stabilizes an uninhibited conformation of dynein to coordinate its localization and activity. *Nat Cell Biol* **22**, 559-569, doi:10.1038/s41556-020-0492-1 (2020).

120   Yamada, M. *et al.* LIS1 and NDEL1 coordinate the plus-end-directed transport of cytoplasmic dynein. *EMBO J* **27**, 2471-2483, doi:10.1038/emboj.2008.182 (2008).

121   Torisawa, T. *et al.* Functional dissection of LIS1 and NDEL1 towards understanding the molecular mechanisms of cytoplasmic dynein regulation. *J Biol Chem* **286**, 1959-1965, doi:10.1074/jbc.M110.169847 (2011).

122   Ferro, L. S. *et al.* Structural and functional insight into regulation of kinesin-1 by microtubule-associated protein MAP7. *Science* **375**, 326-331, doi:10.1126/science.abf6154 (2022).

123   Gennerich, A., Carter, A. P., Reck-Peterson, S. L. & Vale, R. D. Force-induced bidirectional stepping of cytoplasmic dynein. *Cell* **131**, 952-965, doi:10.1016/j.cell.2007.10.016 (2007).

124   Markus, S. M., Punch, J. J. & Lee, W. L. Motor- and tail-dependent targeting of dynein to microtubule plus ends and the cell cortex. *Curr Biol* **19**, 196-205, doi:10.1016/j.cub.2008.12.047 (2009).

125   Raaijmakers, J. A., Tanenbaum, M. E. & Medema, R. H. Systematic dissection of dynein regulators in mitosis. *J Cell Biol* **201**, 201-215, doi:10.1083/jcb.201208098 (2013).

126   Moon, H. M. *et al.* LIS1 controls mitosis and mitotic spindle organization via the LIS1-NDEL1-dynein complex. *Hum Mol Genet* **23**, 449-466, doi:10.1093/hmg/ddt436 (2014).

127 Schmidt, R. *et al.* Two populations of cytoplasmic dynein contribute to spindle positioning in C. elegans embryos. *J Cell Biol* **216**, 2777-2793, doi:10.1083/jcb.201607038 (2017).

128 Tame, M. A. *et al.* Astral microtubules control redistribution of dynein at the cell cortex to facilitate spindle positioning. *Cell Cycle* **13**, 1162-1170, doi:10.4161/cc.28031 (2014).

129 Minke, P. F., Lee, I. H., Tinsley, J. H., Bruno, K. S. & Plamann, M. Neurospora crassa ro-10 and ro-11 genes encode novel proteins required for nuclear distribution. *Mol Microbiol* **32**, 1065-1076, doi:10.1046/j.1365-2958.1999.01421.x (1999).

130 Efimov, V. P. & Morris, N. R. The LIS1-related NUDF protein of Aspergillus nidulans interacts with the coiled-coil domain of the NUDE/RO11 protein. *J Cell Biol* **150**, 681-688, doi:10.1083/jcb.150.3.681 (2000).

131 Sasaki, S. *et al.* A LIS1/NUDEL/cytoplasmic dynein heavy chain complex in the developing and adult nervous system. *Neuron* **28**, 681-696, doi:S0896-6273(00)00146-X [pii] (2000).

132 Niethammer, M. *et al.* NUDEL is a novel Cdk5 substrate that associates with LIS1 and cytoplasmic dynein. *Neuron* **28**, 697-711 (2000).

133 Feng, Y. *et al.* LIS1 regulates CNS lamination by interacting with mNudE, a central component of the centrosome. *Neuron* **28**, 665-679, doi:10.1016/s0896-6273(00)00145-8 (2000).

134 Wang, S. & Zheng, Y. Identification of a novel dynein binding domain in nudel essential for spindle pole organization in Xenopus egg extract. *J Biol Chem* **286**, 587-593, doi:10.1074/jbc.M110.181578 (2011).

135 Zylkiewicz, E. *et al.* The N-terminal coiled-coil of Ndel1 is a regulated scaffold that recruits LIS1 to dynein. *J Cell Biol* **192**, 433-445, doi:10.1083/jcb.201011142 (2011).

136 Nyarko, A., Song, Y. & Barbar, E. Intrinsic disorder in dynein intermediate chain modulates its interactions with NudE and dynactin. *J Biol Chem* **287**, 24884-24893, doi:10.1074/jbc.M112.376038 (2012).

137 Siglin, A. E. *et al.* Dynein and dynactin leverage their bivalent character to form a high-affinity interaction. *PLoS One* **8**, e59453, doi:10.1371/journal.pone.0059453 (2013).

138 Guerrini, R. & Parrini, E. Neuronal migration disorders. *Neurobiol Dis* **38**, 154-166, doi:10.1016/j.nbd.2009.02.008 (2010).

139 Dobyns, W. B., Reiner, O., Carrozzo, R. & Ledbetter, D. H. Lissencephaly. A human brain malformation associated with deletion of the LIS1 gene located at chromosome 17p13. *JAMA* **270**, 2838-2842, doi:10.1001/jama.270.23.2838 (1993).

140 Hirotsune, S. *et al.* Graded reduction of Pafah1b1 (Lis1) activity results in neuronal migration defects and early embryonic lethality. *Nat Genet* **19**, 333-339, doi:10.1038/1221 (1998).

141 Swan, A., Nguyen, T. & Suter, B. Drosophila Lissencephaly-1 functions with Bic-D and dynein in oocyte determination and nuclear positioning. *Nat Cell Biol* **1**, 444-449, doi:10.1038/15680 (1999).

142 Alkuraya, F. S. *et al.* Human mutations in NDE1 cause extreme microcephaly with lissencephaly [corrected]. *Am J Hum Genet* **88**, 536-547, doi:10.1016/j.ajhg.2011.04.003 (2011).

143 Doobin, D. J., Kemal, S., Dantas, T. J. & Vallee, R. B. Severe NDE1-mediated microcephaly results from neural progenitor cell cycle arrests at multiple specific stages. *Nat Commun* **7**, 12551, doi:10.1038/ncomms12551 (2016).